2013-11-14

Towards Macroscopic Quantum Effects Using Optomechanical and Optical Systems

Ghobadi, Roohollah

UNIVERSITY OF CALGARY

Towards Macroscopic Quantum Effects Using Optomechanical and Optical Systems

by

Roohollah Ghobadi

A THESIS

SUBMITTED TO THE FACULTY OF GRADUATE STUDIES

IN PARTIAL FULFILLMENT OF THE REQUIREMENTS FOR THE

DEGREE OF DOCTOR OF PHILOSOPHY

DEPARTMENT OF PHYSICS AND ASTRONOMY

CALGARY, ALBERTA

NOVEMBER, 2013

Abstract

In this thesis, I studied two different approaches which are promising for creating macroscopic quantum superpositions.

The first approach, which is the main focus of this thesis, is based on optomechanical systems. The basic challenge to realize quantum effects in optomechanical systems, is considered to be the weak optomechanical coupling rate compared to the decoherence rates of the system caused by the cavity and mechanical damping. To enhance the optomechanical coupling it has been suggested to pump the cavity with coherent laser light [1]. By this method the strong coupling regime in which the optomechanical coupling rate exceeds all decoherence rates has been demonstrated very recently [2, 3]. It is also known that the optomechanical systems may exhibit nonlinear behaviours such as bistability.

After introducing the basic ideas of optomechanical systems in chapter 1, in chapter 2 we studied the connection between optomechanical entanglement and bistability.

In chapter 3, we studied the drawback of using a laser to enhance the interaction. We studied the effect of the laser phase noise, as an additional decoherence channel, on the optomechanical entanglement. We have shown that the system is very sensitive to this new source of decoherence and the sensitivity is maximum in the bistable threshold. We discussed that our results are independent of how we model the laser phase noise.

In chapter 4, we studied single photon optomechanics. In this regime, we proposed a new scheme to enhance the optomechanical coupling based on post selection. Our scheme is potentially promising to create a superposition of the massive oscillator in different motional states. We also discussed the potential application of our scheme to test some decoherence models.

The second approach that we consider in this thesis is based on amplifying single photons with high gain to create micro-macro superpositions . In chapter 5, we discussed the De

Martini scheme. We then present our scheme for creating optical micro-macro superposition and discussed its experimental realization under realistic conditions when losses are taken into account.

List of published papers

1. B. He, Q. Lin, R. Ghobadi, C. Simon, "Fully Quantum Approach to Optomechanical Entanglement" arXiv:1308.5932.

2. R. Ghobadi, S. Kumar, B. Pepper, D. Bouwmeester, A. Lvovsky, C. Simon, "Optomechanical micro-macro entanglement" Submitted to *Phy. Rev.Lett*.

3. T. Wang, R. Ghobadi, S. Raeisi, C. Simon, "Can coarse measurements reveal macroscopic quantum effects?" arXiv:1307.0732.

4. H. Kaviani, M. Khazali, R. Ghobadi, E. Zahedinejad, K. Heshami, C. Simon, "Quantum Storage and Retrieval of Light by Sweeping the Atomic Frequency" New J. Phys. **15** 085029 (2013).

5. A. I. Lvovsky, R. Ghobadi, C. Simon, A. Chandra, A. S. Prasad,"Observation of micro-macro entanglement of light", *Nature Physics* **9** 541 (2013).

6. R.Ghobadi, A.Lvovsky, C.Simon, "Creating and detecting micro-macro photon-number entanglement by amplifying and de-amplifying a single-photon entangled state", *Phy. Rev.Lett* **110**, 170406 (2013).

7. B. Pepper, E. Jeffry, R.Ghobadi, C. Simon, D. Bouwmeester, "Macroscopic superposition via nested interferometry: finite temperature and decoherence considerations", *New J. Phys* **14**, 115025 (2012).

8. R.Ghobadi, S.Raiesi, C. Simon, "Demonstrating macroscopic entanglement based on Kerr non-linearities requires extreme phase resolution", arXiv:1206.3673.

9. Brian Pepper, Roohollah Ghobadi, Evan Jeffry, Christoph Simon and Dirk Bouwmeester, "Optomechanical superposition via nested interferometry", *Phy. Rev.Lett* **109**,

023601 (2012).

10. R.Ghobadi, A.R.Bahrampour, C.Simon, "Optomechanical entanglement in the presence of laser phase noise" *Phy. Rev. A*, **84**, 063827 (2011).

11. R.Ghobadi, A.R.Bahrampour, C.Simon, "Quantum optomechanics in the bistable regime *Phys. Rev. A*, **84**, 033846 (2011).

Acknowledgements

I would like to thank my supervisor, Dr. Christoph Simon, who has supported me throughout my study with his expertises and knowledge. I appreciate his patience, guidance and constructive criticisms at different stages of my research. As his student, I have been fortunate to have been exposed to a fairly wide range of materials from fundamental to more practical physics.I am always amazed by his ability in simplifying complex subjects.

I would like to thank my friends at the University of Calgary for good times that we had together: Hamidreza, Khabat, Saleh, Jalal, Ehsan, Hossein, Sadegh, Arsalan, Javad, Mahdi and many others.

I would like to thank my committee members for their comments and advises which improves my thesis specially Dr. Paul Barclay, Dr. Aashish Clerck, and Dr. David Feder.

Last but not least, I appreciate my family, especially my parents, Ali and Hanifeh, for their unconditional support and love throughout my life.

Table of Contents

List of Tables

List of Figures and Illustrations

Chapter 1

Introduction to quantum optomechanics: basic principles and potential applications

In this chapter we review some important aspects of optomechanical systems. We start by introducing the Fabry-Perot cavity in Section 1.1. Then we introduce optomechanical systems and their basic physics in Section 1.2. In section 1.3 we derive the Hamiltonian of optomechanical systems.

We briefly discuss some important applications of optomechanical systems such as ground state cooling of mechanical oscillators, observing quantum fluctuations of a mechanical oscillator, optomechanically induced transparency and preparing superpositions of different vibrational states of a mechanical oscillator.

1.1 Basic System: Fabry-Perot Cavity

In this section we briefly review some of the properties of Fabry-Perot cavities. A Fabry-Perot cavity consists of two reflecting mirrors with reflectivity r_1, r_2 and transmittivity t_1 , t_2 at a distance L apart. Fig. (1.1). When the Fabry-Perot cavity is driven by an incident beam with intensity I_0 and wave number k, the intensity of the transmitted light is given by

$$I_T = I_0 \frac{T^2}{(1-R)^2} \frac{1}{1+(\frac{2\mathscr{F}}{\pi})^2 \sin^2(\delta/2)}, \tag{1.1}$$

where $R = |r_1||r_2|$, $T = |t_1||t_2|$ and $\delta = 2kL$ and

$$\mathscr{F} = \frac{\pi\sqrt{R}}{1-R}, \tag{1.2}$$

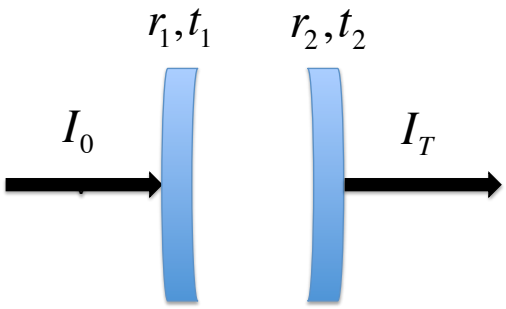

Figure 1.1: A Fabry-Perot cavity consists of two mirrors with reflectivity r_1, r_2 and transmittivity t_1, t_2.

is the cavity finesse. The cavity damping rate is defined in terms of the cavity finesse as

$$\kappa = \frac{\pi c}{L\mathscr{F}}. \tag{1.3}$$

If the Fabry-Perot cavity contains a medium with a nonlinear index like a Kerr medium, the transmitted light from the cavity may display optical bistability, i.e. for some input intensities there are two possible values for the transmitted intensity. To show this, we assume that $\delta \ll 1$, which means the cavity is driven near resonance. In this case Eq.(1.1) can be written as

$$I_T = I_0 \frac{T^2}{(1-R)^2} \frac{1}{1+(\frac{\mathscr{F}}{\pi})^2 \delta^2}. \tag{1.4}$$

The Kerr nonlinear medium causes an intensity-dependent phase shift of the transmitted light:

$$\delta = \delta_0 + \delta_2 I_T. \tag{1.5}$$

We also assume that δ_0 and δ_2 have opposite signs, so that the field can tune the cavity through resonance. Plugging Eq. (1.5) in Eq. (1.4) gives

$$\frac{T^2}{(1-R)^2} I_0 = I_T (1+(\frac{\mathscr{F}}{\pi})^2 (\delta_0 + \delta_2 I_T)^2) \tag{1.6}$$

Eq. (1.6) in general has three solutions for the transmitted light (it is a third order polynomial in I_T). Depending on the parameters in Eq. (1.6), there will be one or two real solutions for the transmitted light. The latter case corresponds to bistability.

1.2 Optomechanical Systems

The simplest optomechanical system (OMS) consists of a Fabry-Perot cavity in which one of its mirrors can move under the influence of the radiation pressure of light inside the cavity, Fig. (1.2). The basic idea with an OMS is to control and manipulate the motion of the mirror with light inside the cavity and vice versa. This idea has been applied to a wide range of scales from macroscopic mirrors in the LIGO [9, 10] to nano or micro mechanical cantilevers [11, 12], microtoroids [13] and membranes [14] and optomechanical crystals [15].

A change in the length of the cavity changes the intracavity light intensity and phase. It was pointed out by Braginsky [16] that these changes produce two main effects. The first one is the optical spring effect, which means that the oscillation frequency of the mirror will change because of the radiation pressure. The second is the change in the damping of the mechanical oscillator. Both of these effects can be used to reduce the temperature of the oscillating mirror. To see how the optical spring effect can reduce the effective temperature of the oscillating mirror, we recall that [17]

$$\langle q^2 \rangle = \frac{k_B T}{m\omega_m^2}, \tag{1.7}$$

where $\langle q^2 \rangle$ represents the fluctuations of the mirror position, m and ω_m are the mass and frequency of the oscillating mirror, respectively. By increasing the resonance frequency of the mirror the fluctuations are reduced, which is similar to the effect of a decrease the temperature.

An induced change in the damping can also lower the effective temperature, this is called cold damping. One can see this from the following expression for the mechanical oscillator energy

$$\frac{d}{dt}\langle E \rangle = -\gamma_m \langle E \rangle + \gamma_m k_B T - \Gamma_{\text{opt}} \langle E \rangle. \tag{1.8}$$

Here γ_m is the intrinsic damping rate of the mirror and Γ_{opt} is the additional damping be-

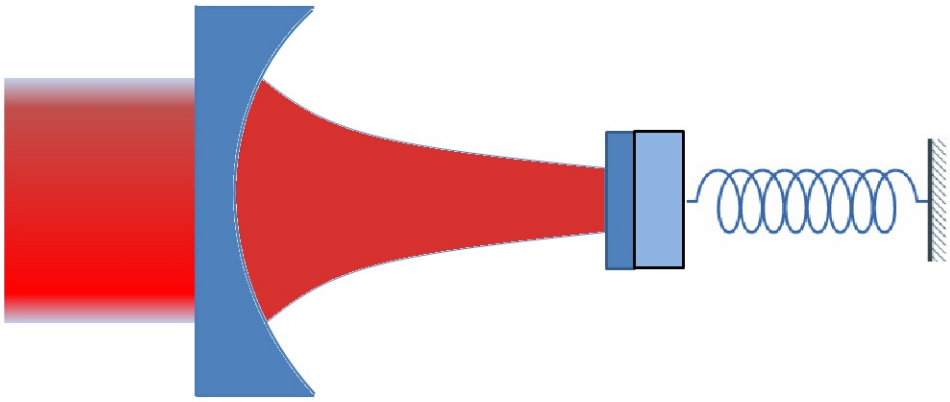

Figure 1.2: A typical optomechancial system consists of an optical cavity with one end movable mirror, modelled as a harmonic oscillator, which moves under the influence of radiation pressure and thermal fluctuations.

cause of the radiation pressure. From the steady state solution ($\frac{d}{dt}\langle E\rangle = 0$) of Eq. (1.8) one sees that the effective temperature is given by

$$T_{\text{eff}} = \frac{\gamma_m T}{\gamma_m + \Gamma_{\text{opt}}} \tag{1.9}$$

For $\Gamma_{\text{opt}} > 0$ one sees that the effective temperature is smaller than the environment temperature.

As a final remark for this section we note that the bistability argument given for the nonlinear medium inside the cavity is applicable to OMS. This is because the phase of the cavity field is determined by the displacement of the movable mirror which is proportional to the light intensity. This means that Eq. (1.5) is applicable to this case. The first observation of optomechanical bistability has been reported in [18]

1.3 Quantum Optomechanics: the Hamiltonian

In this section we derive the optomechanical Hamiltonian [19]. We consider a Fabry-Perot cavity with initial length L_0. One of the mirrors can move under the influence of radiation

pressure due to the light inside the cavity. The position of the mirror at a given time t is given by $L(t)$ and the mirror displacement, denoted by $q(t)$, is given by $q(t) = L_0 - L(t)$. We model the motion of the movable mirror as a mechanical oscillator with mass m and frequency ω_m. The vector potential $A(q,t)$ of the optical field inside the cavity obeys the wave equation ($c = 1$)

$$\frac{\partial^2 A}{\partial q^2} - \frac{\partial^2 A}{\partial t^2} = 0. \tag{1.10}$$

We assume that both mirrors are perfect mirrors so that the vector potential also obeys time-dependant boundary conditions

$$A(0,t) = A(L(t),t) = 0. \tag{1.11}$$

The non relativistic equation of motion for the mirror is given by

$$m\ddot{q} = -\frac{\partial V}{\partial q} + \frac{1}{2}(\frac{\partial A(q,t)}{\partial q})^2|_{q=q(t)}. \tag{1.12}$$

the first term is the simple harmonic force $-m\omega_m^2 q$ and the second term in Eq.(1.12) corresponds to the radiation pressure force. One can understand the second term in Eq.(1.12) easily by moving to the rest frame of the movable mirror. In this frame, the electric field on the mirror surface is zero, as we assume a perfect mirror and the radiation pressure force is given by $\frac{B'^2}{2}$, where $B^{'}$ is the magnetic field on the mirror's surface in the co-moving frame. Now when the velocity of the movable mirror is much smaller than the speed of the light one has $B^{'} = B$ [20], where B is the magnetic field on the mirror surface in the laboratory frame.

We can expand the vector potential in terms of a complete set of orthogonal functions $u_k(x,t)$ which is defined as

$$u_k(q,t) = \sqrt{\frac{2}{L(t)}}\sin(\frac{\pi k q}{L(t)}). \tag{1.13}$$

The vector potential can then be expanded in terms of $u_k(q,t)$ as

$$A(q,t) = \sum_{k=1}^{\infty} Q_k(t) u_k(q,t). \tag{1.14}$$

Plugging Eq.(1.14) into Eq.(1.12) the equation of motion for $Q_k(t)$ can be obtained. We then define P_k as the canonical momentum conjugate to Q_k and, following the standard procedure in canonical quantization, we convert the variables q,p,Q_k,P_k to operators, which obey the following commutation relations

$$[\hat{q},\hat{Q}_j] = [\hat{q},\hat{P}_j] = [\hat{p},\hat{Q}_j] = [\hat{p},\hat{P}_j] = 0, \tag{1.15}$$

$$[\hat{q},\hat{p}] = i\hbar, \tag{1.16}$$

$$[\hat{Q}_j,\hat{P}_k] = i\hbar\delta_{jk}. \tag{1.17}$$

The canonical quantization is accomplished by introducing the cavity-length dependent annihilation and creation operators

$$\hat{a}_k(q) = \sqrt{\frac{1}{2\hbar\omega_k(q)}}[\omega_k(q)\hat{Q}_k + i\hat{P}_k], \tag{1.18}$$

$$\hat{a}_k^{\dagger}(q) = \sqrt{\frac{1}{2\hbar\omega_k(q)}}[\omega_k(q)\hat{Q}_k - i\hat{P}_k]. \tag{1.19}$$

From Eqs. (1.18, 1.19) and using standard canonical field quantization, one can obtain the Hamiltonian [19]:

$$\hat{H} = \frac{(\hat{p}+\hat{\Gamma})^2}{2m} + \hat{V}(q) + \hbar\sum_k \omega(q)[\hat{a}_k^{\dagger}\hat{a}_k + \frac{1}{2}], \tag{1.20}$$

where

$$\hat{\Gamma} = \frac{i\hbar}{2q}\sum_{k,j} g_{kj}(\frac{k}{j})^{1/2}[\hat{a}_k^{\dagger}\hat{a}_j^{\dagger} - \hat{a}_k\hat{a}_j + \hat{a}_k^{\dagger}\hat{a}_j - \hat{a}_j^{\dagger}\hat{a}_k], \tag{1.21}$$

$$\omega_k(q) = \frac{k\pi}{L(t)}, \tag{1.22}$$

$$g_{kj} = \begin{cases} (-1)^{k+j}\frac{2kj}{j^2-k^2} & k \neq j \\ 0 & k = j. \end{cases} \tag{1.23}$$

Considering a single mode cavity, one can simplify the Hamiltonian since $\hat{\Gamma} = 0$ in this case. This approximation is valid if the mechanical frequency is smaller than the spacing between the optical modes, i.e.

$$\triangle\omega = \frac{\pi}{L_0} > \omega_m, \tag{1.24}$$

physically, Eq.(1.24) means that no photon is scattered to other optical modes because of the mirror motion.

Eq.(1.20) is a nonlinear Hamiltonian due to $\hat{\Gamma}$. We are interested in the case for which the potential $V(q)$ keeps the moving mirror oscillating around an equilibrium position and the radiation pressure acts as a perturbation, meaning that the radiation pressure force is much smaller than $V(q)$. One can linearize the Hamiltonian around the equilibrium point and obtain the Hamiltonian

$$\hat{H} = \frac{\hat{p}^2}{2m} + \hat{V}(q) + \hbar\sum_k \omega_{k0}\hat{a}^\dagger_{k0}\hat{a}_{k0} - qF_0 - \frac{\pi\hbar}{24(L_0+q(t))}, \tag{1.25}$$

where a_{k0} and ω_{k0} denote the annihilation operator and frequency in the equilibrium position, respectively and

$$\hat{F}_0 = \frac{\hbar}{2L_0}\sum_{k,j}(-1)^{k+j}\sqrt{\omega_{k0}\omega_{j0}} \times (\hat{a}_{k0}\hat{a}_{j0} + \hat{a}^\dagger_{k0}\hat{a}^\dagger_{j0} + \hat{a}^\dagger_{k0}\hat{a}_{j0} + \hat{a}_{k0}\hat{a}^\dagger_{j0}), \tag{1.26}$$

is the radiation pressure operator. The last term in Eq.(1.25) corresponds to the Casimir energy which can be neglected as it very small compared to other terms. It is interesting to note that the term qF_0 in Eq. (1.25) is analogous to a dipole interaction.

One can further simplify Eq. (1.25) by assuming a single mode cavity. In this special case the optomechanical interaction term in Eq.(1.25) simplifies to $\frac{\hbar\omega_{k0}}{L}\hat{q}\hat{a}^\dagger_{k0}\hat{a}_{k0}$. It is interesting to note that one can easily derive the simplified optomechanical Hamiltonian by starting from the cavity field Hamiltonian with a variable resonance frequency, i.e.

$$\hat{H}_{cavity} = \hbar\omega_c(q)\hat{a}^\dagger\hat{a}. \tag{1.27}$$

Noting that $q(t) \ll L_0$, one can approximate Eq.(1.22) as

$$\omega_c(q) = \frac{\pi}{L+q(t)} \simeq \omega_c(0)(1-\frac{q(t)}{L}), \tag{1.28}$$

where $\omega_c(0)$ is the cavity resonance frequency when $q = 0$. Plugging (1.28) into (1.27) one gets

$$\hat{H} = \hbar\omega_c(0)\hat{a}^\dagger\hat{a} - \hbar\frac{\omega_c(0)}{L}\hat{a}^\dagger\hat{a}\hat{q}. \tag{1.29}$$

From now on we use $\omega_c = \omega_c(0)$ for simplicity. To get the total Hamiltonian one must add the moving mirror Hamiltonian to Eq. (1.29).

1.4 Why is quantum optomechanics attractive?

To study quantum effects in optomechanical systems it is useful to define the position operator of the mirror in terms of creation and annihilation operators as $\hat{q} = x_{zpf}(\hat{b}+\hat{b}^\dagger)$ where $x_{zpf} = \sqrt{\frac{\hbar}{2m\omega_m}}$ is the zero point fluctuation of the mechanical oscillator. The optomechnical Hamiltonian Eq.(1.29) becomes

$$\hat{H} = \hbar\omega_c\hat{a}^\dagger\hat{a} + \hbar\omega_m\hat{b}^\dagger\hat{b} - \hbar G_0\hat{a}^\dagger\hat{a}(\hat{b}+\hat{b}^\dagger), \tag{1.30}$$

where $G_0 = \frac{\omega_c}{L_0}x_{zpf}$ is the single photon optomechanical coupling. The first and second terms are the Hamiltonians of the cavity field and the moving mirror, respectively. The general Hamiltonian should also contain the pumping term. For the case in which the cavity is pumped with coherent light, the pumping term reads

$$H_{\text{pump}} = i\hbar E(\hat{a}^\dagger e^{-i\omega_L t} - \hat{a}e^{i\omega_L t}), \tag{1.31}$$

where E is proportional to the amplitude of the pumping field and ω_L is the frequency of the pump. In the presence of a strong driving field one can linearize the optomechanical interaction by expanding the cavity field and the mirror displacement around their steady state values: $\hat{a} = \alpha_s + \delta\hat{a}$ and $\hat{b} = \beta_s + \delta\hat{b}$ where α_s and β_s describe the steady state behaviour of the cavity

field and the mechanical oscillator, respectively, and δa and δb are the fluctuation around these steady states. Without loss of generality we assume that α_s is real. With these approximations the optomechanical interaction becomes[1] (see also the Eq.(2.7))

$$\hat{H}_{\text{opm}} = -\hbar G_0 \alpha_s (\delta\hat{a} + \delta\hat{a}^\dagger)(\delta\hat{b} + \delta\hat{b}^\dagger) \tag{1.32}$$

One notes that the enhancement of the optomechanical coupling by a factor of α_s. This is analogous to the enhancement of the atom-field interaction in an atomic ensemble.

The optomechanical interaction as shown in Eq. (1.32) consists of two well-known interactions in quantum optics. The term $\delta\hat{a}\delta\hat{b}^\dagger + \delta\hat{a}^\dagger\delta\hat{b}$ is a beam splitter like Hamiltonian. This term describes the energy exchange between the cavity field and the mechanical oscillator, which allows cooling of the mechanical oscillator. This is because of the fact that photons eventually leak from the cavity and hence remove one quantum of mechanical oscillator energy. This is a powerful way for cooling a macroscopic object as it allows ground state cooling of the mechanical oscillator in the so-called resolved sideband regime which occurs when the mechanical frequency (ω_m) is larger than the cavity damping (κ). The resolved sideband condition is necessary to ensure that photons interact with the mechanical oscillator before leaking out of the cavity. It also can be understood in term of Stokes and anti-Stokes scattering of light to the motional sideband. The moving mirror scatters pump photons with frequency ω_L to $\omega_L - \omega_m$ and $\omega_L + \omega_m$. In the red detuned regime ($\omega_L < \omega_c$), the Stokes process ($\omega_L \to \omega_L + \omega_m$) is favoured over the anti-Stokes ($\omega_L \to \omega_L - \omega_m$) because the density of optical mode available for the Stokes process is higher than for the anti-Stokes, see Fig. (1.3). The resolved sideband condition guarantees that the probability of the anti-Stokes process is negligible, see Fig. (1.3).

The second part of the optomechanical Hamiltonian $\delta\hat{a}\delta\hat{b} + \delta\hat{a}^\dagger\delta\hat{b}^\dagger$ is the squeezing Hamiltonian. This term can be useful for preparing the mechanical oscillator in a squeezed state which is important for precise measurement. This term can also produce entangled state of the mechanical oscillation and the cavity field [21, 1] starting from classical states for mechanical

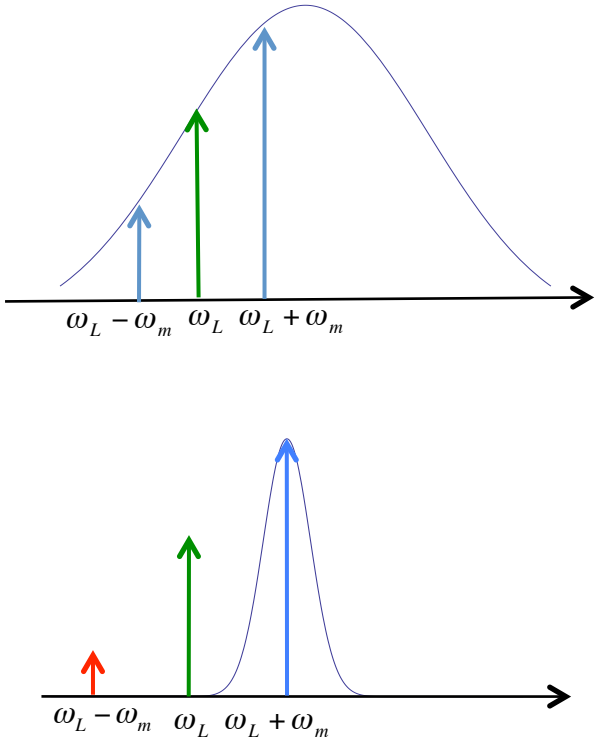

Figure 1.3: Basic principle of ground state cooling. $\omega_m > \kappa$ guarantees that optomechnaical cooling (corresponding to Stokes scattering, $\omega_L + \omega_m$) dominates over optomechanical heating, (corresponding to anti-Stokes scattering, $\omega_L - \omega_m$).

oscillator and the cavity field. This aspect of optomechanical systems is especially important because it may shed some light on the problem of the quantum-classical transition and quantum gravity [22, 8, 23, 24]

1.4.1 Zero-point fluctuation of a mechanical oscillator

Ground state cooling of the mechanical oscillator using the aforementioned method has been realized by different groups [25, 26]. Having reached the ground state cooling regime it is possible to observe some intrinsic quantum effects. For example the zero-point fluctuation (ZPF) of the mechanical oscillator has been observed recently [27]. The experimental observation of ZPF relies on the fundamental asymmetry between absorption and emission [28]. The equation of motion of a harmonic oscillator for the position operator in the Heisenberg picture is

$$\hat{q}(t) = \hat{q}(0)\cos(\Omega t) + \frac{\hat{p}(0)}{m\Omega}\sin(\Omega t). \tag{1.33}$$

A quantity which is usually measured in experiments is the spectral density, defined as

$$S_{qq}(\omega) = \int_{-\infty}^{\infty} dt \langle \hat{q}(t)\hat{q}(0)\rangle e^{-i\omega t}, \tag{1.34}$$

using Eq. (1.33) we obtain

$$\langle \hat{q}(t)\hat{q}(0)\rangle = \langle \hat{q}^2(0)\rangle \cos(\Omega t) + \frac{\langle \hat{p}(0)\hat{q}(0)\rangle}{m\Omega}\sin(\Omega t). \tag{1.35}$$

By writing $\hat{q}$ and $\hat{p}$ in terms of the harmonic oscillator ladder operators, one can show that in the thermal equilibrium, the identities

$$\langle q^2(0)\rangle = x_{\text{zpf}}^2(2\bar{n}+1), \tag{1.36}$$

(with $\bar{n} = \frac{1}{exp(\frac{\hbar\omega_m}{k_B T})-1}$) and

$$\langle p(0)q(0)\rangle = \frac{-i\hbar}{2}, \tag{1.37}$$

hold. Using Eq.(1.36) and Eq.(1.37) in Eq.(1.35) we obtain

$$\langle \hat{q}(t)\hat{q}(0)\rangle = x_{\text{zpf}}^2\{e^{i\Omega t}(\bar{n}+1)+e^{-i\Omega t}\bar{n}\}, \tag{1.38}$$

from which we obtain the spectral density as following

$$S_{qq}(\omega) = x_{\text{zpf}}^2[\bar{n}\delta(\omega+\Omega)+(\bar{n}+1)\delta(\omega-\Omega)] \tag{1.39}$$

In the classical limit where $\bar{n} >> 1$ Eq.(1.39) simplified to

$$S_{qq}(\omega) = x_{\text{zpf}}^2\bar{n}[\delta(\omega+\Omega)+\delta(\omega-\Omega)] \tag{1.40}$$

which means that the spectral density is a symmetric function of frequency. On the other hand, close to the ground state the quantum prediction becomes different from the classical prediction. In the Safavi-Naeini et.al experiment [27], the asymmetry in the spectral density, which is a signature of ground state fluctuations of the mechanical oscillator, has been observed.

1.4.2 Optomechanically Induced Transparency

It is well-known from atomic physics that coherent light-atom interaction can lead to quantum interference between atomic excitations. A prominent example of such effects is electromagnetically induced transparency (EIT) [29]. In EIT, the destructive interference between two pathways causes the medium to become transparent for a weak probe field for a certain window of frequency. It has been predicted theoretically [30] and observed experimentally [25, 31] that the analogous effect can happen in optomechanical systems. The basic idea is to drive the cavity with a strong coupling field (control field) with frequency ω_c and a weak probe field with frequency ω_p. In the presence of the strong control field, which is red-detuned with respect to the cavity frequency ($\omega_c < \omega_{\text{cavity}}$), the beam-splitter like Hamiltonian in the optomechanical interaction is the dominant interaction. The probe field then interacts with this linearized Hamiltonian. Now if the photons from the control field which have been scattered

to the $\omega_c + \omega_m$ channel have almost the same frequency as the probe field, the optomechanical system becomes transparent for the probe field. This transparency can be understood in terms of destructive interference between the scattered photons and the probe field.

1.4.3 Optomechanical superpositions

How does the classical world emerge from quantum mechanics? The standard answer to this question is given by environmentally induced decoherence (EID) theory. According to EID, the interaction of the system with its environment destroys the quantum nature of the system as the environment measures the system. This can be easily understood in terms of the following example. Let us assume that we have a two-level atom which is initially prepared in a superposition of excited and ground states and the environment in the state $|E_0\rangle$, so the initial state of system-environment is

$$|\psi(0)\rangle = (c_g|g\rangle + c_e|e\rangle) \otimes |E_0\rangle \tag{1.41}$$

At a later time the system-environment interaction makes the total state an entangled state like

$$|\psi(t)\rangle = c_g(t)|g\rangle|E_g\rangle + c_e(t)|e\rangle|E_e\rangle \tag{1.42}$$

The state of the system can be obtained after tracing out the environment degrees of freedom. Now if $\langle E_e|E_g\rangle = 0$, it means that the environment measures precisely the system state, so the density matrix of the system becomes a statistical mixture of the ground state and the excited state. Accordingly, one needs to isolate properly the quantum system from its environment to keep the quantum coherence. This isolation gets harder and harder as the size of the system increases.

It is interesting to study the transition from quantum superposition to statistical mixture in different systems. Tracking the quantum to classical transition for massive objects is specially

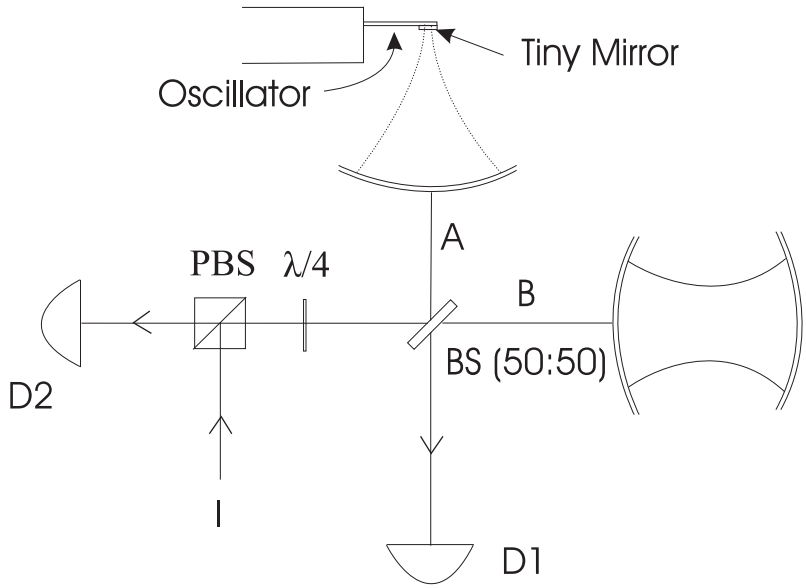

Figure 1.4: The proposed scheme in [8]. A single photon sent to the beam splitter to prepare an entangled state $\frac{|0\rangle_A|1\rangle_B+|1\rangle_A|0\rangle_B}{\sqrt{2}}$. The movable mirror in arm A is prepared in the ground state. If the photon goes into arm A, it will displace the movable mirror and so it prepares the mirror in superposition of vibrational states. The mirror superposition can then be observed by measuring the visibility of the interference in the detectors $D1$ and $D2$.

interesting, as there are some speculations that describe such transitions as a result of a modified Schrodinger equation. For example Diosi [7] and Penrose [6] emphasized the role of gravity in destroying quantum effects.

Here we describe a scheme due to Marshall et.al [8], which suggested the use of optomechanical systems for probing quantum superpositions of a massive object. The basic idea is to use a Mach-Zehnder interferometer with one Fabry-Perot cavity in each of its arms, see Fig.(1.4).

In arm A, one of the mirrors is replaced with a tiny mirror on a micromechanical cantilever. It is assumed that this mirror is cooled close to its motional ground state. Here we assume ground state cooling for simplicity. A single photon is sent to the interferometer to prepare the superposition

$$|\psi(0)\rangle = (\frac{|0\rangle_A|1\rangle_B + |1\rangle_A|0\rangle_B}{\sqrt{2}}) \otimes |0\rangle_m \tag{1.43}$$

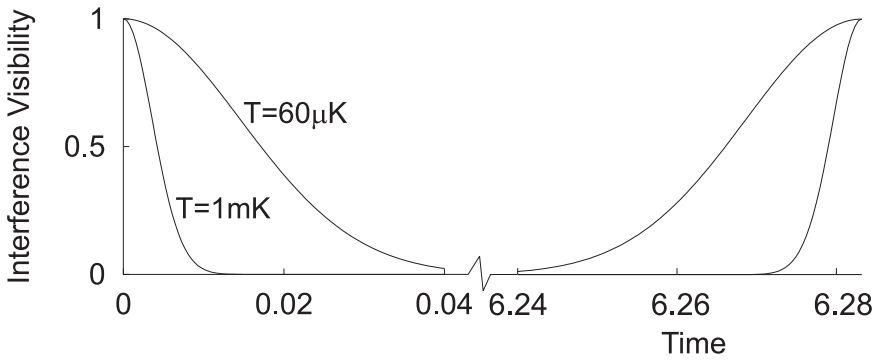

Figure 1.5: Interference visibility as a function of time over one period of the mirror oscillation for $\kappa = 1$, $T = 1mK$ and $T = 60\mu K$.

which means that the photon either takes path A or B. If the photon takes path B the tiny mirror is not affected, while if it takes the other path the radiation pressure of the single photon displaces the mechanical oscillator. The magnitude of displacement depends on the ratio of the single photon coupling and the mechanical oscillator frequency, i.e. G_0/ω_m.

Before proceeding we need to define coherent states. A coherent state is an eigenstate of the annihilation operator and is defined as [32]

$$|\gamma\rangle = e^{-|\gamma|^2/2} \sum_{n=0}^{\infty} \frac{\gamma^n}{\sqrt{n!}} |n\rangle \tag{1.44}$$

It is also possible to define coherent states in term of the displacement operator

$$\hat{D}(\gamma) = exp(\gamma a^+ - \gamma^\star a) \tag{1.45}$$

In this case, the coherent state is defined as

$$|\gamma\rangle = D(\gamma)|0\rangle \tag{1.46}$$

We will use the second definition of the coherent states in Chapter 5.

As a result of optomechanical interaction, the tiny mirror is now in a superposition of the ground state and a coherent state whose amplitude is proportional to G_0/ω_m. The state of the system at time t is given by [33, 8]

$$|\psi(t)\rangle = \frac{1}{\sqrt{2}}(|0\rangle_A|1\rangle_B|0\rangle_m + e^{i\phi}|1\rangle_A|0\rangle_B|(\frac{G_0}{\omega_m})(1-\cos\omega_m t)\rangle_m) \tag{1.47}$$

where $\phi = (\frac{G_0}{\omega_m})^2(\omega_m t - sin\omega_m t)$. Using Eq. (1.47) one can calculate the interference visibility seen by the two single photon detectors $D1$ and $D2$, see Fig. (1.4). The expression for the visibility is given by

$$v(t) = \frac{1}{2}\exp[-(\frac{G_0}{\omega_m})^2\{1-\cos(\omega_m t)\}] \tag{1.48}$$

One sees that this expression reaches its minimum for $t = \pi/\omega_m$, which corresponds to the maximum displacement of the mirror. This can be understood intuitively in term of the distinguishability of the two paths. The important feature of the visibility is its periodicity, which can be seen in Fig. (1.5). This periodicity is the main feature which differentiates EID from other collapse models.

In the realistic case where the mirror is not exactly in the ground state due to the finite temperature of the surrounding environment, the visibility revival is not complete and the modified expression for the visibility is given by [8]

$$v(t) = \frac{1}{2}\exp[-(\frac{G_0}{\omega_m})^2(2\bar{n}+1)\{1-\cos\omega_m t\}] \tag{1.49}$$

The effect of finite temperature is the narrowing of the revival peaks by a factor of $\sqrt{\bar{n}}$. This can be seen by noting that $1-\cos(\omega_m t) = 2\sin^2(\omega_m t/2) \sim (\omega_m t)^2/2$ for small t in (1.49). The experimental requirements to realize the aforementioned proposal are the following. First the system needs to be in the resolved sideband regime to ensure the ground state cooling. Second, the single photon optomechanical coupling must be comparable to the mechanical frequency. This condition guarantees that the displacement of the mechanical oscillator due to the optomechanical interaction, which is proportional to G_0/ω_m (see Eq. (1.47)), is discernible. Third, the single photon must remain in cavity long enough to interact with the oscillator before leaking from the cavity. All these requirements have been met individually but it is still

challenging to satisfy all of them simultaneously. In Chapter 5 we will present a new scheme building on the Marshall et.al[8] proposal which alleviates some of these difficulties.

Chapter 2

Quantum Optomechanics in the Bistable Regime

This chapter is based on [34]. In this chapter we study the simplest optomechanical system, with a focus on the bistable regime. The covariance matrix formalism allows us to study both cooling and entanglement in a unified framework. We identify two key factors governing entanglement, namely the bistability parameter, i.e. the distance from the end of a stable branch in the bistable regime, and the effective detuning, and we describe the optimum regime where entanglement is greatest. We also show that in general entanglement is a non-monotonic function of optomechanical coupling. This is especially important in understanding the optomechanical entanglement of the second stable branch.

2.1 Introduction

Observing quantum effects like superposition states or entanglement at the macroscopic level is a long standing goal. It is a widely held view that this should be possible, provided that enviromentally induced decoherence can be sufficiently suppressed. Note however that there are some theoretical proposals which would rule out the existence of quantum effects at the macroscopic level, see e.g. Ref. [35]. Proposals for the experimental observation of macroscopic quantum effects are often based on the principle of Schrodinger's cat, i.e. on coupling a microscopic quantum system to a macroscopic system in a controlled way, in order to create a macroscopic superposition state [36, 22, 8].

One particularly promising approach in this context is the use of optomechanical systems. The most basic optomechanical system consists of a Fabry-Perot cavity with one movable end mirror. The position of this mirror is determined by the radiation pressure inside the cavity.

Such systems were first studied in the context of high precision measurements and gravitational wave detection [9]. It was suggested in Ref. [22] that the radiation pressure of a single photon in a high finesse optical cavity could in principle create a macroscopic superposition of two spatially distinct locations of a moveable mirror. A potential implementation of this idea was proposed in Ref. [8]. It is very challenging experimentally to achieve sufficiently strong optomechanical coupling at the single-photon level, requiring a system that combines high optical and mechanical finesse, low mechanical resonance frequency and ultra-low temperature.

One way to enhance the optomechanical interaction is to pump the cavity with a strong laser. Using this technique the strong coupling regime in optomechanical systems has recently been reached [3]. In the presence of a strong enough driving laser, the field enhancement inside the high finesse optical cavity is large enough to trigger nonlinear behaviour of the system. Depending on the input power and the detuning of the driving laser with respect to the cavity resonance, optomechanical systems exhibit different types of nonlinear behaviour. For strong enough input power, in the blue detuned regime one obtains multistability[37], instability [38] and chaotic motion [39]. In the red-detuned regime bistability [18, 40] occurs. Here we consider the red detuned regime. This is the appropriate regime for cooling the mechanical oscillator close to the ground state [41, 25], which is usually seen as a prerequisite for observing quantum effects. We are particularly interested in the relationship between bistability and entanglement.

Optomechanical bistability can be understood intuitively as the result of a competition between the mechanical restoring force, which increases linearly when the mirror is moved from its equilibrium position, and the radiation pressure force, which has a maximum at the cavity resonance. For a suitable set of parameters, as in Fig.(2.1), there are three intersection points between the two forces. The leftmost and rightmost intersection points correspond to stable states, because the restoring force grows faster than the radiation pressure (for the rightmost point the radiation pressure even decreases as the mirror is pushed outwards). In contrast, the

Figure 2.1: Mechanical restoring force and radiation pressure force around a cavity resonance. The leftmost and rightmost intersection points are stable equilibrium positions, whereas the middle one is unstable.

middle intersection point is unstable because the radiation pressure force increases faster than the restoring force.

It is known that the optomechanical interaction can squeeze the cavity mode, and this squeezing becomes maximal close to the bistable regime [42]. It has also been noted [43] that under certain conditions, entanglement is maximized at the bistability threshold. This was interpreted as being due to the enhanced optomechanical coupling strength in this region. Here we analyze entanglement close to and in the bistable regime in detail. We show that a lot of insight can be gained by analyzing the situation in terms of two key parameters, namely the effective detuning and the bistability parameter, which quantifies the distance from the end of each bistable branch. Cooling and entanglement can be studied in the same theoretical framework based on the covariance matrix. We identify the optimal regimes for both cooling and entanglement. We also show that, somewhat surprisingly, entanglement is in general a non-monotonic function of the optomechanical coupling strength. (Naively one might have expected it to always increase with optomechanical coupling strength.)

This chapter is organized as follows: Section 2.2 introduces the optomechanical system and

describes the linearization of the equations of motion around the steady state. We also show how bistability arises in the red-detuned regime in this framework, introduce the bistability parameter, and derive the dependence of the photon and phonon number on this parameter, which leads us to a discussion of cooling. Section 2.3 discusses the optomechanical entanglement and its dependence on the bistability parameter and the effective detuning. This allows us to determine the optimum value for the detuning and the maximum achievable entanglement in our system. We discuss the role of the optomechanical coupling constant, show how entanglement varies on both stable branches in the bistable regime, and discuss its robustness under increasing temperature.

2.2 The System

We consider a high-Q Fabry-Perot cavity with decay rate κ. The moveable mirror can move under the influence of radiation pressure and thermal noise. The moveable mirror is initially in equilibrium with a thermal bath at temperature T which results in a mechanical damping rate γ_m and a noise force $\xi(t)$. The system is driven by a laser with frequency ω_L and power P. The general Hamiltonian of such a system is derived in [19]. In the regime of parameters that we are interested in, the general Hamiltonian simplifies to [19, 1]

$$\hat{H} = \hbar\omega_c \hat{a}^\dagger \hat{a} + \frac{\hbar\omega_m}{2}(\hat{p}^2 + \hat{q}^2) - \hbar G_0 \hat{a}^\dagger \hat{a}\hat{q} + i\hbar E(\hat{a}^\dagger e^{-i\omega_L t} - \hat{a}e^{i\omega_L t}), \tag{2.1}$$

where ω_c and $\hat{a}$ are frequency and annihilation operator of the cavity mode,respectively, ω_m, q,p are the frequency and dimensionless position and momentum operators of the mirror,respectively, and $G_0 = \frac{\omega_c}{L}\sqrt{\frac{\hbar}{m\omega_m}}$ is the coupling constant and $E = \sqrt{\frac{2P\kappa}{\hbar\omega_L}}$, where P and ω_L are the input laser power and frequency respectively. The first two terms correspond to two free harmonic oscillators, the third term corresponds to the optomechanical coupling and the last term corresponds to the cavity being driven by the laser.

The Heisenberg-Langevin equations of motion [44] which include the effects of mechanical

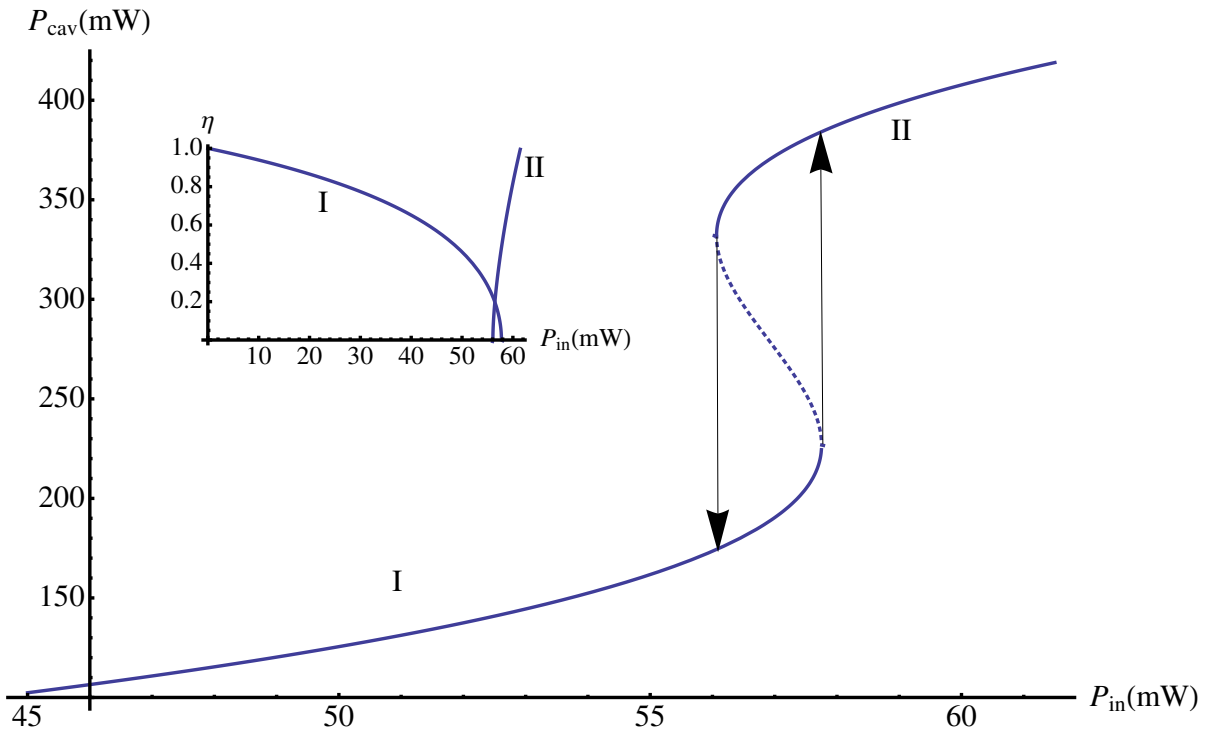

Figure 2.2: Bistability of the intracavity power with respect to the input power. The solid and dotted lines correspond to the stable and unstable branches respectively. The inset shows the bistability parameter η for the two stable branches. The end of each stable branch corresponds to $\eta = 0$.

and optical losses are

$$\dot{\hat{q}} = \omega_m \hat{p}, \tag{2.2}$$

$$\dot{\hat{p}} = -\omega_m \hat{q} - \gamma_m \hat{p} + G_0 \hat{a}^\dagger \hat{a} + \xi(t), \tag{2.3}$$

$$\dot{\hat{a}} = -(\kappa + i\Delta_0)\hat{a} + iG_0 \hat{a}\hat{q} + E + \sqrt{2\kappa}\hat{a}_{\text{in}}, \tag{2.4}$$

where $\Delta_0 = \omega_c - \omega_L$, $\hat{a}_{in}$ is the vacuum input noise of the cavity, and $\xi(t)$ is the noise associated with the damping of the mechanical oscillator [45]. The nonlinear Eqs. (2.3, 2.4) can be linearized by expanding the operators around their steady state values $\hat{O}_i = O_{i,s} + \delta\hat{O}_i$,where $\hat{O}_i = \hat{a}, \hat{q}, \hat{p}$.

From Eqs. (2.2, 2.3, 2.4), the steady-state solutions are $\alpha_s = \frac{E}{\kappa + i(\Delta_0 - G_0 q_s)}$, $q_s = \frac{G_0|\alpha_s|^2}{\omega_m}$, $p_s = 0$, where α_s, q_s and p_s are the stationary values for the cavity amplitude, position and

momentum of the mechanical oscillator respectively. The steady state solutions for cavity amplitude and mechanical oscillator displacement lead to a third order polynomial equation for α_s, which has three roots. The largest and the smallest roots are stable, and the middle one is unstable. Physically this means that the radiation pressure force is larger than the mechanical restoring force for the middle root and this make the system unstable, while for other two roots the restoring force is larger than the radiation pressure force, see also Fig. (2.1). Mathematically, for the smallest and largest roots, the size of the fluctuations does not grow as the system approach these points. This is not the case for the middle root. We will return to this point when we discuss the photon and phonon numbers, see Eqs. (2.16, 2.17). Fig. (2.2) shows the hysteresis loop for the intracavity power. Consider $P_{\rm cav}$ initially on the lower stable branch (I in Fig. (2.2), corresponding to the smallest root). As $P_{\rm in}$ increases past its value for the first turning point, $P_{\rm cav}$ switches to the upper stable branch (II in Fig. (2.2), corresponding to the largest root). For $P_{\rm in}$ larger than its value at this switch point , $P_{\rm cav}$ is given by the upper branch. As $P_{\rm in}$ decreases below this value $P_{\rm cav}$ is still given by the upper branch until $P_{\rm in}$ decreases below its value for the upper turning point. At this point $P_{\rm cav}$ switches back down to the lower branch. We have used the the set of parameters of Ref[1], which is close to several optomechanical experiments[12, 46, 47, 13]. We consider Fabry-Perot cavity with length $L = 1$mm and finesse $\mathscr{F} = 1.07 \times 10^4$, driven by a laser with $\lambda = 810$nm and $\Delta_0 = 2.62\omega_m$. The mechanical oscillator frequency ,damping rate and mass are 10MHz, 100Hz and 5ng respectively with environment temperature $T = 400$mK.

By introducing $\hat{u}^T(t) = (\delta\hat{q}(t), \delta\hat{p}(t), \hat{X(t)}, \hat{Y}(t))$ and $\hat{n}^T(t) = (0, \xi(t), \sqrt{2\kappa}\hat{X}_{\rm in}(t), \sqrt{2\kappa}\hat{Y}_{\rm in}(t))$ where $\hat{X} = \frac{\delta\hat{a}+\delta\hat{a}^\dagger}{\sqrt{2}}$ and $\hat{Y} = \frac{\delta\hat{a}-\delta\hat{a}^\dagger}{\sqrt{2}i}$ and corresponding noises $\hat{X}_{\rm in}$ and $\hat{Y}_{\rm in}$, the linearized dynamics of the system can be written in a compact form

$$\dot{\hat{u}}(t) = A\hat{u}(t) + \hat{n}(t), \tag{2.5}$$

where

$$A = \begin{pmatrix} 0 & \omega_m & 0 & 0 \\ -\omega_m & -\gamma_m & G & 0 \\ 0 & 0 & -\kappa & \Delta \\ G & 0 & -\Delta & -\kappa \end{pmatrix}, \tag{2.6}$$

and $G = \sqrt{2}G_0\alpha_s$, $\Delta = \Delta_0 - G_0 q_s$ are the enhanced optomechanical coupling rate and effective detuning. It is worth mentioning that A (2.6) is anti-Hermitian. This can be understood from the Schrodinger equation $\frac{d}{dt}|\psi\rangle = -\frac{i}{\hbar}\hat{H}|\psi\rangle$. Since the Hamiltonian $\hat{H}$ is Hermitian, $-i\hat{H}$ (which corresponds to A in Eq. (2.5) is anti-Hermitian.

One can obtain the effective optomechanical Hamiltonian, describing the interaction between the optical and mechanical fluctuations, from Eqs. (2.2, 2.6). To do so we neglect the damping and the noise term in Eq. (2.2, 2.6) and obtain

$$\hat{H}_{\text{eff}} = \hbar G \delta\hat{X}\, \delta\hat{q} \tag{2.7}$$

which is identical with Eq.(1.32) when rewritten in terms of the ladder operators.

The solution of Eq.(2.5) is given by

$$\hat{u}(t) = M(t)\hat{u}(0) + \int_0^t ds M(s)\hat{n}(t-s) \tag{2.8}$$

where $M(s) = e^{As}$. Since the initial state of the system is Gaussian and the dynamical equations are linear in the creation and annihilation operators for both the cavity and mechanical modes, the state of the system remains Gaussian at all times. A Gaussian state is fully characterized by its covariance matrix which is defined at any given time t by $V_{ij}(t) = \frac{\langle \hat{u}_i(t)\hat{u}_j(t) + \hat{u}_j(t)\hat{u}_i(t)\rangle}{2}$. Here we are interested in the steady-state solution for our system, which will be reached if all the eigenvalues of the matrix A have negative real parts. In the red detuned regime of operation ($\Delta > 0$), the Routh-Hurwitz criterion [48] gives stability condition

$$\omega_m(\kappa^2 + \Delta^2) - G^2\Delta > 0. \tag{2.9}$$

In the following we assume inequality 2.9 is valid.

From Eq.(2.8), we obtain the following expression for the covariance matrix

$$V_{ij} = \sum_{k,l} \int_0^\infty \int_0^\infty ds ds' M_{ik}(s) M_{jl}(s') \Phi_{kl}(s-s'), \tag{2.10}$$

where $\Phi_{kl}(s-s') = \frac{\langle n_k(s) n_l(s') + n_l(s') n_k(s) \rangle}{2}$.

The mechanical and optical input noise operators are fully characterized by their correlation functions which in the Markovian approximation are given by[1]

$$\langle \hat{a}_{in}(t) \hat{a}_{in}^\dagger(t') \rangle = \delta(t-t'). \tag{2.11}$$

$$\frac{\langle \xi(t)\xi(t') + \xi(t')\xi(t) \rangle}{2} = \gamma_m (2\bar{n}+1)\delta(t-t'). \tag{2.12}$$

where $\bar{n} = [exp(\frac{\hbar\omega_m}{k_B T}) - 1]^{-1}$ is the mean thermal phonon number and k_{B} is Boltzmann's constant. From Eqs.(2.11, 2.12), we have $\Phi_{kl}(s-s') = D_{kl}\delta(s-s')$ with $D = \mathrm{Diag}[0, \gamma_m(2\bar{n}+1), \kappa, \kappa]$ and Eq. (2.10) becomes $V = \int_0^\infty ds M(s) D M^T(s)$. When Eq. (2.9) is satisfied, one obtains the following equation for the steady-state covariance matrix,

$$AV + VA^T = -D. \tag{2.13}$$

In the following we use the dimensionless bistability parameter defined as [49]

$$\eta = 1 - \frac{G^2 \Delta}{\omega_m(\kappa^2 + \Delta^2)} \tag{2.14}$$

which is a positive number between zero and one according to Eq. (2.9) for $\Delta > 0$. We have shown the bistability parameter in the inset of Fig. (2.2). As can be seen from Fig.(2.2), η decreases when approaching the bistable regime and becomes equal to zero at the end of each stable branch.

The stability condition Eq. (2.9) can be intuitively understood by ignoring retardation effects for the radiation pressure. Assuming that the optical field adiabatically follows the mechanical oscillator (i.e. setting $\dot{\delta a} = 0$ in Eq. (2.4)), one has $\delta\hat{a} = \frac{1}{(\kappa + i\Delta)}(\frac{iG}{\sqrt{2}}\delta\hat{q} + \sqrt{2\kappa}\hat{a}_{\mathrm{in}})$.

Using this in Eq. (2.3) we obtain

$$\dot{\delta\hat{p}} = -(\omega_m - \frac{G^2\Delta}{\kappa^2+\Delta^2})\delta\hat{q} - \gamma_m\delta\hat{p} + \xi_T \tag{2.15}$$

where $\xi_T = \xi + G\sqrt{2\kappa}(\frac{a_{\rm in}}{\kappa+i\Delta} + \frac{a_{\rm in}^+}{\kappa-i\Delta})$. From Eq. (2.15) , we see that the mechanical oscillator is stable if the first coefficient is positive. In this case the first term in Eq. (2.15) corresponds to a harmonic restoring force, see also Fig. (2.1) and the associated discussion. This implies Eq. (2.9). The adiabatic approximation is equivalent to treating the response of the cavity field to the moving mirror as instantaneous. It is well known that the delayed nature of this response gives rise to cooling [11], which is however not essential for the above argument. We feel that this argument helps the physical understanding of the stability condition. However, let us emphasize that we will not make the adiabatic approximation in what follows.

In the bistable regime the fluctuations around the steady state solution diverge as one approaches the end of each stable branch. To show this explicitly we solve Eq.(2.13), from which we can obtain the phonon and photon numbers by using $\bar{n}_m = \frac{V_{11}+V_{22}-1}{2}$ and $\bar{n}_o = \frac{V_{33}+V_{44}-1}{2}$. The general solution is complicated and not very illuminating. Simple relations that show the dependence of the fluctuations on the stability parameter can be obtained by assuming a high mechanical quality factor and low temperature environment,i.e. $\frac{\omega_m}{\gamma_m} \gg 1$ and $\frac{\kappa}{\bar{n}\gamma_m} \gg 1$. We find

$$\bar{n}_m = \frac{(\Delta^2+\kappa^2)(1+\eta) - 2\eta\,\omega_m(2\Delta-\omega_m)}{8\Delta\eta\,\omega_m}. \tag{2.16}$$

$$\bar{n}_o = \frac{(1-\eta)(\kappa^2+\Delta^2)}{8\eta\Delta^2}. \tag{2.17}$$

From Eqs. (2.16 , 2.17), it is clear that the phonon and photon numbers diverge as η approaches zero. In order to stay within the range of validity of the linearization approximation, we have made sure that $\bar{n}_o \ll |\ \alpha_s\ |^2$ in all the results shown below.

For $\eta \sim 1$ from Eq. (2.16), the optimum value for the detuning which minimizes the phonon number is given by

$$\Delta_{\rm opt} = \sqrt{\kappa^2+\omega_m^2}. \tag{2.18}$$

Using this optimum in Eq. (13) one finds

$$\bar{n}_m = \frac{1}{2}\left(\frac{\sqrt{\kappa^2+\omega_m^2}}{\omega_m} - 1\right) \tag{2.19}$$

which is identical to Eq. (7) in [50] . In the resolved sideband regime ($\omega_m \gg \kappa$) one sees from Eq. (2.19) that ground state cooling can be achieved ($\bar{n}_m = \frac{\kappa^2}{4\omega_m^2}$) [51, 50]. As a final remark in this section, we remind the reader that the photon numbers given by Eq.(2.17) correspond to $\langle \delta a^\dagger \delta a \rangle$, not $\langle a^\dagger a \rangle$.

2.3 Optomechanical entanglement

As shown in [52], for bipartite Gaussian states the Peres- Horodecki criterion [53, 54] (positivity of the density matrix under partial transposition) is necessary and sufficient for separability. In terms of the covariance matrix formalism this criterion is called logarithmic negativity which is defined as [55]

$$E_N = max\{0, -\ln(2\nu_{\min})\}. \tag{2.20}$$

where $\nu_{\min}$ is the smallest symplectic eigenvalue of the partially transposed covariance matrix, given by $\nu_{\min} = \sqrt{\frac{\Sigma - \sqrt{\Sigma^2 - 4detV}}{2}}$, where $\Sigma = \det A + \det B - 2\det C$, and we represent the covariance matrix (which can be obtained from Eq.(2.13)) as

$$V = \begin{pmatrix} A & C \\ C^T & B \end{pmatrix}. \tag{2.21}$$

Equipped with this measure we go on to study optomechanical entanglement. By optomechanical entanglement we mean the entanglement between the fluctuations of the mechanical oscillator and the cavity field. Fig. (2.3 (a) shows the logarithmic negativity as a function of bistability parameter η and effective detuning Δ. We note that for $\eta \sim 1$, which is required for ground state cooling, there is no optomechanical entanglement. From Fig.(2.3 (a), one can identify three different regimes depending on the effective detuning. In the first regime, corresponding to $\Delta < 0.1\omega_m$ in the figure, there is no optomechanical entanglement. In the second

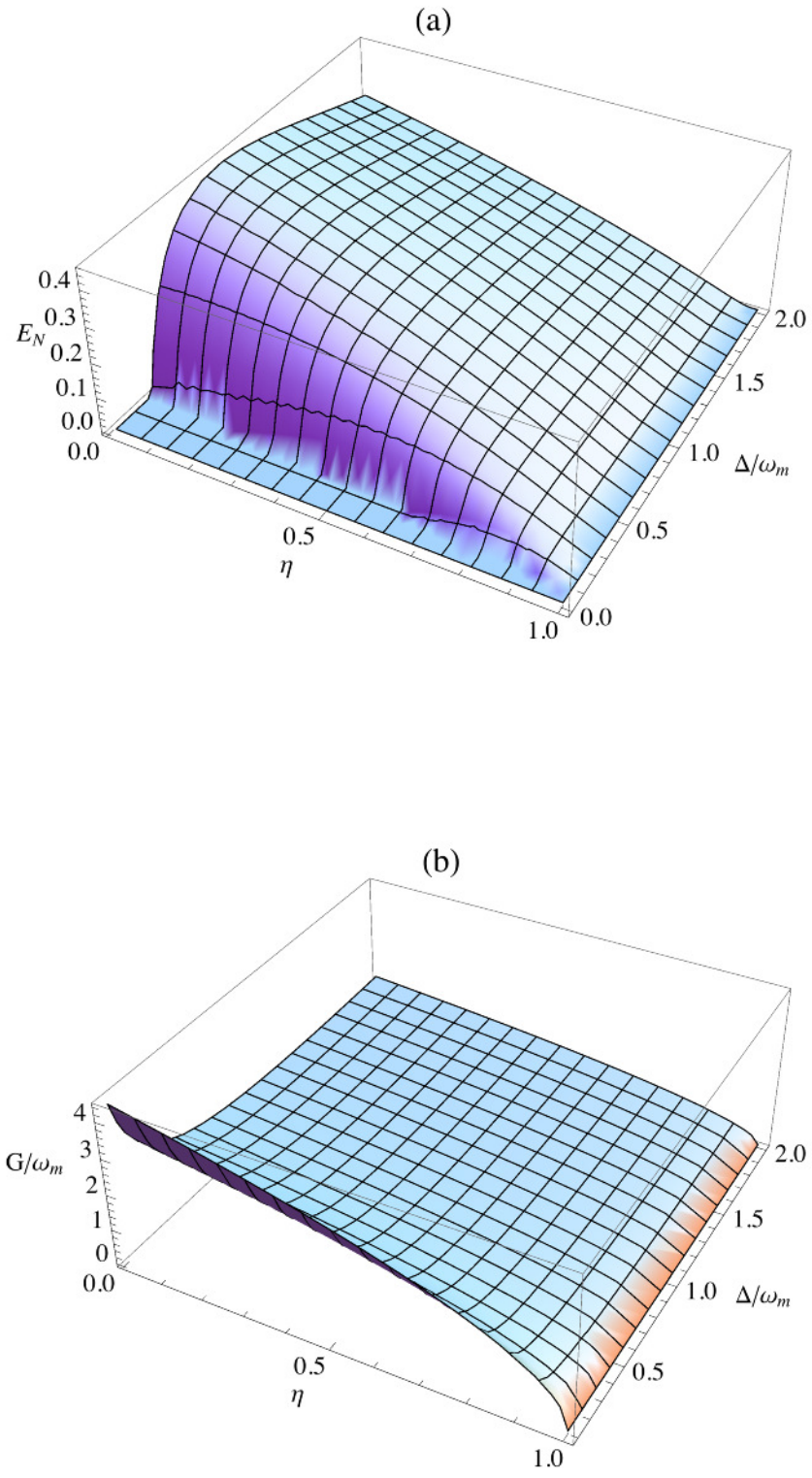

Figure 2.3: Optomechanical entanglement (a) and optomechanical coupling constant (b) as a function of bistability parameter η and normalized effective detuning $\frac{\Delta}{\omega_m}$, for a cavity decay rate $\kappa = 1.4\omega_m$.

regime, corresponding to $0.1\omega_m < \Delta < 0.3\omega_m$ in the figure, there is some optomechanical entanglement but the maximum value for entanglement is attained for values of the bistability parameter η somewhere between zero and one. This shows that for a fixed detuning, the maximum entanglement does not necessarily occur at the end of the bistable branch, (cf. [43]). Finally in the third regime, $\Delta > 0.3\omega_m$ in the figure, there is strong optomechanical entanglement, and for each fixed value of detuning the maximum entanglement is in fact reached at the end of the branch, i.e. for $\eta = 0$. So in short we have $E_{N,1} < E_{N,2} < E_{N,3}$,where $E_{N,i}$ is the logarithmic negativity in the i-th regime.

Fig.(2.3) (b) shows the corresponding optomechanical coupling in the different regimes. From Fig.(2.3) (b) it is clear that the optomechanical coupling is a monotonically decreasing function of effective detuning, i.e $G_1 > G_2 > G_3$ where G_i is the optomechanical coupling constant in the i-th regime. So we see that in general entanglement is not a monotonically increasing function of the coupling constant. These observations suggest that the key variables that determine the entanglement behaviour are the effective detuning and the bistability parameter, not the optomechanical coupling constant. A more quantitative understanding of the different regimes for entanglement is possible by looking at the entanglement behaviour in the vicinity of $\eta = 0$. Assuming that $\frac{\omega_m}{\gamma_m} \gg 1$ and $\frac{\kappa}{\bar{n}\gamma_m} \gg 1$ one finds $\Sigma = a + \frac{b}{\eta}$ and $\det V = c + \frac{d}{\eta}$, where

$$a = \frac{\Delta^2 - 3\kappa^2 + \omega_m^2}{16\Delta^2}, \tag{2.22}$$

$$b = \frac{(\Delta^2 + \kappa^2)(\Delta^2 + \kappa^2 + 5\omega_m^2)}{16\Delta^2\omega_m^2}, \tag{2.23}$$

$$c = \frac{2\Delta^2(\Delta^2 + \kappa^2) + (\Delta^2 - \kappa^2)\omega_m^2}{128\Delta^4}, \tag{2.24}$$

$$d = \frac{(\Delta^2+\kappa^2)(4\Delta^4+4\Delta^2\kappa^2+4\Delta^2\omega_m^2+\omega_m^4)}{256\Delta^4\omega_m^2}, \tag{2.25}$$

We get these expressions by simplifying the solution of Eq. (2.13) using the Mathematica software package. From these equations it is possible to derive a simple form for the logarithmic negativity. Close to the bistability region ($\eta \ll 1$) we have $E_N = \max\{0, \alpha+\beta\eta\}$ where $\alpha = -\ln(2\sqrt{\frac{d}{b}})$ and $\beta = \frac{(abd-b^2c-d^2)}{2db^2}$.

It is worth noting that in contrast to the phonon and photon numbers, which diverge for $\eta = 0$, the logarithmic negativity has a finite limiting value given by α. While our linearization approximation is not justified for the point $\eta = 0$ itself, it does apply in its close vicinity, as the photon number drops precipitously as one moves away from the end point of the stable branch, Eq. (2.17).

Using our expression for the entanglement close to bistability one can easily identify the three regimes shown in Fig. (2.3). The first regime corresponds to $\alpha, \beta < 0$. The second regime corresponds to $\alpha < 0, \beta > 0$ or $\alpha, \beta > 0$ and the third region corresponds to $\alpha > 0, \beta < 0$.

Moreover, as can be seen from Fig. (2.3), the maximum optomechanical entanglement is reached in the bistability region (for η approaching 0) in the third regime. So the maximum achievable optomechanical entanglement is given by α. From Eqs. (2.22 , 2.25) the optimum value for effective detuning where entanglement takes its maximum value is

$$\Delta_{\text{opt}} = \frac{\omega_m}{4}\sqrt{1+\sqrt{16(\frac{\kappa}{\omega_m})^2+81}} \tag{2.26}$$

For $\kappa = 1.4\omega_m$ from Eq.(2.26) we obtain $\Delta_{\text{opt}} = 0.85\omega_m$. Comparing this to Eq. (2.18) one sees that the optimum effective detuning values for cooling and entanglement are not the same. Even more importantly, the cooling performance is optimized for $\eta = 1$, whereas entanglement becomes maximal for $\eta = 0$. Using the optimum value for detuning we obtain the following

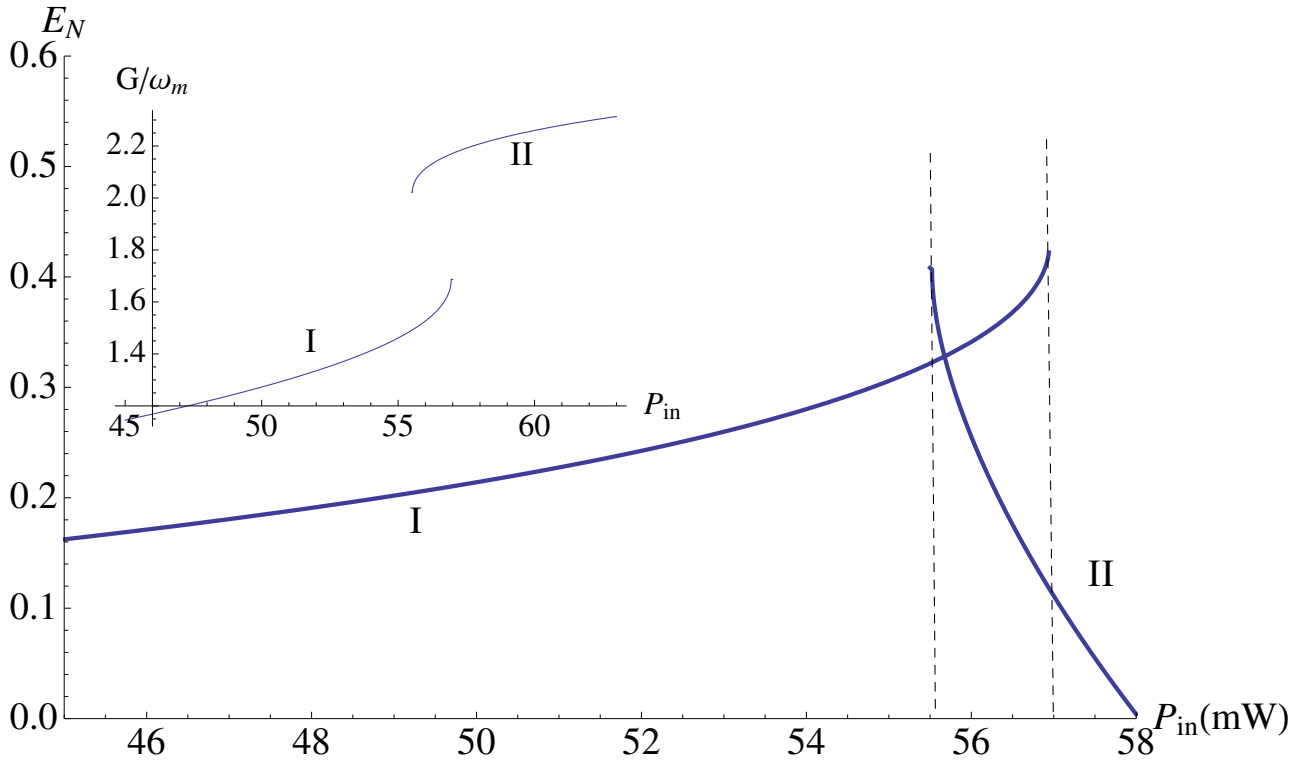

Figure 2.4: Plot of the optomechanical entanglement as a function of input power for both stable branches. The dot dashed (dashed) line corresponds to the end of the first (second) stable branch. The parameters are the same as in Fig. (2.2).

expression for maximum achievable entanglement in our system

$$E_{N,\max} = -\ln\left[\frac{1}{5}\sqrt{9+\frac{128\kappa^2}{8\kappa^2+45\omega_m^2}}\right]. \tag{2.27}$$

Note that this takes its greatest possible value for $\kappa = 0$, giving $E_{N,\max} = -\ln[3/5] = 0.51$.

It is also interesting to look at the optomechanical entanglement for the two stable branches and their behaviour in the bistable regime. Fig. (2.4) shows the logarithmic negativity as a function of the input power for both stable branches. Varying the input power corresponds to varying η, cf. Fig. (2.2). We note the persistence of entanglement in the second stable state in a very narrow window of parameter space. As can be seen in Fig. (2.4) the entanglement is maximum at the end of each branch, corresponding to the third regime. The fast decreasing entanglement for the second branch is in agreement with the bistability parameter behaviour in Fig. (2.2). The inset shows the optomechanical coupling for different stable branches. One sees clearly that the coupling constant is not the decisive parameter for the amount of entanglement in our system, and in particular that the entanglement is a non-monotonic function of the coupling constant.

Until now we studied the entanglement in terms of parameters that are natural to use from a theoretical point of view. It is also interesting to look at entanglement in terms of parameters that can be directly controlled experimentally. Fig. (2.5) shows the bistability parameter and entanglement as a function of bare detuning Δ_0 and laser power P. Note that as we come close to the end of the branch for suitable detuning and large enough input power the entanglement increases.

We have also studied the robustness of entanglement with respect to the temperature. The result is shown in Fig. (2.6). One sees that for higher temperatures the entanglement survives only in the vicinity of the bistable region. Finally we note that in the recent experiment [3], the ratio of the input power to the critical power (the input power for which the bistability happen) is about 0.5. So the bistable regime should definitely be accessible experimentally.

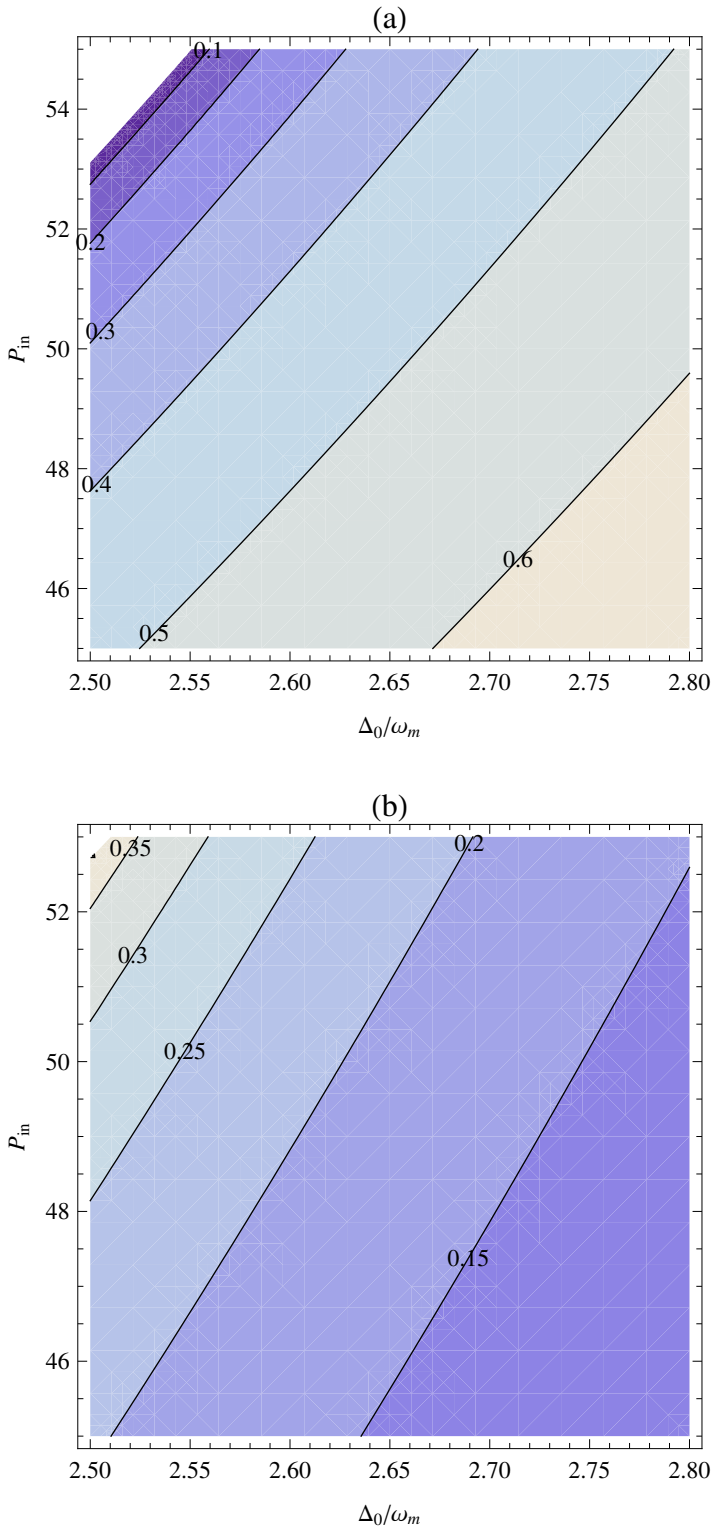

Figure 2.5: Contour plot for bistability parameter (a) and entanglement (b) versus bare detuning Δ_0 and input power P_{in} in mW. The parameters are the same as in Fig. 2

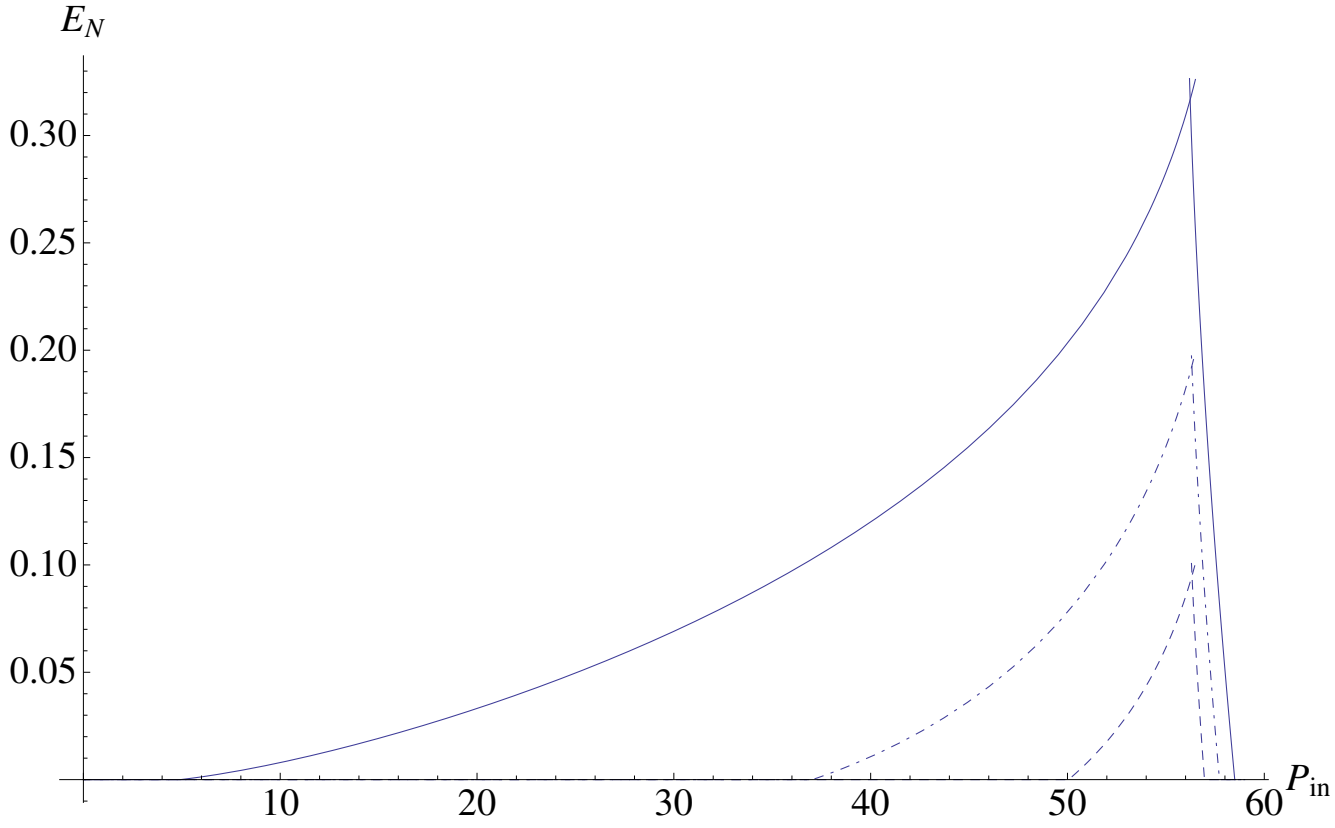

Figure 2.6: Plot of the logarithmic negativity versus the input power for different environment temperatures, $T = 0.4K$ (solid line), $T = 5K$ (dot dashed), and $T = 10K$ (dashed). The other parameters are the same as in Fig. (2.2).

2.4 Conclusion

We have studied the simplest optomechanical system using the covariance matrix formalism with a special emphasis on bistability. We recovered the standard results on optomechanical cooling as a special case of our general expression for the phonon number. However, our focus was on entanglement. We identified two key parameters, namely the effective detuning and the bistability parameter (i.e. the distance from the end of each stable branch in the bistable regime), and we showed that there are different regimes for entanglement as a function of these parameters. In particular we showed that maximum entanglement is achieved when the system is simultaneously close to the red sideband (in terms of effective detuning) and close to the end of each stable branch (bistability parameter close to zero). We also showed that the dependence of entanglement on the optomechanical coupling is counterintuitive, and that in the bistable regime the entanglement is particularly robust with respect to temperature increases.

It would be very interesting to see experimental explorations of the phenomena described in the present chapter. However, it should be noted that measuring the covariance matrix, which lies at the heart of our analysis, requires direct access to the position and momentum variables of the mirror, not just the quadratures of the light. It seems that this would require either an auxiliary measurement cavity, as proposed in Ref. [1], or at least an additional laser beam. A detailed analysis of the resulting more complex dynamics is work for the future. In this Chapter we focused on the entanglement characteristics of the basic system, which are already quite rich and intriguing.

Chapter 3

Optomechanical Entanglement in the Presence of Laser Phase Noise

This chapter is based on [56]. We study the simplest optomechanical system in the presence of laser phase noise (LPN) using the covariance matrix formalism. We show that for any LPN model with a finite correlation time, the destructive effect of the phase noise is especially strong in the bistable regime. This explains why ground state cooling is still possible in the presence of phase noise, as it happens far away from the bistable regime. We also show that the optomechanical entanglement is strongly affected by phase noise.

In Chapter 2 we studied optomechanical cooling (see Eq.(2.16)) and entanglement. In our model we considered both mechanical and optical damping. For realistic values for these decoherence channels, we showed that the mirror motion and the cavity field become quantum mechanically correlated or entangled. We also discussed the dependence of the optomechanical entanglement on the optomechanical coupling and the bistability parameter. We showed that the optomechanical entanglement is especially strong in the bistable regime. In contrast, ground state cooling of the mechanical oscillator happens when the system is far from the bistability threshold. In this Chapter we considered another decoherence channel, which is associated with the phase noise of the input laser.

As we have shown in Chapter 2 by using the cavity with the laser light, the optomechanical interaction was enhanced by factor proportional to the amplitude of the steady-state cavity field. This enhancement is highly desirable as the single photon optomechanical coupling constant is very weak compared to the decoherence channels in the problem. To reduce environmentally induced decoherence one has to cool the mechanical oscillator close to its ground state. For

typical optomechanical systems with the mechanical frequency in the range of MHz, cryogenic cooling is not sufficient to reach the quantum regime. To further cool the mechanical resonator one can use side band laser cooling by a red detuned laser [50, 51]. The laser serves both to cool the mechanical oscillator and to enhance the optomechanical coupling constant. This technique has been used to reach the strong coupling regime [3]. But the price to be paid is that a new source of noise is introduced into the system, namely laser phase noise (LPN).

The conclusion of early studies of the effect of LPN [57], based on modeling it as white noise, suggested that with the current level of LPN ground state cooling is impossible. This is in contrast with several experiments in which low phonon numbers have been observed. This discrepancy has been addressed in Ref. [58] by considering a more realistic model for the LPN.

Here we consider the effect of LPN on optomechanical entanglement. It turns out that optomechanical entanglement is very sensitive to this additional source of noise particularly in the bistable regime, where the maximum entanglement is achieved in the absence of noise [49, 34]. We show that in this regime the LPN is the main decoherence channel.

The chapter is organized as follows: In Section 3.1 we obtain the governing equations in the presence of LPN. In Section 3.2 we introduce the LPN model. Section 3.3 discusses optomechanical cooling. We recover the well-known effect of LPN on the ground state cooling as a special case of our general results. Section3.4 discusses the optomechanical entanglement in the presence of LPN. Section 3.5 is a summary and conclusion.

3.1 The System

Our system is a high finesse Fabry-Perot cavity with one tiny end mirror. This mirror can move under the influence of the radiation pressure inside the cavity and at the same time undergoes Brownian motion as a result of its interaction with the environment. The system is driven by a laser with frequency ω_L and power P. The Hamiltonian of the system is given by $H = H_0 + H_{int}$

where

$$\hat{H}_0 = \hbar\omega_c \hat{a}^\dagger \hat{a} + \frac{\hbar\omega_m}{2}(\hat{q}^2 + \hat{p}^2), \tag{3.1}$$

$$\hat{H}_{\rm int} = \hbar G_0 \hat{a}^\dagger \hat{a}\hat{q} + i\hbar E(\hat{a}^\dagger e^{-i\omega_L t} e^{-i\varphi(t)} - \hat{a} e^{i\omega_L t} e^{i\varphi(t)}), \tag{3.2}$$

where Eq. (3.1) describes the free Hamiltonian of the cavity mode and mechanical oscillator, ω_c and $\hat{a}$ are the frequency and annihilation operator of the cavity mode; and ω_m, $\hat{q}$, and $\hat{p}$ are frequency and dimensionless position and momentum operators of the mirror. The first term in Eq. (3.2) describes the optomechanical interaction, in which $G_0 = \frac{\omega_c}{L}\sqrt{\frac{\hbar}{m\omega_m}}$ is the single photon coupling constant. The second term in Eq. (3.2) describes the cavity pumping with a laser whose phase variation in time is given by $\varphi(t)$, $E = \sqrt{\frac{2P\kappa}{\hbar\omega_L}}$, where κ is the cavity damping rate. In the frame corresponding to a time-dependent phase $\omega_L t + \varphi(t)$, the equations of motion in the presence of damping and noise are

$$\dot{\hat{q}} = \omega_m \hat{p}, \tag{3.3}$$

$$\dot{\hat{p}} = -\omega_m \hat{q} - \gamma_m \hat{p} + G_0 \hat{a}^\dagger \hat{a} + \xi(t), \tag{3.4}$$

$$\dot{\hat{a}} = -(\kappa + i\Delta_0)\hat{a} + i\hat{a}\dot{\varphi} + iG_0 \hat{a}\hat{q} + E + \sqrt{2\kappa}\hat{a}_{\rm in}(t), \tag{3.5}$$

where $\hat{a}_{\rm in}$ and $\xi(t)$ are the optical and mechanical input noise operators respectively, and $\Delta_0 = \omega_c - \omega_L$. One notes that the laser phase noise modifies the equation of motion of the cavity field, see also Eq.(2.4). Now we follow the same procedure as in Chapter 2 to obtain the linearized equations of motion of the system by expanding the operators around their steady state values. This leads to the same equation as in Eq.(2.5, 2.6) with the modified noise vector given by

$$\hat{n}^T = (0, \xi(t), \sqrt{2\kappa}\hat{X}_{in}, \sqrt{2\kappa}\hat{Y}_{in} + \sqrt{2}\alpha_s\dot{\varphi}). \tag{3.6}$$

The steady state covariance matrix is still given by Eq. (2.13) with the matrix element of D given by

$$D_{ij} = \frac{1}{2}\int_0^\infty ds(M_{ik}(s)\langle\{\hat{n}_k(s),\hat{n}_j(0)\}\rangle + M_{jk}(s)\langle\{\hat{n}_i(0),\hat{n}_k(s)\}\rangle), \tag{3.7}$$

Using Eq. (3.6), we get $D = \mathrm{Diag}[0, \gamma_m(2\bar{n}+1), \kappa, \kappa+N]$, where

$$N = \alpha_s^2 \int_0^\infty ds M_{44}(s)\langle\dot{\varphi}(s)\dot{\varphi}(0)\rangle, \tag{3.8}$$

with $M_{44}(s) = \langle 4|e^{As}|4\rangle$ and $|4\rangle^T = (0,0,0,1)^T$.

Using Eq. (2.13) with the modified matrix D and Eq. (3.8), the effect of arbitrary LPN on the behaviour of the optomechanical system can be analyzed.

3.2 The Noise Model

The dynamics of the phase for an ideal single-mode laser far above lasing threshold is given by [59, 60]

$$\ddot{\varphi} + \gamma_c\dot{\varphi} = \xi_{\dot{\varphi}}(t), \tag{3.9}$$

where $\xi_{\dot{\varphi}}(t)$ is a Gaussian random variable obeying[59]

$$\langle\xi_{\dot{\varphi}}(t)\xi_{\dot{\varphi}}(t')\rangle = 2\gamma_c^2\Gamma_L\delta(t-t'). \tag{3.10}$$

Here, Γ_L and γ_c^{-1} describe the laser linewidth and finite correlation time of the phase noise. By taking the Fourier transform of Eq.(3.9) and using Eq.(3.10), we obtain the phase noise spectrum as

$$S_{\dot{\varphi}}(\omega) = \langle\dot{\varphi}(\omega)\dot{\varphi}(\omega)\rangle = \frac{2\Gamma_L}{1+\frac{\omega^2}{\gamma_c^2}}, \tag{3.11}$$

Note that as $\gamma_c \to \infty$, one recovers the white noise case. For a finite correlation time and $\omega \geq \gamma_c$, the power spectrum of the LPN is greatly reduced. This means that a white noise model may result in an overestimation of the LPN effects. From Eq. (3.11) and by applying the Wiener-Khinchin theorem [61], we find

$$\langle \dot{\varphi}(s)\dot{\varphi}(0)\rangle = \int_{-\infty}^{\infty} \langle \dot{\varphi}(\omega)\dot{\varphi}(\omega)\rangle e^{i\omega s} d\omega = 2\gamma_c^2 \Gamma_L e^{-\gamma_c s}. \tag{3.12}$$

Using Eq. (3.12) in Eq. (3.8) we obtain

$$N = 2\alpha_s^2 \gamma_c \Gamma_L \int_0^{\infty} ds M_{44}(s) e^{-\gamma_c s}. \tag{3.13}$$

The general expression for N is very complicated and will not be included here. However, inspection of Eq. (3.13) allows us to gain a good qualitative understanding of the behavior of N. Recall that $M_{44}(s)$ is one of the elements of the matrix $M(s) = \exp(As)$. Far from the bistable regime, all eigenvalues of A are significantly smaller than zero, and all elements of $M(s)$ decay with s, effectively limiting the range of the integral in Eq. (3.13). However, as one approaches the bistable regime, one of the eigenvalues of A approaches zero, and the range of the integral increases until it is limited only by the exponential $e^{-\gamma_c s}$. One thus expects N to take its maximum values in the bistable regime.

In Fig. (3.1), we show N/κ as a function of the effective detuning for two different laser linewidths. We choose the same parameters as in [1], which are close to some experiments [12, 46, 47]. One can see both from Eq. (3.11) and from Fig.(3.1) that the noise is proportional to the laser bandwidth Γ_L. The main message of Fig. (3.1) is that N/κ is maximal for $\eta \sim 0$, in agreement with the above simple argument. Close to the bistability threshold N can be much greater than κ for realistic values of Γ_L. In contrast, the inset of Fig. (3.1) shows N/κ and η far away from the bistable region. One sees that in this region the effect of the LPN is negligible for the set of parameters we used here.

Before proceeding, we would like to emphasize that the above argument is not restricted to the specific LPN model used here. In fact our argument is based on the behaviour of $M_{44}(s)$, which is independent of the LPN model. As long as the system admits a stationary solution (this guarantees that $M_{44}(s)$ is a monotonously decreasing function of s), the above argument

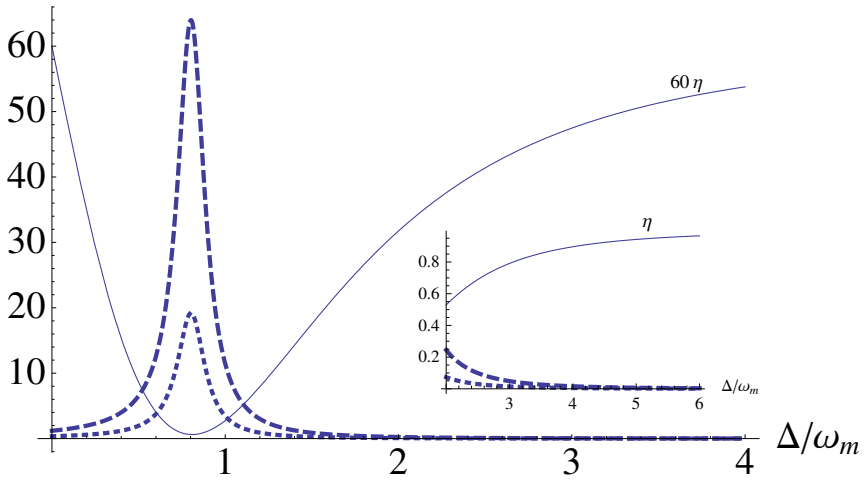

Figure 3.1: Plot of N/κ and η as a function of effective detuning. We consider a Fabry-Perot cavity with length $L = 1$mm, and finesse $F = 10700$, driven by a laser with $\lambda = 810$nm and input power 50mW and $\gamma_c = 10^4$Hz. The mechanical oscillator frequency ω_m, damping rate γ_m, mass m and temperature T are 10MHz, 100Hz, $5ng$ and $0.4K$ respectively. The solid line corresponds to η (multiplied by 60 to be comparable with N/κ). The dashed and dotted curves correspond to $\Gamma_L = 100$ Hz and 30 Hz respectively. The inset shows N/κ and η far away from the bistable region.

is valid for any LPN model with a finite correlation time.

3.3 Optomechanical Cooling

For completeness, in this Section we study optomechanical cooling in the presence of the LPN. From Eq. (2.13) one can obtain the phonon number as $\bar{n}_m = \frac{1}{2}\langle \delta q^2 + \delta p^2 - 1\rangle = \frac{V_{11}+V_{22}-1}{2}$. The quantum limit of the phonon number can be derived by assuming a high mechanical quality factor ($\frac{\omega_m}{\gamma_m} \gg 1$) and low temperature environment ($\frac{\kappa}{\bar{n}\gamma_m} \gg 1$). For $\eta \sim 1$, $\kappa \ll \omega_m$ and $\Delta = \omega_m$, we find

$$\bar{n}_m = \frac{\kappa^2}{4\omega_m^2} + \frac{N}{4\kappa}, \tag{3.14}$$

with

$$N = \frac{2\alpha_s^2 \Gamma_L \gamma_c(\gamma_c + \kappa)}{\omega_m^2 + (\gamma_c + \kappa)^2}. \tag{3.15}$$

For $\omega_m \gg \gamma_c \gg \kappa$ we find

$$\bar{n}_m = \frac{\kappa^2}{4\omega_m^2} + \frac{\alpha_s^2}{2\kappa} S_{\dot{\phi}}(\omega_m), \tag{3.16}$$

which coincides with Eq. (23) in Ref. [58] by adding the effect of the residual thermal occupation due to the mechanical thermal bath. From Eq. (3.11) and Eq. (3.14) it is not difficult to observe that as long as $\omega_m \gg \gamma_c$, the LPN effect on ground state cooling can be small. For $\gamma_c \ll \kappa \ll \omega_m$ by using Eq. (3.15) the second term in Eq. (3.14) becomes $\frac{\alpha_s^2}{2\gamma_c} S_{\dot{\phi}}(\omega_m)$. Intuitively the possibility of ground state cooling in the presence of LPN can be understood as a result of the fact that ground state cooling happens around $\eta \sim 1$, far from the bistability regime, and thus in a region where the effect of LPN is small. See also the discussion of the ground state cooling from the point of view of the bistability parameter in Ref. [56].

As a concluding remark on this section, we would like to note that in [3] the observed phonon number was in agreement with the prediction of optomechanical cooling theory with a noiseless laser.

3.4 Optomechanical Entanglement

In Chapter 2 we studied the optomechanical entanglement for an ideal input laser. There we showed that the optimum regime, in which the optomechanical entanglement is maximum is $\Delta \sim 0.85\omega_m$ and $\eta \sim 0$. We also showed that the maximum value for optomechanical entanglement is equal to 0.51 in the bistable regime for $\kappa \ll \omega_m$, see Eq. (2.27). In this section we consider the effect of LPN on the optomechanical entanglement.

Fig. (3.2) shows the entanglement as a function of the bistability parameter and the detuning for two different laser linewidths. In the absence of phase noise, entanglement is maximal in the bistable regime (i.e. at $\eta \sim 0$). However, it changes dramatically when the laser linewidth is non-zero. For the parameters we used here, the entanglement goes to zero in the bistable region for a linewidth as small as $\Gamma_L = 10$ Hz. For $\Gamma_L = 100$ Hz, only a small amount of entanglement

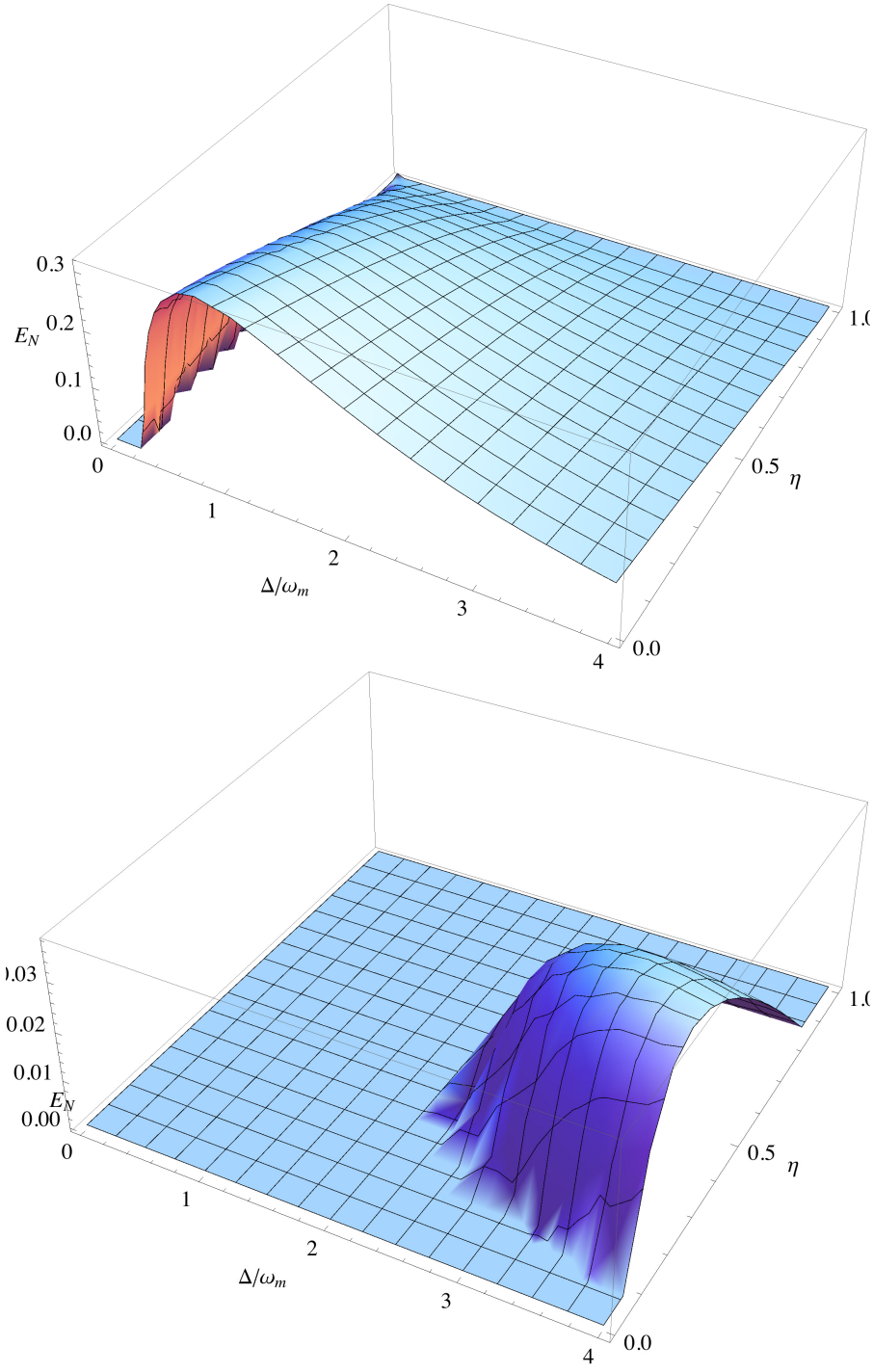

Figure 3.2: Optomechanical entanglement as a function of the bistability parameter η and the normalized detuning Δ/ω_m for two different laser linewidths, Γ_L, from top to bottom, $\Gamma_L = 0$ and 100 Hz. The other parameters are the same as in Fig. (3.1).

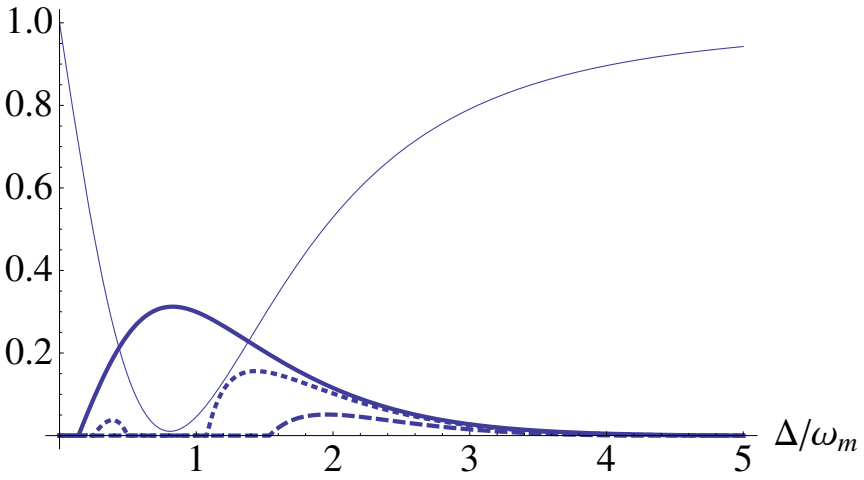

Figure 3.3: Plot of the bistability parameter (thin line) and the optomechanical entanglement for different values of laser linewidth. The solid, dotted and dashed lines correspond to $\Gamma_L = 0, 10, 50Hz$. The other parameters are the same as for Fig.(3.1).

survives , and the region of maximum entanglement is relatively far from the line $\eta = 0$. It is noticeable that for the $\Gamma_L = 100$ Hz entanglement survives only for $\Delta/\omega_m > 2$. This can be understood from Fig.(3.1), because the noise term N becomes very small for these values of the detuning.

Since we used the parameter values of Ref. [1], it is interesting to see how their results change in the presence of the LPN. Figure (3.3) shows the bistability parameter and optomechanical entanglement as a function of normalized detuning for different laser linewidths. First of all, we note that without LPN the maximum value for the entanglement happens at $\eta \simeq 0$. For a laser linewidth as small as 10Hz the maximum value for entanglement is no longer achievable. This can be understood as a result of the strong effect of the LPN in this region. One notes that the region of non-zero entanglement splits into two parts. For larger values of the laser linewidth the maximum entanglement decreases, and the maximum is achieved far from the bistability threshold, as we have seen before.

To experimentally measure the optomechanical entanglement, we need to access both mechanical and optical information. This can be done by using an auxiliary cavity [1] or an

additional laser beam. Our results show that the maximum achievable entanglement in the bistable regime is not accessible in the presence of the LPN. In order to protect the optomechanical system from the LPN one has to work at $\eta \sim 1$. One possible approach is the one proposed in Ref. [62], where the mechanical oscillator is first cooled close to its ground state (which happens for $\eta \sim 1$), then the detuning is switched to blue, which brings the two-mode squeezing part of the Hamitonian into resonance, leading to the generation of entanglement.

3.5 Conclusion

In summary, we studied a generic optomechanical system under realistic conditions, taking into account the effect of the input laser bandwidth. We found that the LPN contribution to the decoherence, characterized by N, is significant in the bistable regime ($\eta \sim 0$), and significantly suppressed elsewhere. This explains why ground state cooling is still possible, as it happens for $\eta \sim 1$. In contrast, optomechanical entanglement in the absence of LPN is maximal in the bistable regime. As a consequence, both the optimum region for the observation of entanglement and the amount of entanglement that can be achieved are strongly affected by LPN. In this chapter we discussed the drawback of using lasers in optomechanical systems. In the next Chapter we discuss a method for observing the optomechanical system with out using the pumping laser.

Note added. When this work was completed, we became aware of a recent related paper[63]. In comparison, the authors of that paper use a different noise model, and they treat the laser phase and amplitude as additional dynamical variables. In contrast we keep the number of dynamical variables fixed and treat the LPN via an additional term in the diffusion matrix, see Eq. (3.8). Finally, we would like to emphasize that our main results are not restricted to a specific LPN model, but are valid for any LPN model with a finite correlation time.

Chapter 4

Optomechanical Superpositions via Nested Interferometry

This chapter is based on [24, 64]. My contribution in this part was the idea of using post-selection to enhance the optomechanical coupling at the single photon level. I also studied the effect of a finite temperature on the proposed scheme here.

Optomechanical systems have been proposed as a method of achieving quantum superposition in mesoscopic systems [22, 8, 1]. However, such proposals impose several demanding experimental requirements, namely: a sideband-resolved cavity for ground state cooling [65, 50, 51, 25, 26, 66], a coupling rate faster than the mechanical frequency in order to displace the mechanical state by more than its zero point fluctuation [8, 65], and strong optomechanical coupling to ensure photons remain in the cavity long enough to produce quantum effects [8, 14, 3]. In practice, many of these requirements can be met individually, but they are extremely difficult to meet simultaneously. For instance, a recent result on diffraction-limited cavities [67] has identified restrictions on achievable optical finesse in cavities with one micromirror end.

One approach to this challenge is to use coherent pumping to reach strong coupling in a device that would otherwise be weakly coupled [1, 14, 3, 68, 69, 70]. This poses problems of its own, as it requires an elaborate readout scheme to distinguish a single photon from a large coherent background [70] and is potentially vulnerable to laser phase noise [63, 56]. Another scheme uses levitated dielectric spheres [23] in the pulsed optomechanics regime [71], but has stringent experimental requirements including extremely high vacuum (10^{-16} torr) and may need to be performed in space [72]. Other quantum effects are also possible, such as squeezing the motion of the mechanical resonator via active feedback [73] or quadratic coupling [74].

In this chapter, we propose using nested interferometers to create and detect macroscopic

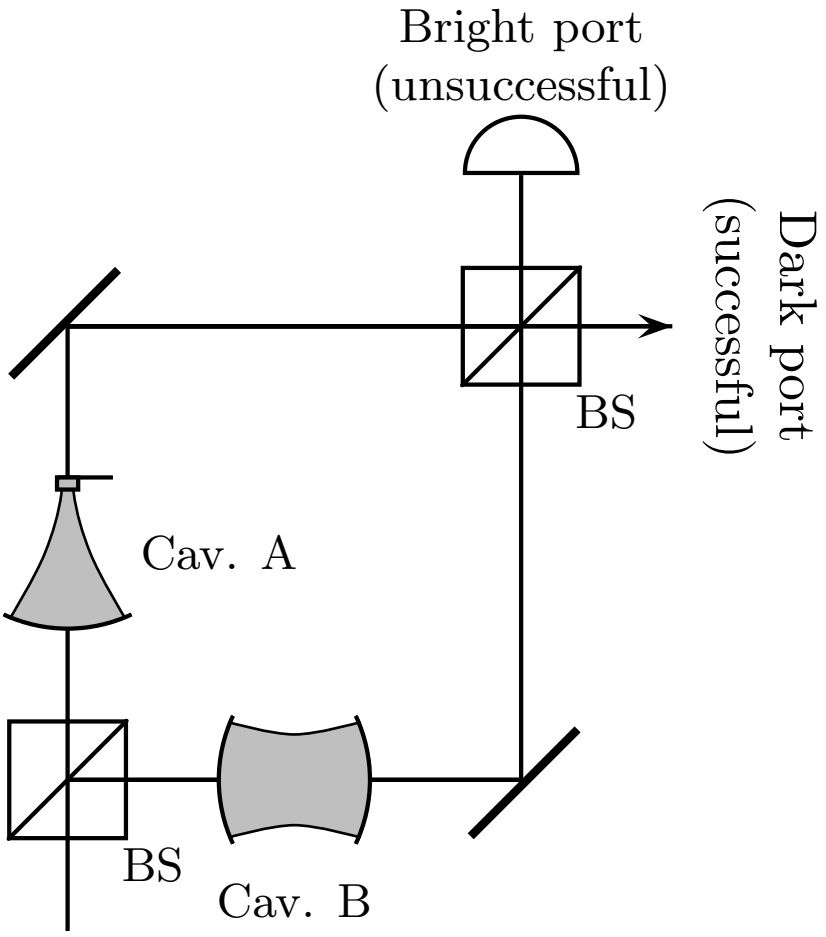

Figure 4.1: The photon enters the first beam splitter of the inner interferometer, followed by an optomechanical cavity (A) and a conventional cavity (B). The cavity in arm B is used to compensate the effect of the cavity in arm A when there is no optomechanical interaction. The photon weakly excites the optomechanical resonator. After the second beam splitter, dark port detection postselects for the case where the resonator has been excited by a phonon.

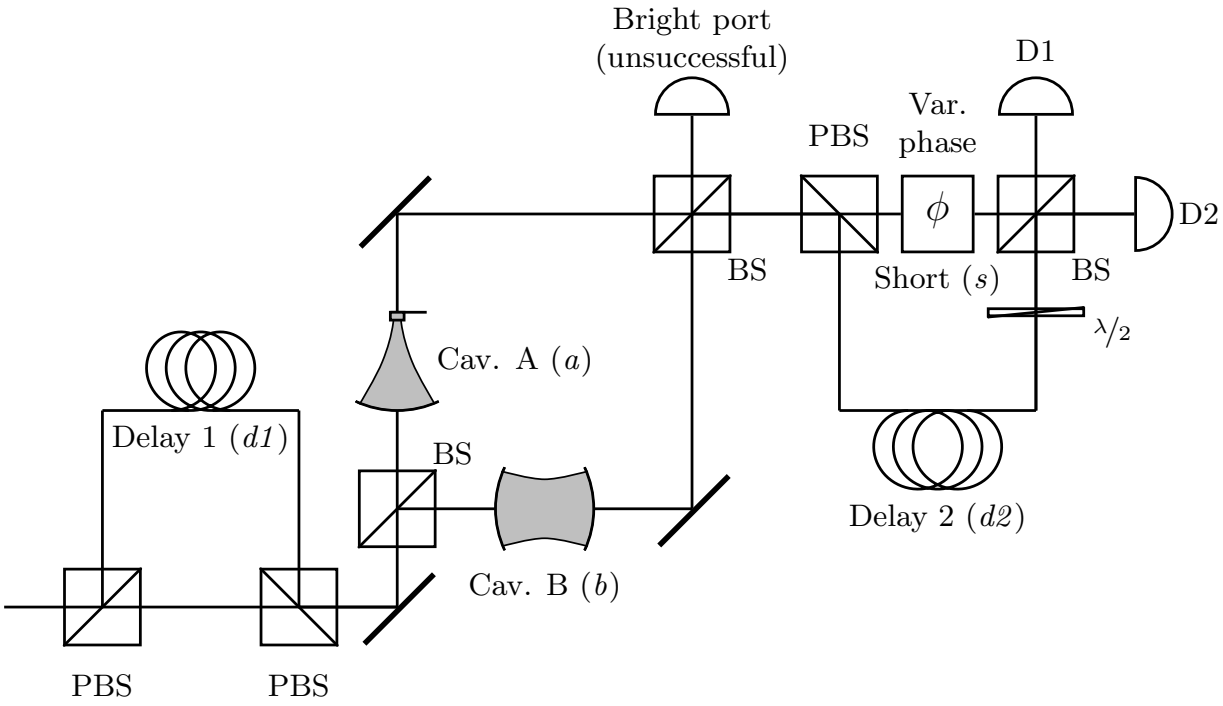

Figure 4.2: Creating a macroscopic superposition via postselection and observing its decoherence. Note that though the two delay lines are depicted separately for clarity, in a realistic system the same delay line might be used twice, in each polarization mode.

quantum superpositions. In the inner interferometer (see Fig(4.1)), we use postselection to amplify the effects of a single photon in the weak coupling regime. In the no-coupling limit photons always exit along bright port, and only when there is an optomechanical interaction can they be detected at the dark port. Postselecting dark port events results in distinguishable mechanical states (states with little overlap with ground state $|0\rangle_m$).

Whereas "dark port detection" has already been proposed in the past, for example in the context of gravitational wave detection [75], the main novelty of our scheme is that the inner interferometer is nested within a Franson [76], or time-bin [77], interferometer (Fig. 4.2). A single-photon state is split into a long and short path before entering the inner interferometer. In the dark port detection arm a second pair of long and short paths are present before the final detection of the photon on either detector D1 or D2. We will explain how the time-bin interferometry allows for the investigation of the coherent properties of the mechanical

resonator in cavity A.

The Hamiltonian for optomechanical systems is given as follows [19], see also Eq.(1.30):

$$\hat{\mathscr{H}} = \hbar\omega_o a^\dagger a + \hbar\omega_m c^\dagger c - \hbar G_0 a^\dagger a(c + c^\dagger) \tag{4.1}$$

where $\hbar$ is the reduced Planck's constant, ω_o is the optical angular frequency, $\hat{a}$ is the optical annihilation operator, ω_m is the mechanical angular frequency, $\hat{c}$ is the mechanical annihilation operator, and coupling strength $G_0 = (\omega_o/L)\sqrt{\hbar/(2m\omega_m)}$, with L the cavity length and m the effective mass of the mechanical mode.

A single photon in an optomechanical cavity interacts weakly with the mechanical mode, producing a periodic coherent displacement (see Eq.(1.44) for the definition of a coherent state) in the mechanical state as described by Eq.(1.47) of $|\psi(t)\rangle_m = exp[i\phi(t)]|\alpha\rangle_m$ with $\phi(t) = \kappa^2(\omega_m t - \sin\omega_m t)$, $\alpha(t) = \kappa(1 - e^{-i\omega_m t})$ and $\kappa = G_0/\omega_m$. Since the interaction is weak, $\alpha(t) \ll 1$ at all times, making the displacement of the mechanical state hard to detect.

Now consider a Mach-Zehnder interferometer, where one arm contains an optomechanical cavity, and the other contains a stationary Fabry-Pérot cavity (with annihilation operator $\hat{b}$), as in [8]. This is shown in Fig. 4.1. The optomechanical device is cooled to the ground state using sideband-resolved cooling techniques [50, 51], and the cooling beam is switched off. A single photon is input to the interferometer, and after the first beam splitter the state of the system is $\frac{1}{\sqrt{2}}(|1\rangle_a|0\rangle_b + |0\rangle_a|1\rangle_b)$. The photon weakly interacts with the optomechanical device, resulting in an overall state of:

$$|\psi\rangle = \frac{1}{\sqrt{2}}[|1\rangle_a|0\rangle_b|\psi(t)\rangle_m + |0\rangle_a|1\rangle_b|0\rangle_m] \approx \frac{1}{\sqrt{2}}[|1_a\rangle|0_b\rangle e^{-|\alpha|^2/2}\{|0\rangle_m + \alpha(t)|1\rangle_m\} + |0_a\rangle|1_b\rangle|0\rangle_m]. \tag{4.2}$$

The second beam splitter postselects for an optical state $|\psi\rangle_f$ tuned such that the $|0\rangle_m$ components cancel each other out. Technically, this will vary depending on how long the photon remained in the cavity, but for $|\alpha(t)| \ll 1$ it will always be approximately $|\psi\rangle_f =$

$1/\sqrt{2}(|1\rangle_a|0\rangle_b - |0\rangle_a|1\rangle_b)$. When photons exit the dark port of the interferometer, the state $|\psi\rangle_f$ is postselected, resulting in an unnormalized state of:

$$|\psi\rangle \approx \frac{e^{-|\alpha(t)|^2/2}-1}{2}|0\rangle_m + \frac{\alpha(t)}{2}e^{-|\alpha(t)|^2/2}|1\rangle_m. \tag{4.3}$$

For $|\alpha(t)| \ll 1$, this is approximately $|\psi\rangle \approx (\alpha(t)/2)|1\rangle_m$, or $|1\rangle_m$ with an $|\alpha(t)|^2/4$ chance of the postselection succeeding. We have thus probabilistically amplified the optomechanical effect of the photon (amplifying in the sense that the probability of having the mechanical oscillator in the first excited state is larger than being in the ground state).

This aspect of our scheme is related to the weak measurement formalism [78, 79], with the optomechanical device essentially acting as a "pointer" which weakly measures photon number. However, it operates outside the weak measurement regime [80, 81] due to its totally orthogonal postselection. For more discussion on this point see the Appendix. B.

We propose to use this postselection to create macroscopic superpositions and measure their decoherence. Fig. 4.2 shows an extended optical setup, featuring an outer interferometer with two delay lines of equal length, one before the inner interferometer and one after it. The input photon is split by a polarizing beam splitter (PBS) into an early component and a late component which enters delay line 1. The early component immediately enters the inner interferometer and interacts with the device, and only the small component associated with mechanical state $|1\rangle_m$ passes through. After this component exits the dark port of the inner interferometer it is put into a second delay line via the polarizing beam splitter. At this point we have an entangled state, with a large component in delay line 1 associated with mechanical state $|0\rangle_m$, and a small component in delay line 2 associated with mechanical state $|1\rangle_m$, see Eq.(4.4). The late component then exits delay line 1 and enters the inner interferometer, where again only the component associated with $|1\rangle_m$ passes through. Finally, both components are interfered with each other at the end of the outer interferometer to check for visibility.

We sort the photons detected at the end of the outer interferometer into bins by arrival time.

If the delay lines are of equal length τ_d, then a photon detected at $t = \tau_d + t_c$ after the initial photon entered corresponding to a photon that remained in the cavities for time t_c. However, this conveys no information about whether it took the early or late path. Thus, both components will have had the same value of $\alpha(t_c)$, and both $|1\rangle_m$ components will have the same magnitude. Thus the early and late paths will be balanced and can interfere with perfect visibility.

Conditioned on the early component leaving the dark port of the inner interferometer, we will have an unnormalized state of:

$$|\psi\rangle \approx \frac{1}{\sqrt{2}}(|1\rangle_{d1}|0\rangle_{d2}|0\rangle_m + \frac{\alpha(t_c)}{2}|0\rangle_{d1}|1\rangle_{d2}|1\rangle_m), \tag{4.4}$$

with $d1$ and $d2$ labeling the first and second delay lines, respectively. This shows entanglement between the photon and the macroscopic mechanical state. Now, the components can be delayed for any length, optical losses allowing. After the late component has passed through the inner interferometer, we apply a variable phase ϕ to the early component, in order to observe fringes. Assuming no decoherence the state will be:

$$|\psi\rangle \approx \frac{\alpha(t_c)}{2\sqrt{2}}(e^{i\phi}|1\rangle_{s2}|0\rangle_{d2}|1\rangle_m + |0\rangle_{s2}|1\rangle_{d2}|1\rangle_m), \tag{4.5}$$

with $s2$ representing the short path of the late photon prior to the final beam splitter.

For increasing delay times, however, eventually the mechanical components will undergo decoherence of some kind. This could be traditional environmentally-induced decoherence due to imperfect isolation from the environment [82], or it could be a proposed novel form of decoherence [4, 5, 83, 84, 6, 7].

After the final beamsplitter, there are two quantities that can be measured to characterize the superposition. First, we can determine the arrival rate of photons versus time. Here we assume a single photon enters the cavity at a specific time, valid in the short-pulse limit [85]. The probability density of a photon in a cavity being released after time t_c is $\Gamma_c \exp(-\Gamma_c t_c)$, where Γ_c is the decay rate of the cavity. The probability of a successful postselection of a photon being released after t_c is approximately $|\alpha(t_c)|^2/4 = \kappa^2 \sin^2(\omega_m t_c/2)$. Multiplying these results

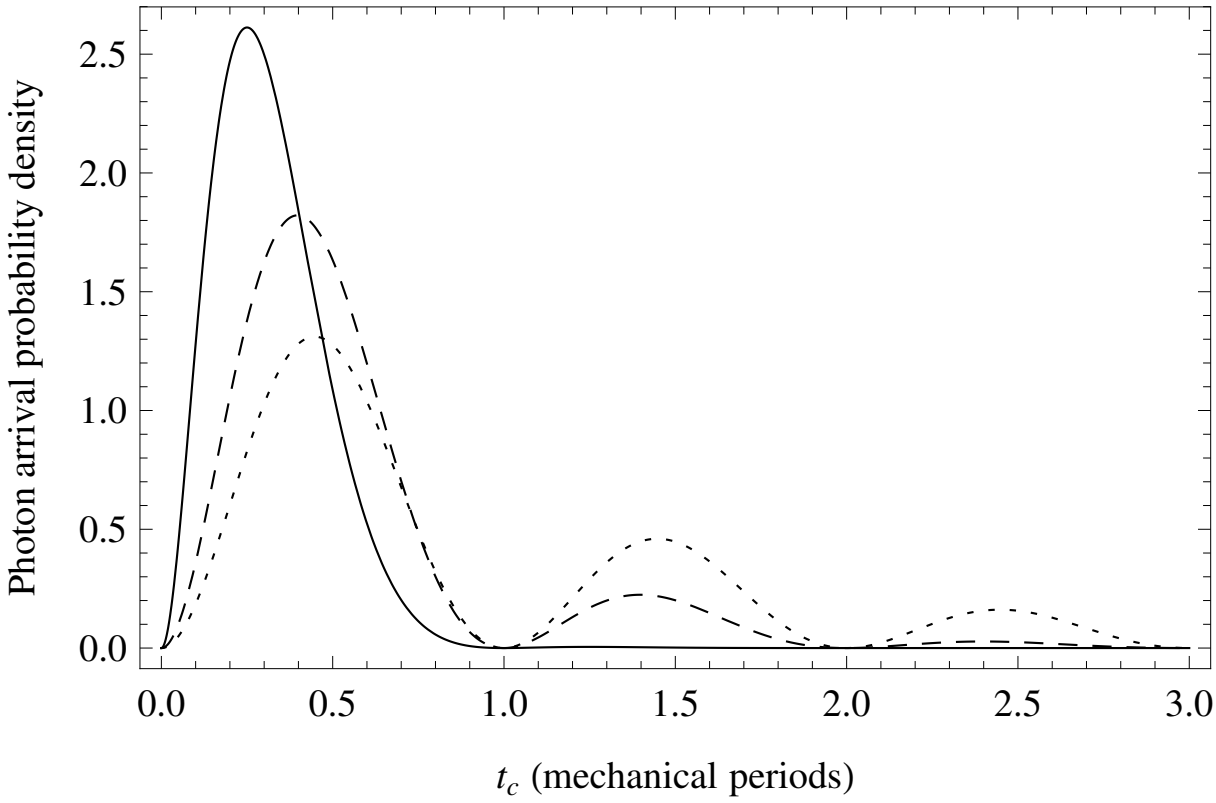

Figure 4.3: Solid: (unnormalized) probability density of a photon count vs. arrival time given a successful postselection for a sideband-resolved device with $\omega_m = \Gamma_c$. Dashed: $\omega_m = 3\Gamma_c$. Dotted: $\omega_m = 6\Gamma_c$.

in a characteristic oscillation (Fig. 4.3) in arrival rate at the mechanical frequency of the optomechanical device. We can detect this oscillation by binning the photons by arrival time and comparing arrival rates. This indicates a successful postselection involving the device, ruling out counts on the dark port of an imperfectly aligned inner interferometer or entanglement with some other degree of freedom. Integrating, we get the overall probability of a single photon successfully creating a $|1\rangle_m$ state:

$$\kappa^2\Gamma_c \int_0^\infty \sin^2\left(\frac{\omega_m t_c}{2}\right) e^{-\Gamma_c t_c} dt_c = \frac{1}{2}\frac{\kappa^2\omega_m^2}{\Gamma_c^2 + \omega_m^2}. \tag{4.6}$$

Second, we can measure the interference visibility by varying the phase in the outer interferometer ("Var. phase" in Fig. 4.2). The visibility should not vary with arrival time in a given

experiment; both components will have been put into the same mechanical state (Eqn. 4.5). However, we can jointly vary the delay line lengths and plot visibility versus delay time. As delay time increases, visibility will eventually be lost due to some form of decoherence. Definitively determining the cause of any observed decoherence is difficult, but it will be possible to test its dependence on parameters like mass, frequency, environmental temperature, and mechanical Q, putting bounds on proposed macroscopic decoherence mechanisms.

4.1 Finite Device Temperature

Before discussing the experimental requirements for our scheme we consider the realistic case in which the mechanical oscillator is not in the ground state. We assume that the mechanical oscillator is initially in the coherent state $|\gamma\rangle$. After weakly interacting ($\kappa \ll 1$, $|\alpha(t)| \ll 1$) with the optomechanical resonator for time t, the state will be:

$$|\psi(t)\rangle = \frac{1}{\sqrt{2}}[e^{i\phi}|1\rangle_a|0\rangle_b|\gamma+\alpha(t)\rangle_m + |0\rangle_a|1\rangle_b|\gamma\rangle_m]. \tag{4.7}$$

By postselecting for photons which exit the dark port, we select the $|\psi\rangle_f = 1/\sqrt{2}(|1\rangle_a|0\rangle_b - |0\rangle_a|1\rangle_b)$ component. The state of the mechanical oscillator after post-selection is given by $|\psi_{ps}(t)\rangle_m =_f \langle\psi|\psi(t)\rangle$. Keeping to the lowest order in κ:

$$|\psi_{ps}(t)\rangle_m = \frac{1}{2}[e^{i\phi(t)}|\gamma e^{-i\omega_m t} + \alpha(t)\rangle_m - |\gamma e^{-i\omega_m t}\rangle_m] \approx \frac{1}{2}[e^{-i\kappa\gamma sin\omega_m t}\hat{D}(\alpha(t)) - 1]|\gamma e^{-i\omega_m t}\rangle_m \tag{4.8}$$

where $D(\eta)$ is the displacement operator defined by Eq.(1.45). In deriving Eq.(4.8) we used the Eq.(1.45) to write

$$|\gamma e^{-i\omega_m t} + \alpha(t)\rangle = D(\gamma e^{-i\omega_m t} + \alpha(t))|0\rangle \tag{4.9}$$

then we used the following identity for coherent states[44]

$$D(\gamma_1 + \gamma_2) = e^{iIm(\gamma_1\gamma_2^*)}D(\gamma_1)D(\gamma_2) \tag{4.10}$$

using which we get

$$|\gamma e^{-i\omega_m t} + \alpha(t)\rangle = e^{i\kappa\gamma sin\omega_m t}D(\gamma e^{-i\omega_m t})|0\rangle \tag{4.11}$$

In the $\gamma = 0$ case, where the resonator has been cooled to its ground state, the above simplifies to a postselected state of:

$$|\psi_{ps}(t)\rangle_m = \frac{\alpha(t)}{2}|1\rangle_m. \tag{4.12}$$

Thus in this case, the resonator is placed into the first excited state with probability $|\alpha(t)|^2/4$ (see Eq.(4.3)). The weak interaction between the photon and the device is probabilistically amplified. Using Eq.(4.8) one obtains the overall probability of successful postselection for an initial coherent state to lowest order in κ as:

$${}_m\langle\psi|\psi\rangle_m \simeq \frac{1}{2}\{\kappa^2(1-cos\omega_m t) + \frac{1}{2}\kappa^2\gamma^2 sin^2\omega_m t\} \tag{4.13}$$

Note that$|\langle\gamma(t)|\psi_{ps}(t)\rangle|^2 \approx \frac{1}{4}\kappa^2|\gamma|^2 sin^2\omega_m t$, precisely the second term of Eqn. 4.13. Thus the first term represents our signal, while the second term represents a background noise of dark port events due to finite temperature rather than successfully conveying a phonon to the device. Considering a mechanical resonator initially in a thermal state, a statistical mixture of coherent states[44]:

$$\hat{\rho}_{th} = \frac{1}{\pi\bar{n}_{th}}\int e^{-|\gamma|^2/\bar{n}_{th}}|\gamma\rangle\langle\gamma|d^2\gamma \tag{4.14}$$

where

$$\bar{n}_{th} = \frac{1}{e^{\hbar\omega_m/k_B T}-1} \tag{4.15}$$

is the mean thermal occupation number and k_{B} represents the Boltzmann constant. Averaging Eqn. 4.13 over the thermal distribution Eq.(4.14), we arrive at:

$$\langle{}_m\langle\psi|\psi\rangle_m\rangle_{th} \simeq \frac{1}{2}\{\kappa^2(1-cos\omega_m t) + \frac{1}{2}\kappa^2\bar{n}_{th} sin^2\omega_m t\} \tag{4.16}$$

So for the signal to be larger than the noise, we must have $\bar{n}_{\mathrm{th}} \ll 4\left[\sin(\omega_m t/2)/\sin\omega_m t\right]^2 = \sec^2(\omega_m t/2)$. This implies that the nested interferometry proposal will only be successful if $\bar{n} \ll 1$, that is $T \ll \hbar\omega_m/k_B$. Thus, ground state cooling is essential for the success of this scheme. For a sideband-resolved device, this can be accomplished by driving the red (anti-Stokes) sideband of the cavity with a coherent beam [50, 51, 25, 26]

4.2 Experimental Requirements

We now discuss this scheme's experimental requirements. First, the optomechanical device must be capable of cooling to the mechanical ground state. For the low-frequency devices considered here, cooling by conventional means, such as in [86], is impractical. This means they must be in the sideband-resolved regime, $\omega_m > \Gamma_c$, to allow optical ground state cooling [50, 51]. Further, they must be a few times sideband-resolved,$\omega_m = 3\Gamma_c$, in order to allow observation of the oscillations in arrival rate shown in Fig.(4.3). Many sideband-resolved devices [87, 88, 89, 25, 26, 66] have been demonstrated, and two have been successfully cooled to the ground state [25, 26].

The device must also have κ high enough to make successful postselections common, though the precise value required will depend on the dark count rate of the detectors and the stability of the setup. As shown in Eq.(4.6), a device with $\omega_m = 3\Gamma_c$ will have successful postselections with probability approximately $9\kappa^2/20$. The window in which the detectors will need to be open for photons is approximately $1/\Gamma_c$, leading to a requirement that the dark count rate be lower than $9\kappa^2\Gamma_c/20$. The best silicon avalanche photodiodes (APDs) have a dark count rate of $\sim$2 Hz, requiring $\kappa \sim 0.0009$ for a 300 kHz device with $\omega_m = 3\Gamma_c$, and $\kappa \sim 0.007$ for a 4.5 kHz device.

However, an emerging option is superconducting transition edge sensors (TESs) [90], which have negligible dark counts caused only by background thermal radiation [91]. Dark counts this low would result in interferometer alignment being the limiting factor on κ. Though compared to APDs they have low maximum count rates ($\sim$100 kHz), poor time resolution ($\sim$0.1 μs) and require sub-Kelvin temperatures, none of these are problematic for the proposed experiment.

Table 4.1 shows the parameters for two resonator devices [66], representing the current state of the art, in terms of maximizing κ. It also shows two sets of proposed parameters representing devices with $\kappa \simeq 0.001$–0.005 and $\omega_m \simeq 3\Gamma_c$, with only slight improvements over existing

devices. The required finesse ranges from 300,000–2,000,000. For comparison, the highest reported finesse in an optical Fabry-Pérot cavity is 1.9×10^6 [92], and the highest reported between micromirrors is 1.5×10^5 [93]. This indicates that a sideband-resolved device with sufficient κ for the proposed experiment is a realistic goal. For the proposed devices presented in Table 4.1 it should be possible to collect a usable amount of data in times ranging from hours to days. These times depend on the specific device as well as the timescale of the decoherence being probed.

Further, the delay lines must be capable of storing the photons for multiple mechanical periods without significant losses. For delays up to $\sim$100 μs simple fiber optic delay lines are sufficient; at 1550 nm fiber optic delay lines have acceptable losses (0.2 dB/km) for this purpose. For shorter wavelengths fiber optic losses are too high but free space delay lines such as a Herriott cell may be used [94, 95], allowing $\sim$70 μs of delay. This could be increased to tens of milliseconds with ultrahigh reflectivity mirrors and very long cell lengths (lengths up to 1 km have been demonstrated). In the future, much longer delay times may be possible using quantum optical memory [96, 97].

In addition, the base temperature from which optical cooling starts must be low enough that the ground state can withstand environmentally induced decoherence for multiple mechanical periods. This requirement is given as $T \ll T_{\mathrm{EID}} \equiv \hbar\omega_m Q_m/k_B$ [82, 8, 65]. This means that mechanical quality factor Q_m must be high enough that it is possible to cool below T_{EID} prior to optical cooling. The values of T_{EID} for the devices in Table 4.1 are easily met by a standard dilution refrigerator.

It is important to note that the proposed scheme is potentially useful for other types of weakly coupled optomechanical devices, even in very different frequency regimes. For instance, optomechanical crystals with $\omega_m = 7.4\Gamma_c = 2\pi \times 3.68$ GHz and $\kappa = 0.00025$ have been demonstrated [26]. Though the lower value of κ lowers the chance of a successful postselection and places stricter requirements on the alignment of the inner interferometer, the higher

frequency might allow experimental runs to be performed in similar amounts of time.

Device	M	f_m	L	F	Q_m	T_{EID}	κ	ω_m/Γ_c
Resonator #1 [66]	60	158	5	38,000	43,000	0.3	0.000034	2.0
Resonator #2 [66]	110	9.71	5	29,000	940,000	0.4	0.0016	0.09
Proposed device #1	1	300	0.5	300,000	20,000	0.3	0.001	3.0
Proposed device #2	100	4.5	5	2,000,000	2,000,000	0.4	0.005	3.0

Table 4.1: Effective mass of the mechanical mode (ng), mechanical frequency (kHz), cavity length (cm), optical finesse, mechanical quality factor, environmentally induced decoherence temperature (K), and $\kappa = g/\omega_m$ of two recent devices with κ high enough to attempt the proposed scheme. Trampoline resonator #1 has insufficient κ while #2 has insufficient finesse to be sideband-resolved. Improved parameters for two devices with $\omega_m \simeq 3\Gamma_c$ and $\kappa \simeq 0.001$–0.005 are also presented. Proposed device #2 could be used to observe novel decoherence mechanisms [4, 5, 6, 7].

4.3 Decoherence

In the following section we study the possibility of probing some decoherence models using our scheme. The basic idea is to prepare the superposition states for the mechanical oscillator using the aforementioned method and then observe how the superposition evolves.

4.3.1 Environmentally Induced Decoherence

Most devices proposed for ground state cooling [25, 26, 66] require that the device be optically cooled below the temperature T_{env} that the surrounding environment can reach by conventional cooling (there is one notable exception [86]). This is also true of the devices proposed in Tab. 4.1.

In this situation, the mechanical resonator is modeled as coupled to an infinite bath of harmonic oscillators [82, 65]. In the limit of $k_{\mathrm{B}}T_{\mathrm{env}} \gg \hbar\omega_m$, mechanical quality factor $Q_m \gg 1$, and a Markovian regime with no memory effects in the bath, the bath degrees of freedom can

be eliminated and the system can be described by the master equation for the reduced density matrix $\hat{\rho}$ [82, 65, 98]:

$$\frac{d}{dt}\hat{\rho} = \frac{i}{\hbar}\left[\hat{\rho}, \hat{\mathscr{H}}\right] - \frac{i\gamma_m}{\hbar}\left[\hat{x}, \{\hat{p}, \hat{\rho}\}\right] - \frac{D}{\hbar^2}\left[\hat{x}, [\hat{x}, \hat{\rho}]\right], \tag{4.17}$$

with $\hat{\mathscr{H}}$ the Hamiltonian from Eq.(4.1), the damping coefficient $\gamma_m = \omega_m/Q_m$, and the diffusion coefficient $D = 2m\gamma_m k_B T_{\text{env}}$. The first term represents the unitary evolution of the system under the Hamiltonian from Eq.(4.1), while the second term represents the damping and the third term represents the diffusion. In the macroscopic regime the diffusion term proportional to $D/\hbar^2$ dominates Eq.(4.17) [82, 65]. Thus the resulting time scale for decoherence is:

$$\tau_{\text{EID}} \approx \frac{\hbar^2}{D(\Delta x)^2} = \frac{\hbar Q_m}{2k_B T_{\text{env}}}, \tag{4.18}$$

with the superposition size $\Delta x = \sqrt{\frac{\hbar}{2m\omega_m}}$. It is helpful at this point to define an environmentally induced decoherence temperature [65]:

$$T_{\text{EID}} = \frac{\hbar\omega_m Q_m}{k_B}. \tag{4.19}$$

We note that the inverse of the decoherence time scale is $\tau_{\text{EID}}^{-1} = 2\omega_m(T_{\text{env}}/T_{\text{EID}})$. Thus for the environmentally induced decoherence to act on a time scale slower than the mechanical frequency it is necessary that $T_{\text{env}} \ll T_{\text{EID}}$.

We will consider EID with a base temperature of $T_{\text{env}} = 1$ mK, obtainable with a dilution refrigerator. For this case, with the 300 kHz proposed device, $\tau_{\text{EID}} \approx 150\ \mu$s. For the 4.5 kHz proposed device, $\tau_{\text{EID}} \approx 15$ ms.

4.3.2 Gravitationally Induced Decoherence

Gravitationally induced decoherence, proposed independently by Diósi [7] and Penrose [6]. In their model, the decoherence rate for superpositions scale by the difference between the corresponding Newtonian field strengths. The time scale for such decoherence is:

$$\tau_{\text{P}} = \hbar/\Delta_{\text{P}} \tag{4.20}$$

with the Δ_P defined as follows:

$$\Delta_P = 4\pi G \iint \frac{(\rho_1(\vec{x}) - \rho_2(\vec{x}))(\rho_1(\vec{y}) - \rho_2(\vec{y}))}{|\vec{x} - \vec{y}|} d^3x d^3y, \tag{4.21}$$

with $\rho_1(\vec{x})$ and $\rho_2(\vec{x})$ the mass distributions of the two superposed states. Intuitively Eq.(4.21) means that superpositions between two states with a larger difference between densities wii decohere faster.

As in [65], we model the system as a set of spheres with mass m, representing nuclei. The Penrose energy for one sphere is given by $\Delta_P^0 = 4\pi(E_{1,2}^0 + E_{2,1}^0 - E_{1,1}^0 - E_{2,2}^0)$, with $E_{m,n}^0 = -G\iint \rho_m(\vec{x})\rho_n(\vec{y})/|\vec{x} - \vec{y}| d^3x d^3y$. The spheres considered are far enough apart and displaced little enough that their most significant interaction is with themselves, and not neighboring spheres. This means that we can merely multiply by the number of spheres, M/m, to get the total energy $\Delta_P = (M/m)\Delta_P^0 = 4\pi(E_{1,2} + E_{2,1} - E_{1,1} - E_{2,2})$, with $E_{m,n} = (M/m)E_{m,n}^0$

For all cases, we will consider two spherical mass distributions with radii a equal to the size of the specific mass distribution that will be chosen, separated by $\Delta x = x_0 = \sqrt{\hbar/(2m\omega_m)}$, the zero point motion of the resonator. Note that this is mathematically equivalent to the model of one sphere at $x = 0$ for $|0\rangle_m$, and two half-mass spheres at $x = \pm x_0$ for $|1\rangle_m$.

As the radius of the two spheres will be greater than x_0 regardless of mass distribution used, there will always be significant overlap in the distributions. This will greatly complicate evaluation of Eq.(4.21). This has no effect on the self-energy terms but does affect the interaction terms. The $1/r$ potential between overlapping spheres has been evaluated previously [99]:

$$E_{1,2} = \begin{cases} -GMm/\Delta x & \Delta x > 2a \\ -GMm[\frac{12a^2 - 5\Delta x^2}{10a^3} - \frac{\Delta x^5 - 30\Delta x^3 a^2}{160a^6}] & 0 \leq \Delta x \leq 2a \end{cases} \tag{4.22}$$

For the $E_{1,1}$ and $E_{2,2}$ terms, we can just plug $\Delta x = 0$ into Eq.(4.22). This gives $E_{1,1} = E_{2,2} = -\frac{6GMm}{5a}$. There is considerable theoretical disagreement about the proper mass distribution to use for gravitationally induced decoherence [8, 100, 65, 101, 23]. Previous papers have used the zero point motion of the resonator itself, the nuclear radius of the nuclei making up the

resonator, the zero point motion of the nuclei making up the resonator, and a completely homogeneous mass with no nuclear granularity. At this point, we will define the mass distribution to be considered in this chapter.

In the Debye model, the zero point motion of nuclei in a lattice is given (Eq.(12.3.10) in [102]):

$$a = x_{0,\mathrm{nuc}} = \frac{3\hbar}{2\sqrt{k_B \Theta_D M}}. \tag{4.23}$$

with Θ_D the Debye temperature and M the atomic mass. Since the largest component of the mass of a Ta_2O_5/SiO_2 dielectric mirror will be tantalum, we will make the simplifying assumption that the mirrors are composed of tantalum. The Debye temperature of tantalum is $\Theta_D = 240$ K [103], and the atomic mass $M = 181$ amu. Thus $a \approx 5$ pm.

For this case, for the proposed 300 kHz device, $\tau_{\mathrm{P}} \approx 1.8 \times 10^6$ s. For the proposed 4.5 kHz device, $\tau_{\mathrm{P}} \approx 28 \times 10^3$ s. This type of decoherence would not be testable, as it is slower than EID in both devices.

4.3.3 Continuous Spontaneous Localization

Continuous spontaneous localization is a proposed position-localized decoherence mechanism in which a nonlinear stochastic classical field interacts with objects causing collapse of macroscopic superpositions. Proposed by Ghirardi, Rimini, Weber and Pearle [104, 83], the master equation and decay rate for position-localized decoherence have the following form [105, 6, 104, 83, 7, 106, 5, 4]:

$$\langle x|\dot{\rho}(t)|x'\rangle = \frac{i}{\hbar}\langle x|[\rho, H]|x'\rangle - \Gamma(x-x')\langle x|\rho|x'\rangle \tag{4.24}$$

where Γ is the decay rate of the coherence in the position basis given by

$$\Gamma(x) = \gamma(1 - exp[-\frac{x^2}{4a^2}]) \approx \begin{cases} \Lambda x^2 & x \ll 2a \\ \gamma & x \gg 2a \end{cases} \tag{4.25}$$

with $\Lambda = \gamma/(4a^2)$ the localization parameter, γ the localization strength, and a the localization distance. For the macroscopic resonators considered in tabel 4.1 we are in the $x \ll 2a$ limit. For the single nucleon case, the continuous spontaneous localization model [83] gives values $a_{\mathrm{CSL}} = 100$ nm and $\gamma^0_{\mathrm{CSL}} = 10^{-16}$ Hz based on phenomenological arguments.

Following [107, 23], the value of the localization parameter Λ_{CSL} can be shown to be:

$$\Lambda_{\mathrm{CSL}} = \frac{M^2}{m_0^2} \frac{\gamma^0_{\mathrm{CSL}}}{4a^2_{\mathrm{CSL}}} f(R,b,a) \tag{4.26}$$

with M the resonator mass, m_0 the nucleon mass, R the radius of the sphere and $f(R,b,a)$ a parameter depending on the geometry of the device. Disk geometry was considered in [107]. For motion perpendicular to the disk face f is evaluated (see [107], Sec. 5.2, App. A, and Eqn. A.11):

$$f(R,b,a) = 4(\frac{2a}{R})^4(\frac{2a}{b})^2[1 - e^{-b^2/4a^2}] \int_0^{R/2a} x dx \int_0^{R/2a} x' dx' e^{-(x^2+x'^2)} I_0(2xx') \tag{4.27}$$

with R the disk radius, b the disk thickness, $I_0(x)$ the $n = 0$ modified Bessel function of the first kind, and a the localization distance (for CSL, $a_{\mathrm{CSL}} = 100$ nm). In the $(R/2a)^2 \gg 1$ and $(b/2a)^2 \gg 1$ limits, applicable in this case, $f \approx (2a/R)^2(2a/b)^2$.

Thus, for the 300 kHz device, using a thickness of ~ 5 μm and a radius of ~ 4 μm (values consistent with the proposed finesse and mass), we obtain a decoherence time of order $\tau_{\mathrm{CSL}} = 10^7$ s. For the 4.5 kHz device, using a thickness of ~ 5 μm and a radius of ~ 40 μm, we obtain a decoherence time of order $\tau_{\mathrm{CSL}} = 1.5 \times 10^5$ s. This type of decoherence would not be testable, as it is slower than EID in both devices.

4.3.4 Quantum Gravity

It has been proposed that quantum gravity might cause a form of position-localized decoherence due to coupling of the system to spacetime foam. This was first proposed by Ellis, Nanopoulos, Hagelin, and Srednicki [4] and subsequently elaborated on [106, 5] by others. Notably, this model is phenomenologically equivalent to the CSL model with altered values for the constants [23]: $a_{\mathrm{QG}} = \hbar m_{\mathrm{P}}/2cm_0^2$ with $m_{\mathrm{P}} = \sqrt{\hbar c/G}$ the Planck mass, and $\gamma_{\mathrm{QG}}^0 = 4a_{\mathrm{QG}}^2 c^4 m_0^6/\hbar^3 m_P^3$. This gives us:

$$\Lambda_{\mathrm{QG}} = \frac{M^2}{m_0^2}\frac{\gamma_{\mathrm{QG}}^0}{4a_{\mathrm{QG}}^2} f(R,b,a) = \frac{c^4 M^2 m_0^4}{\hbar^3 m_P^3} f(R,b,a) \tag{4.28}$$

with $f(R,b,a)$ as in Eqn. 4.27. However, since $R \ll a_{\mathrm{QG}}$ and $b \ll a_{\mathrm{QG}}$, we can set f to 1 [107]:

$$\Lambda_{\mathrm{QG}} \approx \frac{c^4 M^2 m_0^4}{\hbar^3 m_P^3} \tag{4.29}$$

Thus, for the 300 kHz device, using a thickness of $\sim 5\ \mu$m and a radius of $\sim 4\ \mu$m, we get a decoherence time of order $\tau_{\mathrm{QG}} = 7.1$ s. For the 4.5 kHz device, using a thickness of $\sim 5\ \mu$m and a radius of $\sim 40\ \mu$m, we get a decoherence time of order $\tau_{\mathrm{QG}} = 1.1$ ms. This type of decoherence might potentially be testable in the 4.5 kHz device, as it is faster than EID.

4.4 Conclusion

In conclusion we proposed a method of post-selected interferometry for the creation and investigation of macroscopic quantum superposition. This scheme has a couple of notable advantages over the previous optical scheme [8]. The proposed scheme only requires weakly coupled optomechanical systems, and the mechanical decoherence times that can be investigated are not limited by the optical storage time within the optomechanical system but only by the optical storage time in the external delay. We have also investigated the temperature dependence of the scheme and find that ground state cooling is necessary for implementation. We also investigate the time scales on which the novel decoherence mechanisms would be expected to operate.

Chapter 5

Creating and Detecting Micro-Macro Photon-Number Entanglement by Amplifying and De-Amplifying a Single-Photon Entangled State

This chapter is based on [108]

The goal of pushing the observation of quantum effects such as superpositions and entanglement towards the macroscopic level is currently being pursued in a number of different fields, including trapped ions [109], superconducting circuits [110], nano-mechanics [86], microwave cavities interacting with atoms in Rydberg states [111], atomic ensembles [112], and non-linear optics [113, 114, 115, 116]. Within non-linear optics, one can distinguish proposals based on Kerr non-linearities [113], and proposals and experiments based on parametric down-conversion [114, 115, 116]. The latter area has recently seen significant activity, a lot of which was stimulated by Ref. [116], which claimed the creation and detection of entanglement in polarization between a single photon on one side and thousands of photons on the other. The state was created starting from a single polarization entangled photon pair, by greatly amplifying one of the photons using stimulated type-II parametric down-conversion (i.e. a two-mode squeezing interaction involving both polarization modes). Ref. [117, 118] subsequently showed that the evidence for micro-macro entanglement given in Ref. [116] was not conclusive, and Ref. [119] showed that in order to rigorously prove the presence of entanglement for the state of Ref. [116], one would need to be able to count the photons on the macro side with single-photon resolution, which is a significant technological challenge. Several other results also suggest that the observation of entanglement by direct measurement on macroscopic systems generally requires very high resolution, which also implies very low photon loss in the case of

multi-photon states [120, 121, 114, 122].

These results inspired the work of Ref. [123], which proposed to prove the existence of micro-macro polarization entanglement by de-amplifying the macro part of the state of Ref. [116] back to the single-photon level. As entanglement cannot be created locally, if entanglement is detected at the single-photon level, this proves that micro-macro entanglement had to exist after the amplification stage. This approach has two advantages. On the one hand, the final measurement can be done by single-photon detection, which is much simpler than counting large photon numbers with single-photon resolution. On the other hand, the entanglement is primarily sensitive to loss between the amplification and de-amplification stages, which is easier to minimize in practice than the overall loss, which also includes detection inefficiency.

Most of the previous work in this area was concerned with polarization (or spin) entanglement [114, 116, 120, 121, 122, 123]. Here we propose to apply the amplification-deamplification approach to create and detect a different - quite striking - type of entanglement, namely micro-macro entanglement in photon number. Instead of starting from a polarization entangled photon pair, we propose to start from a single-photon entangled state, which can be created by sending a single photon onto a beam splitter [124, 125, 126, 127]. The presence of single-photon entanglement can be proven experimentally by homodyne tomography [125], and also by a combination of interference and single-photon detection [128]. Using single-photon entanglement as a starting point, one can create a micro-macro photon-number entangled state by amplifying one side via stimulated type-I parametric down-conversion (i.e. a single-mode squeezer). The resulting state is a superposition of two components with largely different mean photon numbers. This distinguishes our proposal from another recent proposal, where micro-macro entanglement is created by displacing (rather than squeezing) one half of a single-photon entangled state [129]. In that case the mean photon numbers of the two superposed components are very similar. Micro-macro photon number entanglement as suggested here could in principle be used to test proposals for fundamental decoherence in

energy [130, 131, 132]. In the next section we describe De Martini's proposal [133] and its experimental realization[116].

5.1 The De Martini Proposal

In 1998, De Martini suggested a scheme for creating the optical superposition of micro-macro state based on amplifying an initial micro state [133, 116]. The first step in the De Martini scheme is to prepare an entangled pair of photons by pumping a non linear crystal with a strong UV pulse as shown in Fig.(5.1). The entangled photon creates in spontaneous down conversion (SPDC) process, where a photon from the pump with frequency ωp splits to two photons with smaller frequency ω_s and ω_i called the signal and idler, respectively. In order for this process to happen, the two following conditions called phase matching conditions, should be satisfied:

$$\omega_p = \omega_s + \omega_i \tag{5.1}$$

$$\overrightarrow{k}_p = \overrightarrow{k}_s + \overrightarrow{k}_i \tag{5.2}$$

These conditions guarantee the conservation of energy and momentum, respectively. There are two type of phase matching in terms of polarization. In type I the signal and idler have the same polarization while in type II they have orthogonal polarizations. In the De Martini scheme type II phase matching is used to create the state

$$|\psi\rangle_{AB} = \frac{|H\rangle_A|V\rangle_B - |V\rangle_A|H\rangle_B}{\sqrt{2}} \tag{5.3}$$

The photon in arm A is directly measured and the photon in arm B amplified using the optical parameter amplifier (OPA). The amplification by an OPA is described by the Hamiltonian

$$\hat{H} = i\hbar\chi(\hat{a}_H^\dagger \hat{a}_V^\dagger - \hat{a}_H \hat{a}_V) \tag{5.4}$$

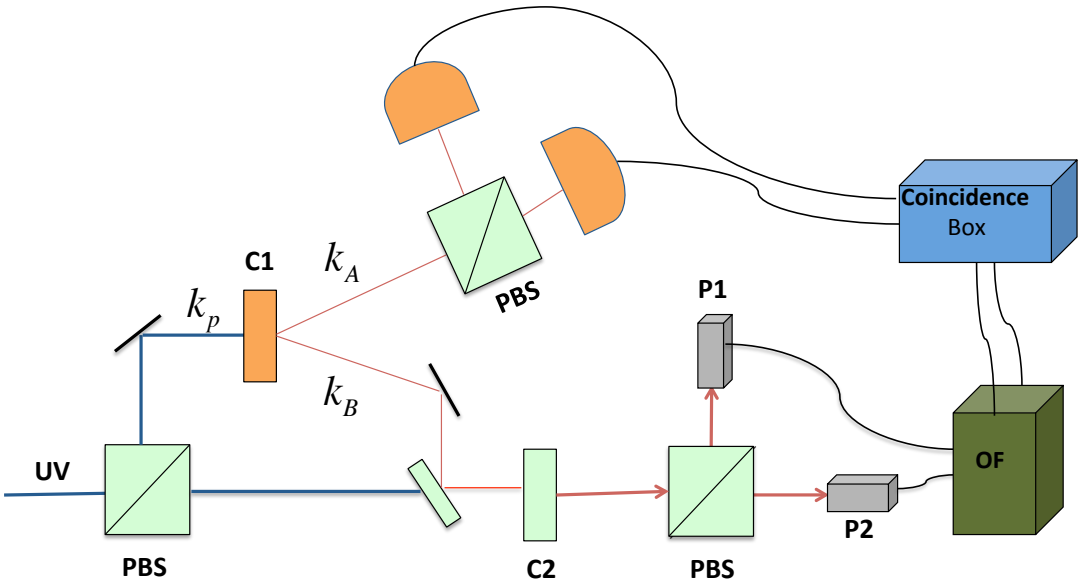

Figure 5.1: Schematic of the De Martini experiment. A nonlinear crystal creates the initial state(5.3). The photon in mode A is directly measured. The photon in mode B is amplified by pumping another nonlinear crystal ($C2$) to create many imperfect copy of the the original photons. The "orthogonality filter" (OF) is used in mode B to discriminate the two macroscopic states in this mode. The correlation between micro macro sates is then inferred by coincidence statistics.

The fact that Hamiltonian (5.4) describes the amplification process can be shown easily by writing down the Heisenberg equation of motion for $\hat{a}_H$ and $\hat{a}_V$. To show this we note that the equation of motions is given by

$$\frac{d}{dt}\hat{a}_H = \frac{i}{\hbar}[H, \hat{a}_H] = \chi \hat{a}_V^\dagger \tag{5.5}$$

$$\frac{d}{dt}\hat{a}_V = \frac{i}{\hbar}[H, \hat{a}_V] = \chi \hat{a}_H^\dagger \tag{5.6}$$

The solution to the above coupled equations for $\hat{a}_H$ is given by

$$\hat{a}_H(t) = \cosh(\chi t)\hat{a}_H(0) + \sinh(\chi t)\hat{a}_V(0) \tag{5.7}$$

From Eq.(5.7) one obtains the followoing relation for photon number with H polarization

$$\langle \hat{a}_H^\dagger(t) a_H(t) \rangle = \cosh^2(\chi t)\langle \hat{a}_H^\dagger(0) a_H(0) \rangle + \sinh^2(\chi t)\langle \hat{a}_V^\dagger(0) a_V(0) \rangle \tag{5.8}$$

The same equation can be obtain for V polarization. From Eq.(5.8) it is clear that the photon number in mode H is increasing with time.

It is interesting to note that the Hamiltonian (5.4) is invariant under the effect of rotation in the equator of the Bloch sphere. To see this we define the annihilation operator on the equator of the Bloch sphere as

$$\hat{a}_\phi = \frac{\hat{a}_H + e^{i\phi}\hat{a}_V}{\sqrt{2}} \tag{5.9}$$

$$\hat{a}_{\phi\perp} = \frac{\hat{a}_H - e^{i\phi}\hat{a}_V}{\sqrt{2}} \tag{5.10}$$

The Hamiltonian (5.4) can then be rewritten in term of the aforementioned operator as

$$\hat{H} = i\chi\{(\hat{a}_\phi^\dagger)^2 + (\hat{a}_{\phi\perp}^\dagger)^2\} + h.c. \tag{5.11}$$

The total state after amplification, expressed in term of equatorial basis, is given by [116]

$$|\Sigma\rangle_{AB} = \frac{1}{\sqrt{2}}(|1\phi^{\perp}\rangle|\Phi^{\phi}\rangle_B - |1\phi\rangle|\Phi^{\phi^{\perp}}\rangle) \tag{5.12}$$

with the orthogonal macroscopic states

$$|\Phi^{\phi}\rangle_B = \sum_{i,j=0}^{\infty} \gamma_{ij} \frac{\sqrt{(2i+1)!(2j)!}}{i!\,j!} |(2i+1)\phi;(2j)\phi^{\perp}\rangle \tag{5.13}$$

$$|\Phi^{\phi^{\perp}}\rangle_B = \sum_{i,j=0}^{\infty} \gamma_{ij} \frac{\sqrt{(2i+1)!(2j)!}}{i!\,j!} |(2j)\phi;(2i+1)\phi^{\perp}\rangle \tag{5.14}$$

where $\gamma_{ij} \equiv C^{-2}(-\frac{\Gamma}{2})^i \frac{\Gamma^j}{2}$, $C \equiv \cosh(g)$, $\Gamma \equiv \tanh(g)$ and g is the nonlinear gain. In Eq.(5.12), $|p\phi;q\phi^{\perp}\rangle$ means p photons with polarization a_{ϕ} and q photons with polarization $a_{\phi\perp}$. Eq.(5.12) describes the superposition of a macroscopic state with a microscopic state. It is important to note that the single photon is in superposition with a classically distinguishable macroscopic state. To see this we note the mean photon number of the state $|\Phi^{\phi}\rangle$ and $|\Phi^{\phi^{\perp}}\rangle$. The mean photon number for the polarization ϕ is $\sinh^2(g)$ for $|\Phi^{\phi^{\perp}}\rangle$ and $3\sinh^2(g)+1$ for $|\Phi^{\phi}\rangle$. The mean photon number for the polarization $\phi^{\perp}$ is $3\sinh^2(g)+1$ for $|\Phi^{\phi}\rangle$ and $\sinh^2(g)$ for $|\Phi^{\phi}\rangle$.

In[116], experimental realization of the De Martini scheme has been reported. The experimental challenge in the experiment is to verify the entanglement in the final state Eq.(5.12). The experimental detection of the micro-macro entanglement in [116] is based on the violation of the following inequality

$$V_1 + V_2 + V_3 \leq 1 \tag{5.15}$$

with $V_i = |\langle \Sigma_i^A \otimes \sigma_i^B \rangle|$, $\Sigma_i = |\Phi^{\Psi_i}\rangle\langle\Phi^{\Psi_i}| - |\Phi^{\Psi_i\perp}\rangle\langle\Phi^{\Psi_i\perp}|$, $\sigma_i = |\Psi_i\rangle\langle\Psi_i| - |\Psi_i^{\perp}\rangle\langle\Psi_i^{\perp}|$ where $\{\Psi_i, \Psi_i^{\perp}\}$ are two orthogonal qubits corresponding to basis $\{\Psi_1, \Psi_1^{\perp}\} = \{|H\rangle, |V\rangle\}$, $\{\Psi_2, \Psi_2^{\perp}\} = \{|\frac{|H\rangle - i|V\rangle}{\sqrt{2}}, \frac{|H\rangle + i|V\rangle}{\sqrt{2}}\}$, $\{\Psi_3, \Psi_3^{\perp}\} = \{\frac{|H\rangle + |V\rangle}{\sqrt{2}}, \frac{|H\rangle - |V\rangle}{\sqrt{2}}\}$.

To test entanglement it is then necessary to measure the correlation between $|\sigma_i^A\rangle$ and $|\Sigma_i^B\rangle$. One also needs to be able to distinguish $|\Phi^{\phi}\rangle$ and $|\Phi^{\phi^{\perp}}\rangle$. In principle if one can determine whether the photon number in mode B is odd or even one can discriminate $|\Phi^{\phi}\rangle$ from $|\Phi^{\phi^{\perp}}\rangle$,

but this resolution is out of reach of the current detectors. Instead one can use the probability distributions of photon numbers to distinguish $|\Phi^{\phi}\rangle$ and $|\Phi^{\phi\perp}\rangle$. One can look at the photo current (which is proportional to the photon numbers) from the detectors behind the PBS in arm B. If the difference between the two currents exceeds a certain threshold the measurement counts as a conclusive measurement, otherwise it discarded. This postselection process opens the loop hole in the De Martini experiment as discussed in [117, 118, 123]

5.1.1 Our Scheme

In the following we describe our proposal in more detail, taking into account the effects of photon loss, see also Figure5.2. We start by sending a single photon onto a balanced beam splitter. The output state is a single-photon entangled state

$$|\psi_{in}\rangle = \frac{|1\rangle_A|0\rangle_B + |0\rangle_A|1\rangle_B}{\sqrt{2}}. \tag{5.16}$$

The photon in arm B is then subjected to the unitary evolution $\hat{S} = e^{-i\hat{H}t}$ where

$$\hat{H} = i\chi(\hat{a}^2 - \hat{a}^{\dagger^2}) \tag{5.17}$$

is the single-mode squeezing Hamiltonian, which can be implemented by type-I parametric down conversion. The total state after the application of S becomes

$$|\psi_s\rangle = \frac{|1\rangle_A|S_0\rangle_B + |0\rangle_A|S_1\rangle_B}{\sqrt{2}}, \tag{5.18}$$

where

$$|S_0\rangle = \hat{S}|0\rangle = \frac{1}{\sqrt{\cosh r}} \sum_{n=0}^{\infty} \frac{\sqrt{(2n)!}}{2^n n!} (-\tanh r)^n |2n\rangle \tag{5.19}$$

and

$$|S_1\rangle = \hat{S}|1\rangle = \frac{1}{\sqrt{(\cosh r)^3}} \sum_{n=0}^{\infty} \frac{\sqrt{(2n+1)!}}{2^n n!} (-\tanh r)^n |2n+1\rangle, \tag{5.20}$$

with $r = \chi t$. For derivation of Eq.(5.19, 5.20) see Appendix C. For large enough squeezing parameter r the state $|\psi_s\rangle$ is a superposition of two components with largely different mean

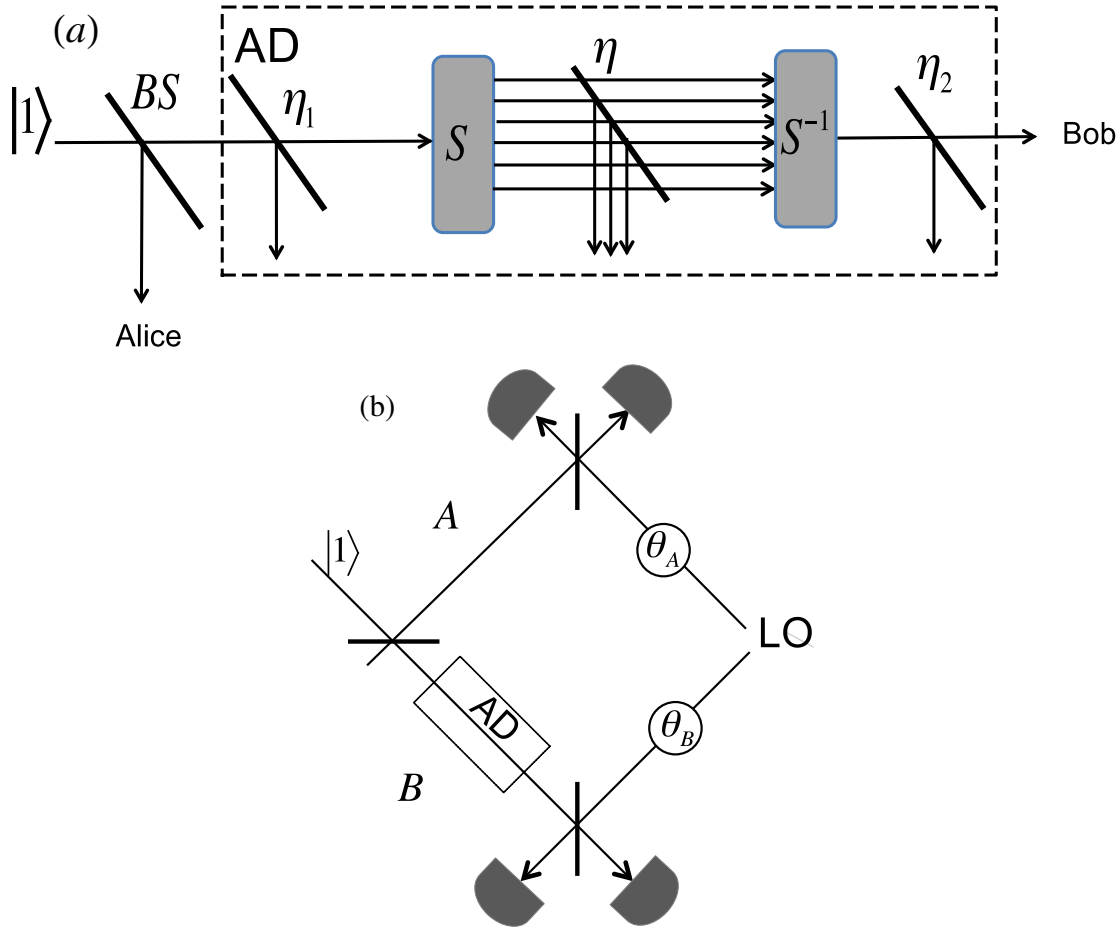

Figure 5.2: Schematic of the proposed experiment. (a) A single photon is sent onto the beam splitter *BS*, which creates the single-photon entangled state of Eq. (5.18). Mode A is directly measured, see below. Mode B is first amplified by the single-mode squeezer S and then de-amplified by S^{-1}. The pump laser beams necessary for implementing S and S^{-1} are not shown for simplicity. Losses before S, between S and S^{-1}, and after S^{-1} are taken into account through transformation factors η_1, η and η_2, respectively. If the modes A and B are found to be entangled at the end, one can infer the existence of micro-macro entanglement between the applications of S and S^{-1}. (b) Measurement scheme including the local oscillator *LO* (which is a laser) which is essential for performing homodyne tomography (means to reconstruct the wave function of the photons) of the final state. The box *AD* represents the amplification and de-amplification process described in (a).

photon numbers. To see this, we calculate

$$n_0 = \langle S_0|\hat{a}^\dagger \hat{a}|S_0\rangle = \sinh^2(r) \tag{5.21}$$

and

$$n_1 = \langle S_1|\hat{a}^\dagger \hat{a}|S_1\rangle = 1 + 3\sinh^2(r). \tag{5.22}$$

For large enough values of r one has $n_1/n_0 \sim 3$. In Fig.(5.3) we show the photon number distributions for the states $|S_0\rangle$ and $|S_1\rangle$, as well as their Wigner functions. Note that values of r much greater than those used in the figure were achieved in the experiment of Ref. [116], where thousands of photons were created on the macro side.

So far we have discussed the amplification process. In order to study the effects of photon loss and subsequent de-amplification as shown in Fig(5.2), it is most convenient to work with the Wigner function. The Wigner function corresponding to the state of Eq. (5.16) is given by

$$W_{in}(X_A, P_A, X_B, P_B) = \frac{1}{2}\sum_{m,n=0}^{m,n=1} W_{m,n}(X_A, P_A) W_{1-m,1-n}(X_B, P_B), \tag{5.23}$$

where $W_{0,0}(X_i, P_i) = \frac{e^{-(X_i^2+P_i^2)}}{\pi}$, $W_{1,0}(X_i, P_i) = \frac{\sqrt{2}(X_i+iP_i)e^{-(P_i^2+X_i^2)}}{\pi} = W_{0,1}^*(X_i, P_i)$ and $W_{1,1}(X_i, P_i) = \frac{(-1+2X_i^2+2P_i^2)e^{-(P_i^2+X_i^2)}}{\pi}$ with $i = A, B$. X_i,P_i are the position and momentum quadratures respectively.

The effect of squeezing in the phase space is simply given by the following transformation: $X_B \to e^r X_B$, $P_B \to e^{-r} P_B$. This implies that the Wigner function after squeezing is given by $W_s(X_A, P_A, X_B, P_B) = W_{in}(X_A, P_A, e^r X_B, e^{-r} P_B)$.

In the absence of photon loss, the prepared macroscopic state in arm B would now undergo the de-amplification operation S^{-1}, which can be realized by changing the sign of χ. Experimentally this can be done either by inverting the phase of the pump laser or by inverting the sign of the non-linear coefficient of the second non-linear crystal, in analogy to what is done in periodic poling [134]. In practice the de-amplification will always be preceded by a certain amount of photon loss. In this case the final state is no longer exactly equal to the initial state,

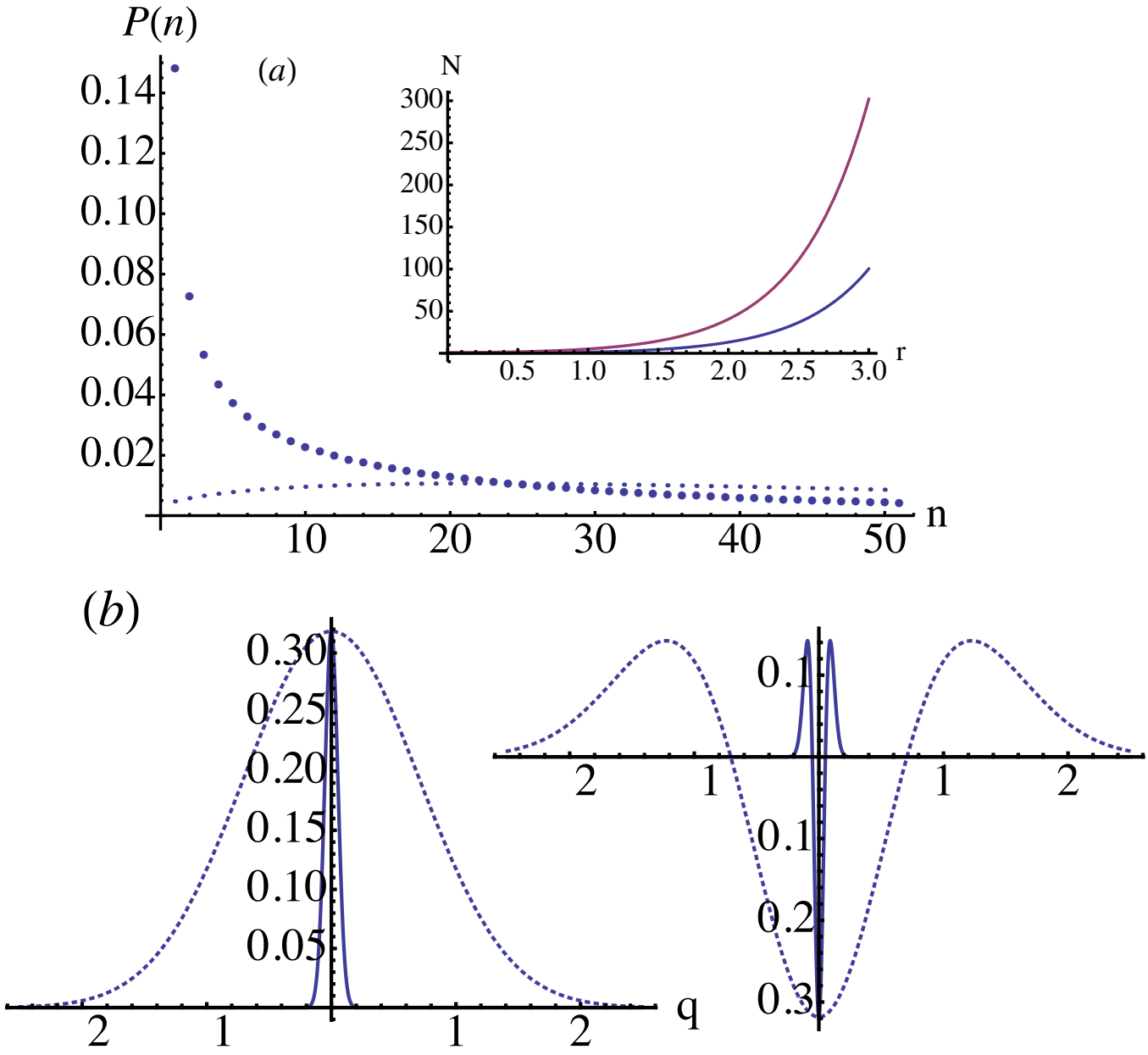

Figure 5.3: (a) Photon probability distributions of $|S_0\rangle$ (big dots) and $|S_1\rangle$ (small dots) for $r = 2.6$. The inset shows the mean photon numbers for the same two states as a function of r, see also Eqs. (5.21) and (5.22). (b) Cross section of the Wigner function of $|S_0\rangle$ (left) and $|S_1\rangle$ (right) for the cutting plane $P = 0$. The dotted curves are the Wigner functions of $|0\rangle$ and $|1\rangle$, respectively. Note that the other quadrature (which is not shown here) is correspondingly elongated due to the Heisenberg uncertainty principle.

in particular there will be higher order excitations in the number basis (beyond one). We will first discuss only loss between S and S^{-1}, which is the most critical imperfection; loss before S and after S^{-1} will be discussed below.

The effect of loss in phase space is described by a convolution [135]

$$W_{s,\eta}(X_A,P_A,X_B,P_B) = \int_{-\infty}^{\infty} dX'_B dP'_B W_s(X_A,P_A,X'_B,P'_B) F_\eta(X_B,P_B,X'_B,P'_B) \tag{5.24}$$

with the attenuation kernel

$$F_\eta(X_B,P_B,X'_B,P'_B) = \frac{\exp[-\frac{\eta}{1-\eta}((X'_B-\frac{X_B}{\sqrt{\eta}})^2+(P'_B-\frac{P_B}{\sqrt{\eta}})^2))]}{\pi(1-\eta)}. \tag{5.25}$$

The Wigner function of the final state after de-squeezing is given by $W_{s,\eta,s^{-1}}(X_A,P_A,X_B,P_B) = W_{s,\eta}(X_A,P_A,e^{-r}X_B,e^{r}P_B)$.

To determine the density matrix of the final state in the photon number basis we use the following property of the Wigner function [135]

$$tr[\hat{O}_1\hat{O}_2] = 2\pi \int_{-\infty}^{\infty} dX dP W_1(X,P) W_2(X,P) \tag{5.26}$$

where $W_1$and W_2 are the Wigner functions of operators $\hat{O}_1$ and $\hat{O}_2$, respectively. If we set $\hat{O}_2 = |m\rangle\langle n|$ and $\hat{O}_1 = \hat{\rho}$ in Eq.(5.26) we obtain the following expression for the density matrix in the photon number basis,

$$\rho_{mn} = 2\pi \int_{-\infty}^{\infty} dX dP W(X,P) W_{mn}(X,P) \tag{5.27}$$

As mentioned above, on the B side the final state will in general have higher-order components in the Fock basis. As it is difficult to quantify entanglement in high-dimensional systems, we will here focus on the projection of the final state onto the zero and first excitation subspace for mode B, i.e

$$\hat{\rho}_p = (\hat{I}_A \otimes \hat{P}_B)\hat{\rho}(\hat{I}_A \otimes \hat{P}_B), \tag{5.28}$$

where $\hat{I}_A$ is the identity operator in mode A and P_B is the projection in subspace $\{|0\rangle_B, |1\rangle_B\}$ in arm B. Since the local projection $\hat{P}_B$ cannot create entanglement, any entanglement present in

$\hat{\rho}_p$ also had to be present in $\hat{\rho}$. Similarly, any entanglement present in $\hat{\rho}$ had to be present in the micro-macro state created by the amplification stage because the loss and de-amplification are also local processes.

The projected density matrix $\hat{\rho}_p$ has the following form in the Fock state basis,

$$\hat{\rho}_p = \begin{pmatrix} p_{00} & 0 & 0 & d' \\ 0 & p_{01} & d & 0 \\ 0 & d^* & p_{10} & 0 \\ d'^* & 0 & 0 & p_{11} \end{pmatrix}, \tag{5.29}$$

where p_{ij} is the probability to find i photons in arm A and j photons in arm B; d is the coherence term between $|1\rangle_A|0\rangle_B$ and $|0\rangle_A|1\rangle_B$, d' is the coherence between $|0\rangle_A|0\rangle_B$ and $|1\rangle_A|1\rangle_B$. One should note that the projected density matrix is not normalized. In fact the success probability of projection is given by $Tr(\hat{\rho}_p) = p_{00} + p_{01} + p_{10} + p_{11}$. In the initial state $p_{01} = p_{10} = d = \frac{1}{2}$, with all other coefficients equal to zero. One sees that the combination of amplification, loss in between, and de-amplification can create new population terms as well as a new coherence. However, certain coherences are still exactly zero (under otherwise ideal conditions). This can be understood by noting that neither the Hamiltonian nor the loss can create coherence between neighboring photon number states (in a given mode). The zero elements in Eq. (5.29) can also be understood in term of the reflection symmetry of the initial state and attenuation kernel Eq. (5.25).

To characterize entanglement we use the concurrence[136] which is defined as

$$C(\hat{\rho}_p) = \max(0, \lambda_1 - \lambda_2 - \lambda_3 - \lambda_4) \tag{5.30}$$

where λ_i are the eigenvalues in decreasing order of the Hermitian matrix $\sqrt{\sqrt{\hat{\rho}_p}\tilde{\rho}_p\sqrt{\hat{\rho}_p}}$ with $\tilde{\rho}_p = (\hat{\sigma}_y \otimes \hat{\sigma}_y)\hat{\rho}_p^*(\hat{\sigma}_y \otimes \hat{\sigma}_y)$. For the density matrix in Eq.(5.29) the concurrence is given by

$$C(\hat{\rho}_p) = \max\{0, 2(|d| - \sqrt{p_{00}p_{11}}), 2(|d'| - \sqrt{p_{10}p_{01}})\}. \tag{5.31}$$

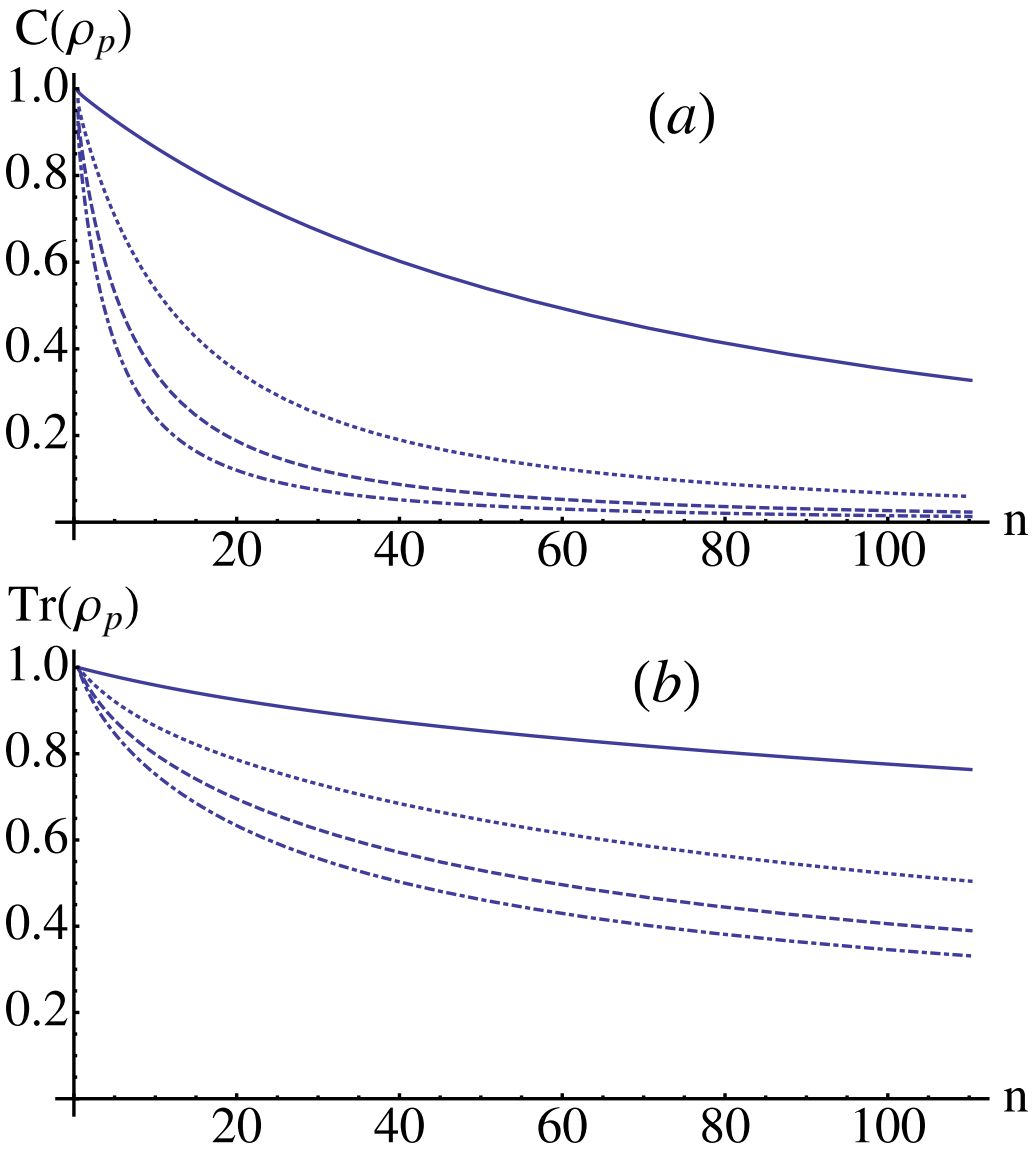

Figure 5.4: (a) Concurrence of the final state as a function of the mean photon number after the amplification, $n = \frac{n_0+n_1}{2}$, for different values of the attenuation between amplification and de-amplification, η. The solid, dotted, dashed and dot-dashed curves correspond to $\eta = 0.99, 0.95, 0.9, 0.85$, respectively. (b) Probability of projecting the final state into the subspace spanned by the zero and one photon states for the same values of η.

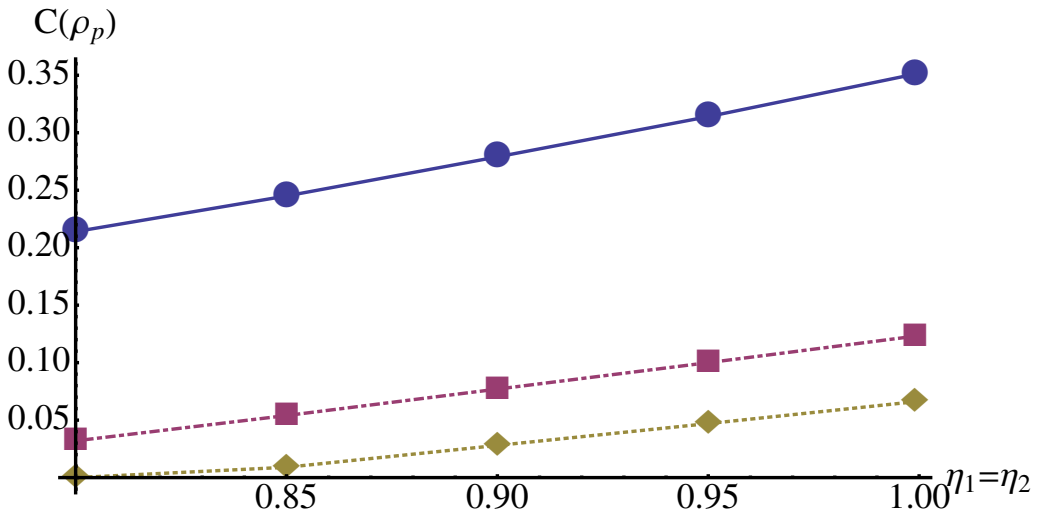

Figure 5.5: Concurrence of the final state for a fixed mean photon number $n = 100$ for different values of η, for $\eta_1 = \eta_2$ varying together. Circles, cubes and diamonds correspond to $\eta = 0.99, 0.97, 0.95$ respectively. One can see that the entanglement is much more sensitive to η than to η_1 and η_2.

Fig.(5.4)(a) shows the concurrence as a function of mean photon number $n = \frac{n_0+n_1}{2}$ after squeezing for different values of attenuation η. One notes the high sensitivity of the concurrence to the attenuation. However, in practice it should be possible to keep losses between the two non-linear crystals very low, values of η as high as 0.99 should be realistic. One promising approach would be to realize amplification and de-amplification in a single solid-state system, where the two active non-linear sections could be separated by a non-active spacer layer. Note that the experiment would typically be performed with femtosecond pulses, so it would not be difficult to make non-active layer thick enough to contain the entire pulse. The macro component of the micro-macro entangled state would then exist for a short span of time in that spacer layer. Fig. 3(b) shows that the success probability for projecting the system into the zero-or-one photon subspace decreases as the amount of loss and the mean photon number are increased, but that it is still quite significant in the regime under consideration.

Fig.(5.4) suggests that micro-macro entanglement involving hundreds of photons might be observable with the proposed scheme. To confirm this suggestion, it is still important to study

the effect of losses before the amplification and after the de-amplification, η_1 and η_2. These losses are harder to minimize in practice. In particular, η_2 also includes detector inefficiency. However, values of order $\eta_1 = \eta_2 = 0.9$ should be achievable [137]. Figure (5.5) shows that a substantial amount of entanglement is still present in the system under these conditions for a mean photon number $n = 100$. One can see that the micro-macro photon-number entanglement is much less sensitive to η_1 and η_2 than to η, similarly to the results of Ref. [123] for micro-macro polarization entanglement.

The entanglement can be demonstrated experimentally by using full homodyne tomography, which was already used to demonstrate the non-locality of single-photon entanglement in Ref. [125]. In this method the full density matrix is reconstructed from the joint quadrature statistics $p_{\theta_A,\theta_B}(X_A, X_B)$ for different values of the local oscillator phases θ_A and θ_B. In particular this allows one to reconstruct the density matrix in the zero and one-photon subspace which is relevant for us here.

5.2 Conclusion

We have proposed to create and detect micro-macro photon-number entanglement by amplifying and then de-amplifying a single-photon entangled state. In particular, the present approach should allow the creation and detection of entangled states that are superpositions of two components with very different mean photon numbers (for example, 50 and 150).

Conclusion and Outlook

In conclusion we have studied macroscopic quantum effects in optomechancial and optical systems. We studied optomechanical entanglement and also discussed how it will change in the presence of the laser phase noise. Our results show that optomechanical entanglement is very sensitive to the laser phase noise. This motivated us to study single photon optomechanics. We proposed that one can enhance the weak optomechancial coupling constant in the single photon regime by using post selection and then described a scheme for probing the optomechancial superpositions. The experimental requirements for realizing this scheme have been discussed.

Motivated by recent experiment by De Martini et.al [116] and very recent studies in [119, 123], we presented a new scheme for creating and detecting micro- macro entanglement based on amplifying a single photon entangled state. The focus in this part is to understand how precise the measurements should be to be able to verify micro- macro entanglement.

The next logical step is to study the experimental requirements for observing optomechanical entanglement with special emphasis on the measurement precision. In other words, how sensitive should the measurements be in order to be able to verify the optomechancial entanglement.

Another interesting problem is to combine our scheme for creating optical Schrodinger cat with the optomechanics. One advantage of this method is that it allows larger values for the optomechanical coupling.

Appendix A

An introduction to Gaussian states

In this appendix, we briefly review some important aspects of continues variable (CV) state. We also briefly discuss the entanglement measure that we used in chapters 2 and 3.

In the phase space description of classical mechanics the state of the system consisting of N particles is described by the position and momentum variables which fulfil the following relations

$$\{R_i, R_j\} = \sigma_{ij} \tag{A.1}$$

where, denotes the Poisson bracket, $R = (x_1, p_1, , x_N, p_N)^T$ and σ is the symplectic matrix defined as

$$\sigma = \oplus_{i=1}^{N} \begin{pmatrix} 0 & 1 \\ -1 & 0 \end{pmatrix} \tag{A.2}$$

In quantum mechanics the previous description is still valid if we replace position and momentum variables with their corresponding operators,i.e. $x_n \to \hat{x}_n$,$p_n \to \hat{p}_n$, Poisson bracket with commutator $[,]$. Now instead of Eq.(A.1) we have

$$[\hat{R}_j, \hat{R}_k] = i\sigma_{jk}\hat{1} \tag{A.3}$$

with $\hat{R} = (\hat{x}_1, \hat{p}_1, ..., \hat{x}_N, \hat{p}_N)$.

From quantum mechanics we also know that the complete description of a system is given by its density matrix, denoted by ρ. The density matrix is the analogue of the probability distribution of the classical system. It is also known that the probability distribution can be completely characterized by its moments which are experimentally accessible. This is also true for the density matrix.

The first and second order moments of a state ρ, known as displacement vector and covariance matrix,respectively, defined as

$$\langle \hat{R} \rangle = tr[\rho \hat{R}_j] \tag{A.4}$$

$$V_{ij} = tr[\rho \{\hat{R}_i - \langle \hat{R}_i \rangle, \hat{R}_j - \langle \hat{R}_j \rangle\}] \tag{A.5}$$

using Eq.(A.3) we can rewrite Eq.(A.5)

$$V_{ij} = 2tr[\rho (\hat{R}_i - \langle \hat{R}_i \rangle)(\hat{R}_j - \langle \hat{R}_j \rangle)] - i\sigma_{ij} \tag{A.6}$$

Now one can show that Eq.(A.6) implies that

$$V + i\sigma \geq 0 \tag{A.7}$$

It is interesting that Eq.(A.7) is exactly the uncertainty relation. To see this, it is enough to check Eq.(A.7) for one-mode state. In this case we have

$$V + i\sigma = \begin{pmatrix} 2\langle \hat{q}^2 \rangle & i \\ -i & 2\langle \hat{p}^2 \rangle \end{pmatrix} \tag{A.8}$$

now Eq.(A.7) implies $\langle \hat{q}^2 \rangle \langle \hat{p}^2 \rangle \geq \frac{1}{4}$ which is the uncertainty relation.

A.0.1 Gaussian states

For the transformation from Hilbert space to phase space we need to define the Weyl operator defined as

$$\hat{W}_\xi = e^{i\xi^T \sigma \hat{R}} \tag{A.9}$$

The important properties Weyl operators are

$$\hat{W}_\xi \hat{W}_\zeta = e^{-i\xi^T \sigma \zeta} \hat{W}_{\xi+\zeta} \tag{A.10}$$

$$tr(\hat{W}_\xi \hat{W}_\zeta) = (2\pi)^N \delta^{2N}(\xi - \zeta) \tag{A.11}$$

Eq.(A.10) is called orthogonality condition for Weyl operator. It makes it possible to expand any linear bounded operator in term of the Weyl operator,i.e.

$$\hat{A} = \frac{1}{(2\pi)^{2N}} \int d^{2N}\xi \, f_A(-\xi)\hat{W}_\xi \tag{A.12}$$

f_A is the unique weighting function. Using the orthogonality property of Weyl operator,Eq.(A.10), one can show

$$f_A(\xi) = tr(\hat{A}\hat{W}_\xi) \tag{A.13}$$

we can also expand the density matrix in term of the Weyl operator. the coefficient of expansion in this case is called the characteristic function which is denoted by $\chi_\rho(\xi)$ which is given by

$$\chi_\rho(\xi) = tr(\hat{\rho}\hat{W}_\xi) \tag{A.14}$$

means that it is expectation value of the Weyl operator.

Characteristic function allow us to map any density matrix to $\mathscr{L}^2$ space. The inverse Fourier transform of the characteristic function,which is called Wigner function, is analogous to the probability distribution in the phase space. More explicitly we have

$$W(\xi) = \frac{1}{(2\pi)^{2N}} \int d\eta \, \chi_\rho(\eta) e^{-i\xi^T \sigma \eta} \tag{A.15}$$

The Wigner function is not always a probability distribution as it takes negative values because of the quantum nature of the system.

The *Gaussian* state are states which their characteristic function can be written as:

$$\chi_\rho(\xi) = exp[-\frac{1}{4}(\sigma\xi)^T V(\sigma\xi)] \tag{A.16}$$

This means that the Gaussian states are completely determined by their covariance matrix V.

A quantum state ρ of the bipartite system is *separable* if and only if it can be expressed as:

$$\hat{\rho} = \sum_i p_i \hat{\rho}_{i1} \otimes \hat{\rho}_{i2} \tag{A.17}$$

where $p_i \geq 0$ and ρ_1,ρ_2 are the density matrix for system one and two respectively.

From Eq.(A.17) it is clear that if the state be separable then the partial transposed state is still a density matrix as

$$\hat{\rho}^{T_2} = \sum_i p_i \hat{\rho}_{i1} \otimes \hat{\rho}_{i2}^T = \hat{\rho} \tag{A.18}$$

This is the basic idea behind the Peres- Horodecki criterion.

Peres- Horodecki criterion: Let ρ be a density matrix in the Hilbert space $\hat{\mathscr{H}} = \hat{\mathscr{H}}_A \otimes \hat{\mathscr{H}}_B$ with non-positive partial transpose. Then the state is the entangled.

A.0.2 Simon criterion

R.Simon extend the Peres-Horodecki criterion for CV states. The basic idea is that the partial transpose operation in the phase space is equivalent to time reversal of a subsystem, so equivalent to momentum inversion. To see this we start with a following representation of the Wigner function for bipartite CV system

$$W(\xi) = \frac{1}{(2\pi)^2} \int d^2x \langle q - x|\hat{\rho}|q + x\rangle e^{-ixp} \tag{A.19}$$

with $\xi = (q_1, q_2, p_1, p_2)^T$, $q = (q_1, q_2)^T$, $p = (p_1, p_2)$ and $x = (x_1, x_2)$. Let say we take partial transpose with respect to the second subsystem. By definition we have $\langle q_1, q_2|\hat{\rho}^{T_2}|q_1^{'}, q_2^{'}\rangle = \langle q_1, q_2^{'}|\hat{\rho}|q_1^{'}, q_2\rangle$ The Wigner function of the partially transposed matrix is then given by

$$W^{PT}(\xi) = \frac{1}{(2\pi)^2} \int d^2x \langle q - x|\hat{\rho}^{T_2}|q + x\rangle e^{-i(Zx)^T p} \tag{A.20}$$

where $Z = diag[1,-1]$. This implies that partial transpose operation inverts the associated momentum p_2. From this observation we arrive to the following statement

$$W^{PT}(\xi) = W(\Lambda\xi) \tag{A.21}$$

where $\Lambda = diag[1,1,1,-1]$. It is simple to verify that the effect of partial transposition on the covariance matrix is given by

$$V \to \Lambda V \Lambda \tag{A.22}$$

With this interoperation of the partial transposition for CV state, we can apply the Peres-Horodecki criterion to Gaussian states.

Simon criterion: A Gaussian bipartite state (which completely determined by its covariance matrix) is entangled if and only if

$$\Lambda V \Lambda + i\sigma \leq 0 \tag{A.23}$$

We used this criterion in chapter 2 and 3 for quantifying optomechanical entanglement.

Appendix B

Weak measurment

I briefly introduce the basic idea of weak measurement[78, 79].

In standard (projective) measurement, one projects the system of interest (which is in superposition of different state) to one of its eigenvectors of the measured observable. The basic idea behind the weak measurement is to weakly touch the system to reduce the effect associated with measurement process. We don't gain so mush information in this way unless we post select the state of the system after weak measurement. To show this, suppose we have a two level system which is in the initial state $|\psi(0)\rangle = \beta_0|0\rangle + \beta_1|1\rangle$. Where $|0\rangle$ and $|1\rangle$ are the eigenvectors of the observable to be measured which we call it A, $\hat{A}|0\rangle = |0\rangle$ and $\hat{A}|1\rangle = -|1\rangle$. The system is coupled to the measurement apparatus (initially at the state $|M(s)\rangle$) through the Hamiltonian $H = gPA$ where g is the coupling strength between meter (measurement device) and the system which is very small number and P is the momentum operator for the meter. The state of the system at time t is given by $|\psi(\Delta t)\rangle = e^{-i\tau PA}|M(x)\rangle|\psi(0)\rangle = \beta_0|M_0\rangle|0\rangle + \beta_1|M_1\rangle|1\rangle$ where $\tau = g\Delta t$. Now we note that in the projective measurement we have $\langle M_0|M_1\rangle = 0$ which means that the meter completely determines the state of the system. Since we consider the weak coupling between system and meter we do not expect that this condition be fulfilled, instead we expect to have $\langle M_0|M_1\rangle \sim 1$. This means that the state of the meter before and after the measurement is almost the same. The difference between $|M_0\rangle$ and $|M_1\rangle$ is such small that the detector can not resolve them (The signal is smaller than the detector noise). Now let assume that after measurement we post select the state of the system to the state $|\varphi\rangle$. The state of the meter is now given by $\langle\varphi|e^{-i\tau PA}|M(x)\rangle|\psi(0)\rangle$, which can be written as

$$\langle\varphi|\psi(0)\rangle(1-\tau PA_w)|M(x)\rangle \simeq \langle\varphi|\psi(0)\rangle e^{-i\tau A_w P}|M(x)\rangle \tag{B.1}$$

where A_w is called the weak value and is given by

$$A_w = \frac{\langle \varphi | A | \psi(0) \rangle}{\langle \varphi | \psi(0) \rangle} \tag{B.2}$$

Now if the post selected state chosen such that it almost be orthogonal to the initial state ($\langle \varphi | \psi(0) \rangle \sim 0$) then the weak value can be large number. In term of meter displacement this means that we now have $|M(x \pm \tau A_w)\rangle$, which shows the meter displacement may increase in such a way that it can be used to infer the state of the system.

In our proposed scheme for post-selection in chapter.4 the states $|\psi\rangle$ and $|\varphi\rangle$ are

$$|\psi\rangle = \frac{|1_A 0_B\rangle + |0_A 1_B\rangle}{\sqrt{2}} \tag{B.3}$$

$$|\varphi\rangle = \frac{|1_A 0_B\rangle - |0_A 1_B\rangle}{\sqrt{2}} \tag{B.4}$$

Our post selection scheme is different from weak measurement because of the orthogonality of initial state and the post selected state.

Appendix C

Derivation of Equations 5.19 and 5.20

We start with the following identity for the vacuum state

$$\hat{a}|0\rangle = 0 \tag{C.1}$$

Multiplying Eq.(C.1) from left by $\hat{S}$ and using the fact that $\hat{S}(r)$ is unitary we can write

$$\hat{S}(r)\hat{a}\hat{S}^{\dagger}(r)\hat{S}(r)|0\rangle = 0 \tag{C.2}$$

or

$$\hat{S}(r)\hat{a}\hat{S}^{\dagger}(r)|S_0\rangle = 0 \tag{C.3}$$

Now we use the following identity[44]

$$\hat{S}(r)\hat{a}\hat{S}^{\dagger}(r) = coshr\hat{a} + sinhr\hat{a}^{\dagger} \tag{C.4}$$

we can rewrite Eq.(C.3) as

$$(coshr\hat{a} + sinhr\hat{a}^{\dagger})|S_0\rangle = 0 \tag{C.5}$$

Now we expand the state $|S_0\rangle$ in term the number state

$$|S_0\rangle = \sum_{n=0}^{\infty} c_n|n\rangle \tag{C.6}$$

substituting Eq.(C.6) in Eq.(C.5) we get the following recursion relation

$$c_{n+1} = -tanhr(\frac{n}{n+1})^{1/2}c_{n-1} \tag{C.7}$$

from Eq.(C.7) and using the normalization condition for $|S_0\rangle$ we obtain

$$c_{2n} = (-1)^n \frac{\sqrt{(2n)!}}{2^n n!} \frac{(tanhr)^n}{\sqrt{coshr}} \tag{C.8}$$

Thus the squeezed vacuum state is (5.19)

$$|S_0\rangle = \sum_{n=0}^{\infty} (-1)^n \frac{\sqrt{(2n)!}}{2^n n!} \frac{(tanhr)^n}{\sqrt{coshr}} |2n\rangle \tag{C.9}$$

We now drive Eq.(5.20).

$$\hat{S}|1\rangle = \frac{1}{coshr} a^\dagger \hat{S}|0\rangle \tag{C.10}$$

which using Eq.(C.9) immediately results

$$|S_1\rangle = \sum_{n=0}^{\infty} (-1)^n \frac{\sqrt{(2n+1)!}}{2^n n!} \frac{(tanhr)^n}{(coshr)^{3/2}} |2n+1\rangle \tag{C.11}$$

Bibliography

[1] D. Vitali, S. Gigan, A. Ferreira, H. R. Bohm, P. Tombesi, A. Guerreiro, V. Vedral, A. Zeilinger, and M. Aspelmeyer, "Optomechanical entanglement between a movable mirror and a cavity field," *Phys. Rev. Lett*, vol. 98, p. 030405, 2007.

[2] E. Verhagen, S. Deléglise, S. Weis, A. Schliesser, and T. Kippenberg, "Quantum-coherent coupling of a mechanical oscillator to an optical cavity mode," *Nature*, vol. 482, p. 63, 2012.

[3] S. Groblacher, K. Hammerer, M. R. Vanner, and M. Aspelmeyer, "Observation of strong coupling between a micromechanical resonator and an optical cavity field," *Nature*, vol. 460, p. 724, 2009.

[4] J. Ellis, J. Hagelin, D. Nanopoulos, and M. Serdnicki, "Supersymmetric relics from the big bang," *Nucl. Phys. B*, vol. 241, p. 381, 1984.

[5] J. Ellis, N. Mavromatos, and D. Nanopoulos, "String theory modifies quantum mechanics," *Phys. Lett. B*, vol. 293, p. 37, 1992.

[6] R. Penrose, "On gravity's role in quantum state reduction," *Gen. Relativ. Gravit*, vol. 28, p. 581, 1996.

[7] L.Diosi, "Models for universal reduction of macroscopic quantum fluctuations," *Phys. Rev. A*, vol. 40, p. 1165, 1989.

[8] W.Marshall, C. Simon, R. Penrose, and D.Bouwmeester, "Towards quantum superpositions of a mirror," *Phys. Rev. Lett.*, vol. 91, p. 130401, 2003.

[9] V. B. Braginsky, *Measurement of Weak Forces in Physics Experiments*. University of Chicago Press, Chicago, 1977.

[10] T. Corbitt, Y. Chen, E. Innerhofer, H. Muller-Ebhardt, D. Ottaway, H. Rehbein, D. Sigg, S. Whitcomb, C. Wipf, and N. Mavalvala, "An all-optical trap for a gram-scale mirror," *Phys. Rev. Lett*, vol. 98, p. 150805, 2007.

[11] C. H. Metzger and K. Karrai, "Cavity cooling of a microlever," *Nature*, vol. 432, p. 1002, 2004.

[12] D. Kleckner and D. Bouwmeester, "Sub-kelvin optical cooling of a micromechanical resonator," *Nature*, vol. 444, p. 75, 2006.

[13] T. Carmon, H. Rokhsari, L. Yang, T. J. Kippenberg, and K. J. Vahala, "Temporal behavior of radiation-pressure-induced vibrations of an optical microcavity phonon mode," *Phys. Rev. Lett*, vol. 94, p. 223902, 2005.

[14] J. Thompson, B. Zwickl, A. M. Jayich, F. Marquardt, S. Girvin, and G. Harris, "Strong dispersive coupling of a high-finesse cavity to a micromechanical membrane," *Nature*, vol. 452, p. 72, 2008.

[15] M. Eichenfield, J. Chan, R. M. Camacho, K. J. Vahala, and O. Painter, "Optomechanical crystals," *Nature*, vol. 462, p. 78, 2009.

[16] V. B. Braginsky and A. Manukin *Sov. Phys. JETP*, vol. 25, p. 653, 1967.

[17] P. Pathria, *Statistical Mechanics*. Butteworth Heineman, 1996.

[18] A. Dorsel, J. D. McCullen, P. Meystre, E. Vignes, and H. Walther, "Optical bistability and mirror confinement induced by radiation pressure," *Phys. Rev. Lett*, vol. 51, p. 1550, 1983.

[19] C.K.Law, "Interaction between a moving mirror and radiation pressure: A hamiltonian formulation," *Phys. Rev. A*, vol. 51, p. 2537, 1995.

[20] J. D. Jackson, *Classical Electrodynamics*. John Wiley Sons, 3rd ed., 1998.

[21] S. Mancini, V. Giovannetti, D. Vitali, and P. Tombesi, "Entangling macroscopic oscillators exploiting radiation pressure entangling macroscopic oscillators exploiting radiation pressure," *Phys. Rev. Lett*, vol. 88, p. 120401, 2002.

[22] S. Bose, K. Jacobs, and P. Knight, "Scheme to probe the decoherence of a macroscopic object," *Phys. Rev. A*, vol. 59, p. 3204, 1999.

[23] O. Romero-Isart, A. Pflanzer, F. Blaser, R. Kaltenbaek, N. Kiesel, and M. Aspelmeyer, "Large quantum superpositions and interference of massive nanometer-sized objects," *Phys. Rev. Lett*, vol. 107, p. 020405, 2011.

[24] B. Pepper, R. Ghobadi, E. Jeffrey, C. Simon, and D. Bouwmeester, "Quantum supperpositions via nested interferometry," *Phys. Rev. Lett*, vol. 109, p. 023601, 2012.

[25] J. D. Teufel, T. Donner, D. Li, J. H. Harlow, M. S. Allman, K. Cicak, A. J. Sirois, J. D. Whittaker, K. W. Lehnert, and R. W. Simmonds, "Sideband cooling micromechanical motion to the quantum ground state," *Nature*, vol. 475, p. 359, 2011.

[26] J.Chan, T.P.M.Alegre, .H.Safavi-Naeini, J. Hill, A. Krause, S. Groblacher, M. Aspelmeyer, and O. Painter, "Laser cooling of a nanomechanical oscillator into its quantum ground state," *Nature*, vol. 478, p. 89, 2011.

[27] A. H. Safavi-Naeini, J. Chan, J. T. Hill, T. P. M. Alegre, A. Krause, and O. Painter, "Observation of quantum motion of a nanomechanical resonator," *Phys. Rev. Lett*, vol. 108, p. 033602, 2012.

[28] A. A. Clerk, M. H. Devoret, S. M. Girvin, F. Marquardt, and R. J. Schoelkopf, "Introduction to quantum noise, measurement, and amplification," *Rev. Mod. Phys*, vol. 88, p. 1155, 2010.

[29] K.-J. Boller, A. Imamolu, and S. E. Harris, "Observation of electromagnetically induced transparency," *Phys. Rev. Lett.*, vol. 66, p. 2593, 1991.

[30] G. S. Agarwal and S. Huang, "Electromagnetically induced transparency in mechanical effects of light," *Phys. Rev. A*, vol. 81, p. 041803, 2010.

[31] S. Weis, R. Riviere, S. Deleglise, E. Gavartin, O. Arcizet, A. Schliesser, and T. J. Kippenberg, "Optomechanically induced transparency," *Science*, vol. 330, no. 6010, p. 1520, 2010.

[32] R. J. Glauber, "Coherent and incoherent states of the radiation field," *Phys. Rev*, vol. 131, p. 2766, 1963.

[33] S. Bose, K. Jacobs, and P. Knight, "Preparation of nonclassical states in cavities with a moving mirror," *Phys. Rev. A*, vol. 56, p. 4175, 1997.

[34] R. Ghobadi, A. Bahrampour, and C. Simon, "Quantum optomechanics in the bistable regime," *Phys. Rev. A*, vol. 84, p. 033846, 2011.

[35] R. Penrose, *Mathematical Physics*. Imperial Colledge, London, 2000.

[36] A. D. Armour, M. P. Blencowe, and K. C. Schwab, "Entanglement and decoherence of a micromechanical resonator via coupling to a cooper-pair box," *Phys. Phys.Rev. Lett*, vol. 88, p. 148301, 2002.

[37] F. Marquardt, J. G. E. Harris, and S. M. Girvin, "Dynamical multistability induced by radiation pressure in high-finesse micromechanical optical cavities," *Phys. Rev. Lett.*, vol. 96, p. 103901, 2006.

[38] O. Arcizet, P.-F. Cohadon, T. Briant, M. Pinard, and A. Heidmann, "Radiation-pressure cooling and optomechanical instability of a micromirror," *Nature*, vol. 444, p. 71, 2006.

[39] T. Carmon, M. C. Cross, and K. J. Vahala, "Chaotic quivering of micron-scaled on-chip resonators excited by centrifugal optical pressure," *Phys. Rev. Lett*, vol. 98, p. 167203, 2007.

[40] M. Karuza, C. Biancofiore, M. Galassi, R. Natali, G. D. Giuseppe, P. Tombesi, and D. Vitali, "Quantum dynamics of a vibrational mode of a membrane within an optical cavity," 2010.

[41] R. Riviere, S. Deleglise, S. Weis, E. Gavartin, O. Arcizet, A. Schliesser, and T. J. Kippenberg, "Optomechanical sideband cooling of a micromechanical oscillator close to the quantum ground state," *Phys. Rev. A*, vol. 83, p. 063835, 2011.

[42] C. Fabre, M. Pinard, S. Bourzeix, A. Heidmann, E. Giacobino, and S. Reynaud, "Quantum-noise reduction using a cavity with a movable mirror," *Phys. Rev. A*, vol. 49, p. 1337, 1994.

[43] C. Genes, A. Mari, P. Tombesi, and D. Vitali, "Robust entanglement of a micromechanical resonator with output optical fields," *Phys. Rev. A*, vol. 78, p. 032316, 2008.

[44] M. O. Scully and M. S. Zubairy, *Quantum Optics*. Cambridge University Press, 1 edition ed., 1991.

[45] C. Gardiner and P. Zoller, *Quantum Noise: A Handbook of Markovian and Non-Markovian Quantum Stochastic Methods with Applications to Quantum Optics*. Springer, 3rd ed., 2004.

[46] S. Gigan, H. R. Bohm, M. Paternostro, F. Blaser, G. Langer, J. B. Hertzberg, K. C. Schwab, D. Bauerle, M. Aspelmeyer, and A. Zeilinger, "Self-cooling of a micromirror by radiation pressure," *Nature*, vol. 444, p. 66, 2006.

[47] D. Kleckner, W. Marshall, M. J. A. de Dood, K. N. Dinyari, B.-J. Pors, W. T. M. Irvine, and D. Bouwmeester, "High finesse opto-mechanical cavity with a movable thirty-micron-size mirror," *Phys. Rev. Lett*, vol. 96, p. 173901, 2006.

[48] E. DeJesus and C. Kaufman, "Routh-hurwitz criterion in the examination of eigenvalues of a system of nonlinear ordinary differential equations," *Phys. Rev. A*, vol. 35, p. 5288, 1987.

[49] C. Genes, D. Vitali, P. Tombesi, S. Gigan, and M. Aspelmeyer, "Ground-state cooling of a micromechanical oscillator: Comparing cold damping and cavity-assisted cooling schemes," *Phys. Rev. A*, vol. 77, p. 033804, 2008.

[50] I.Wilson-Rae, N.Nooshi, W.Zwerger, and T.J.Kippenberg, "Theory of ground state cooling of a mechanical oscillator using dynamical backaction," *Phys. Rev. Lett*, vol. 99, p. 093901, 2007.

[51] F. Marquardt, J. P. Chen, A. A. Clerk, and S. M. Girvin, "Quantum theory of cavity-assisted sideband cooling of mechanical motion," *Phys. Rev. Lett*, vol. 99, p. 093902, 2007.

[52] R. Simon, "Peres-horodecki separability criterion for continuous variable systems," *Phys. Rev. Lett*, vol. 84, p. 2726, 2000.

[53] A. Peres, "Separability criterion for density matrices," *Phys. Rev. Lett*, vol. 77, p. 1413, 1996.

[54] P. Horodecki, "Separability criterion and inseparable mixed states with positive partial transposition," *Phys.Lett.A*, vol. 232, p. 333, 1997.

[55] G. Adesso, A. Serafini, and F. Illuminati, "Extremal entanglement and mixedness in continuous variable systems," *Phys. Rev. A*, vol. 70, p. 022318, 2004.

[56] R. Ghobadi, A. Bahrampour, and C. Simon, "Optomechanical entanglement in the presence of laser phase noise," *Phys. Rev. A*, vol. 84, p. 063827, 2011.

[57] L. Diosi, "Laser linewidth hazard in optomechanical cooling," *Phys. Rev. A*, vol. 78, p. 021801, 2008.

[58] P. Rabl, C. Genes, K. Hammerer, and M. Aspelmeyer, "Phase-noise induced limitations on cooling and coherent evolution in optomechanical systems," *Phys. Rev. A*, vol. 80, p. 063819, 2009.

[59] H.Haken, *Laser Theory*. Springer-Verlag, Berlin, 1970.

[60] T. Kennedy, T. Derson, and D. Walls, "Effects of laser phase fluctuations on squeezing in intracavity second-harmonic generation," *Phys. Rev. A*, vol. 40, p. 1385, 1989.

[61] W. Goodman, *Statistical Optics*. Wiley, New York, 1986.

[62] M. Aspelmeyer, S. Groblacher, K. Hammerer, and N. Kiesel, "Quantum optomechanics—throwing a glance," *J. Opt. Soc. Am. B*, vol. 27, p. A189, 2010.

[63] M. Abdi, S. Barzanjeh, P. Tombesi, and D. Vitali, "Effect of phase noise on the generation of stationary entanglement in cavity optomechanics," *Phys. Rev. A*, vol. 84, p. 032325, 2011.

[64] B. Pepper, E. Jeffrey, R. Ghobadi, C. Simon, and D. Bouwmeester, "Macroscopic superpositions via nested interferometry: finite temperature and decoherence considerations," *arXiv:1207.1946*, 2012.

[65] D. Kleckner, I. Pikovsky, E. Jeffrey, L.Ament, E. Eliel, J. van den Brink, and D. Bouwmeester, "Creating and verifying a quantum superposition in a micro-optomechanical system," *New J. Physics*, vol. 10, p. 095020, 2008.

[66] D. Kleckner, B. Pepper, E. Jeffrey, P. Sonin, S. Thon, and D. Bouwmeester, "Optomechanical trampoline resonators," *Opt. Express*, vol. 19, p. 19708, 2011.

[67] D. Kleckner, W. T. M. Irvine, S. R. Oemrawsingh, and D. Bouwmeester, "Polychromatic photonic quasicrystal cavities," *Phys. Rev. A*, vol. 81, p. 043814, 2010.

[68] O. Romero-Isart, M. Juan, R. Quidant, and J. Cirac, "Toward quantum superposition of living organisms," *New J. Physics*, vol. 12, p. 033015, 2010.

[69] F. Khalili, S. Danilishin, H. Miao, H. Huller-Ebhardt, H. Yang, and Y. Chen, "Preparing a mechanical oscillator in non-gaussian quantum states," *Phys. Rev. Lett*, vol. 105, p. 070403, 2010.

[70] U. Akram, N. Kiesel, M. Aspelmeyer, and G. Milburn, "Single-photon opto-mechanics in the strong coupling regime," *New J. Physics*, vol. 12, p. 083030, 2010.

[71] M. Vanner, I. Pikovsky, G. Cole, M. Kim, C. Brukner, K. Hammerer, G. Milburn, and M. Aspelmeyer, "Pulsed quantum optomechanics," *PNAS*, vol. 108, p. 16182, 2011.

[72] R. Kaltenbaek, G. Hechenblaikner, N. Kiesel, O. Romero-Isart, K. C. Schwab, U. Johann, and M. Aspelmeyer, "Macroscopic quantum resonators," *Exp.Astron*, vol. 34, p. 123, 2012.

[73] A. A. Clerk, F. Marquardt, and K. Jacobs, "Back-action evasion and squeezing of a mechanical resonator using a cavity detector," *New J. Physics*, vol. 10, p. 095010, 2008.

[74] A. Nunnenkamp, K. Borkje, J. Harris, and S. Girvin, "Cooling and squeezing via quadratic optomechanical coupling," *Phys. Rev. A*, vol. 82, p. 021806, 2010.

[75] R. Weiss, "Electromagnetically coupled broad band gravitational antenna," *MIT Res. Lab. Electron. Q. Prog. Rep*, vol. 105, p. 54, 1972.

[76] J. Franson, "Two-photon interferometry over large distances," *Phys. Rev. A*, vol. 44, p. 4552, 1991.

[77] W. Tittel, J. Brendel, H. Zbinden, and N. Gisin, "Violation of bell inequalities by photons more than 10 km apart," *Phys. Rev. Lett*, vol. 81, p. 3563, 1998.

[78] Y. Aharonov, D. Albert, and L. Vaidman, "How the result of a measurement of a component of the spin of a spin-1/2 particle can turn out to be 100," *Phys. Rev. Lett*, vol. 60, p. 1351, 1988.

[79] Y. Aharonov and L. Vaidman, "Properties of a quantum system during the time interval between two measurements," *Phys. Rev. A*, vol. 41, p. 11, 1990.

[80] T. Geszti, "Postselected weak measurement beyond the weak value," *Phys. Rev. A*, vol. 81, p. 044102, 2010.

[81] S. Wu and Y. Li, "Weak measurements beyond the aharonov-albert-vaidman formalism," *Phys. Rev. A*, vol. 83, p. 052106, 2011.

[82] W. Zurek, "Decoherence, einselection, and the quantum origins of the classical," *Rev. Mod. Phys*, vol. 75, p. 715, 2003.

[83] G. Ghirardi, P. Pearle, and A. Rimini, "Markov processes in hilbert space and continuous spontaneous localization of systems of identical particles," *Phys. Rev. A*, vol. 42, p. 78, 1990.

[84] P. Pearle, "Combining stochastic dynamical state-vector reduction with spontaneous localization," *Phys. Rev. A*, vol. 39, p. 2277, 1989.

[85] T.Hong, H. Yang, H. Miao, and Y. Chen, "Open quantum dynamics of single-photon optomechanical devices," *arXiv*, 2011.

[86] A. OConnell, M. Hofheniz, M. Ansmann, R. Bialczak, M. Lenander, E. Lucero, M. Neeley, D. Sank, H. Wang, M. Weides, J. Wenner, J. M. Martinis, and A. Cleland, "Quantum ground state and single-phonon control of a mechanical resonator," *Nature*, vol. 464, p. 697, 2010.

[87] A. Schliesser, R.Riviere, G. Anetsberger, O. Arcizet, and T.J.Kippenberg, "Resolved-sideband cooling of a micromechanical oscillator," *Nat. Phys*, vol. 4, p. 415, 2008.

[88] Y. Park and H. Wang, "Resolved-sideband and cryogenic cooling of an optomechanical resonator," *Nat. Phys*, vol. 5, p. 489, 2009.

[89] A. Schliesser, O. Arcizet, R. Riviere, G. Anetsberger, and T.J.Kippenberg, "Resolved-sideband cooling and position measurement of a micromechanical oscillator close to the heisenberg uncertainty limit," *Nat. Phys*, vol. 5, p. 509, 2009.

[90] A. Lita, A. Miller, and S. W. Nam, "Counting near-infrared single-photons with 95

[91] B. Cabrera, R. Clarke, P. Colling, A. Miller, S. Nam, and R. Romani, "Detection of single infrared, optical, and ultraviolet photons using superconducting transition edge sensors," *App. Phys. Lett*, vol. 73, p. 735, 1998.

[92] G. Rempe, R. Thompson, H. Kimble, and R. Lalezari, "Measurement of ultralow losses in an optical interferometer," *Opt. Lett*, vol. 17, p. 3631, 1992.

[93] A. Muller, E. Flagg, J. Lawall, and G. Solomon, "Ultrahigh-finesse, low-mode-volume fabry–perot microcavity," *Opt. Lett*, vol. 35, p. 2293, 2010.

[94] D. Herriott and H. Schulte, "Folded optical delay lines," *Appl. Opt*, vol. 4, p. 883, 1965.

[95] V.Vali, R. Goldstein, and K. Fox, "Verylongpath absorption cell for molecular spectroscopy," *App. Phys. Lett*, vol. 22, p. 391, 1973.

[96] R. Zhang, S. Garner, and L. Hau, "Creation of long-term coherent optical memory via controlled nonlinear interactions in bose-einstein condensates," *Phys. Rev. Lett*, vol. 103, p. 233602, 2009.

[97] A. Radnaev, Y. Dudin, R. Zhao, H. Jen, S. Jenkins, A. Kuzmich, and T. Kennedy, "A quantum memory with telecom-wavelength conversion," *Nat. Phys*, vol. 6, p. 894, 2010.

[98] A. Caldeira and A. Leggett, "Path integral approach to quantum brownian motion," *Physica A: Statistical mechanics and its Applications*, vol. 121(3), p. 587, 11983.

[99] M. Kermode, M. Mustafa, and N. Rowley, "Coulomb potential between two uniformly charged heavy ions," *Jounal of Physics G: Nuclear and Particle Physics*, vol. 16(12), p. L299, 1990.

[100] L.Diosi, "Notes on certain newton gravity mechanisms of wavefunction localization and decoherence," *J. Phys. A*, vol. 40, p. 2989, 2007.

[101] F. Maimone, G. Scelza, A. Naddeo, and V. Plenio, "Quantum superpositions of a mirror for experimental tests for nonunitary newtonian gravity," *Phys. Rev. A*, vol. 83, p. 062124, 2011.

[102] J. Solyom, *Fundamentals of the Physics of Solides: Volume 1: Structure and Dynamics*. Springer, 2007.

[103] C. Kittel, *Introduction to Solid State Physics*. Wiley, 2004.

[104] G. Ghirardi, A. Rimini, and T. Weber, "Unified dynamics for microscopic and macroscopic systems," *Phys. Rev. D*, vol. 34, p. 470, 1986.

[105] O. Romero-Isart, "Quantum superposition of massive objects and collapse models," *Phys. Rev. A*, vol. 84, p. 052121, 2011.

[106] J. Ellis, S. Mohanty, and D. V. Nanopoulos, "Quantum gravity and the collapse of the wave function," *Phys. Lett. B*, vol. 221(2), pp. 113–119, 1989.

[107] B. Collett and P. Pearle, "Wavefunction collapse and random walk," *Found. Phys*, vol. 33, p. 1495, 2003.

[108] R. Ghobadi, A. Lvovsky, and C. Simon, "Creating and detecting micro-macro photon-number entanglement by amplifying and de-amplifying a single-photon entangled state," *arXiv:1210.1514*, 2012.

[109] C. Monore, D. M. Meekhof, B. King, and D. Winwland, "A" schrodinger cat" superposition state of an atom," *Science*, vol. 272, p. 1131, 1996.

[110] J. Friedman, V. Patel, W. Chen, S. Tolpygo, and J. Lukens, "Quantum superposition of distinct macroscopic states," *Nature*, vol. 406, p. 43, 2000.

[111] S. Deleglise, I. Dorsenko, C. Sayrin, J. Bernu, M. Brune, J. M. Raimond, and S. Haroche, "Reconstruction of non-classical cavity field states with snapshots of their decoherence," *Nature*, vol. 455, p. 510, 2008.

[112] B. Julsgaard, A. Kozhekin, and E. Polzik, "Experimental long-lived entanglement of two macroscopic objects," *Nature*, vol. 413, p. 400, 2001.

[113] B. Yurke and Stoler, "Generating quantum mechanical superpositions of macroscopically distinguishable states via amplitude dispersion," *Phys. Rev. Lett*, vol. 57, p. 13, 1986.

[114] C. Simon and D. Bouwmeester, "Theory of an entanglement laser," *Phys. Rev. Lett*, vol. 91, p. 053601, 2003.

[115] A. Ourjoumtsev, H. Jeong, R. Tualle-Brouri, and P. Grangier, "Generation of optical 'schrodinger cats' from photon number states," *Nature*, vol. 448, p. 784, 2007.

[116] F. D. Martini, F. Sciarrino, and C. Vitelli, "Entanglement test on a microscopic-macroscopic system," *Phys. Rev. Lett*, vol. 100, p. 253601, 2008.

[117] P. Sekatski, N. Brunner, C. Branciard, N. Gisin, and C. Simon, "Towards quantum experiments with human eyes as detectors based on cloning via stimulated emission," *Phys. Rev. Lett*, vol. 103, p. 113601, 2009.

[118] P. Sekatski, B. Sanguinetti, E. Pomarico, N. Gisin, and C. Simon, "Cloning entangled photons to scales one can see," *Phys. Rev. A*, vol. 82, p. 250401, 2010.

[119] S. Raeisi, P. Sekatski, and C. Simon, "Coarse graining makes it hard to see micro-macro entanglement," *Phys. Rev. Lett*, vol. 107, p. 250401, 2011.

[120] N. Mermin, "Quantum mechanics vs local realism near the classical limit: A bell inequality for spin s," *Phys. Rev. D*, vol. 22, p. 356, 1980.

[121] A. Peres, *Quantum Theory: Concepts and Methods*. Klouwer-Dordrecht, 2002.

[122] N. Spagnolo, C. Vitelli, M. Paternostro, F. D. Martini, and F. Sciarrino, "Hybrid methods for witnessing entanglement in a microscopic-macroscopic system," *Phys. Rev. A*, vol. 84, p. 032102, 2011.

[123] S. Raeisi, W. Tittel, and C. Simon, "Proposal for inverting the quantum cloning of photons," *Phys. Rev. Lett*, vol. 108, p. 120404, 2012.

[124] K. Banaszek and K. Wodkiewicz, "Testing quantum nonlocality in phase space," *Phys. Rev. Lett*, vol. 82, p. 2009, 1999.

[125] S. A. Babichev, J. Appel, and A. Lvovsky, "Homodyne tomography characterization and nonlocality of a dual-mode optical qubit," *Phys. Rev. Lett*, vol. 92, p. 193601, 2004.

[126] S. V. Enk, "Single-particle entanglement," *Phys. Rev. A*, vol. 72, p. 064306, 2005.

[127] O. Morin, J. D. Bancal, M. Ho, P. Sekatski, V. D'Auria, N. Gisin, J. Laurat, and N. Sangouard, "Witnessing single-photon entanglement with local homodyne measurements," *arXiv: 1206.5734*, 2012.

[128] C. Chou, H. de Reidmatten, D. Felinto, S. Polyakov, S. V. Enk, and H. Kimble, "Measurement-induced entanglement for excitation stored in remote atomic ensembles," *Nature*, vol. 438, p. 828, 2008.

[129] P. Sekatski, N. Sangouard, M. Stobinska, F. Bussieres, M. Afzelis, and N. Gisin, "Exploring macroscopic entanglement with a single photon and coherent states," *arXiv*, no. 1206.1870, 2012.

[130] G. Milburn, "Intrinsic decoherence in quantum mechanics," *Phys. Rev. A*, vol. 44, p. 5401, 1991.

[131] R. Gambini, R. Porto, and J. Pullin, "Loss of quantum coherence from discrete quantum gravity," *Class. Quantum Grav*, vol. 21, p. L51, 2004.

[132] C. Simon and D. Jaksch, "Possibility of observing energy decoherence due to quantum gravity," *Phys. Rev. A*, vol. 70, p. 052104, 2004.

[133] F. D. Martini, "Amplification of quantum entanglement," *Phys. Rev. Lett*, vol. 81, p. 2842, 1998.

[134] J. Armestrong, N. Bloembergen, J. Ducuing, and P. Pershan, "Interactions between light waves in a nonlinear dielectric," *Phys. Rev. Lett*, vol. 127, p. 1918, 1962.

[135] U. Leonhardt, *Measuring the Quantum State of Light*. Cambridge University Press, Cambidge, 1997.

[136] W. Wootters, "Entanglement of formation of an arbitrary state of two qubits," *Phys. Rev. Lett*, vol. 80, p. 2245, 1998.

[137] H. Vahlbruch, M. Mehmet, S. Chelkowski, B. Hage, A. Franzen, N. Lastzka, S. Gobler, K. Danzmann, and R. Schnabel, "Observation of squeezed light with 10-db quantum-noise reduction," *Phys. Rev. Lett*, vol. 100, p. 033602, 2008.